SYNTHESIS AND CHARACTERIZATION OF SILICA-BASED NANOPARTICLES FOR BIOANALYTICAL APPLICATIONS

By

ROVELYN TAPEC DYTIOCO

A DISSERTATION PRESENTED TO THE GRADUATE SCHOOL OF THE UNIVERSITY OF FLORIDA IN PARTIAL FULFILLMENT OF THE REQUIREMENTS FOR THE DEGREE OF DOCTOR OF PHILISOPHY

UNIVERSITY OF FLORIDA

2002

ACKNOWLEDGMENTS

I would like to express my gratitude to my research advisor, Dr. Weihong Tan for his guidance and generous support. I would also like to thank the members of the Tan Research group, all of whom I enjoyed working with. I am greatly indebted to Dr. Swadeshmukul Santra for being a great mentor and a good friend. I owe Dr. Peng Zhang, Dr. Jianwei Li, Dr. Xiajun Zhao, Dr. Gang Yao, and Dr. Xiaohong Fang great appreciation for their advice and support in many of the work I have done. I am also very thankful to Karina Kerns, Monde Qhobosheane, Jane Hua Lou, Lisa Hillard, Zehui Cao, Tim Drake, and Marie Vicens for their friendship, encouragement, and help.

I would like to show my appreciation to Dr. Arthur Hebard and Nikoleta Theodoroupoulou of the Physics Department for working with us on the silica-coated magnetic nanoparticles. I am very grateful to Ms. Karen Kelley of the ICBR and Mr. Gil Brubaker of the ERC for their assistance in the characterization of my samples. I am especially thankful to the member of my research committee- Dr. Ben Horenstein, Dr. Robert Kennedy, Dr. M. Ian Phillips, and Dr. Jim D. Winefordner- for their assistance and encouragement.

I am extremely grateful to my friends for their belief and constant encouragement. I owe Celeste Aida Regino and Danilo Ortillo great appreciation for their friendship and continuous support. I am very thankful to Janina Gutierrez, Camilla Yandoc, Gino Ables,

Suzette and Ed Pabit, and Stephen and Czarina Carino for their gracious advice and warm-hearted nature.

My heartfelt thanks to my husband, Daniel Dytioco, for his interest in the research, helping in any way he can, and for being patient.

I am deeply indebted to my parents for their unending support and the best encouragement I received, their confidence in me.

TABLE OF CONTENTS

page

ACKNOWLEDGMENTS. ii

LIST OF TABLES..... vi

LIST OF FIGURES..... vii

ABSTRACT. xi

CHAPTER

1 INTRODUCTION 1

Nanoparticles and Biotechonology 3
Nanoparticle Synthesis Routes..... 6
Nanoparticle Characterization 9
Silica as a Matrix 10
Surface Modification and Bioconjugation 10
Dissertation Overview..... 15

2 SYNTHESIS AND CHARACTERIZATION OF INORGANIC DYE-DOPED SILICA NANOPARTICLES 17

Introduction 17
Experimental Section 19
Results 22
Discussion 42
Conclusions 47

3 SYNTHESIS AND CHARACTERIZATION OF ORGANIC DYE-DOPED SILICA NANOPARTICLE..... 49

Introduction 49
Experimental Section 53
Results 55
Discussion 64
Conclusions 67

4 SYNTHESIS AND CHARACTERIZATION OF MAGNETIC NANOPARTICLES 69

Introduction 69
Experimental Section 71
Results 74
Discussion 83
Conclusions 88

5 ULTRA-LUMINESCENT NANOPARTICLES FOR SEQUENCE-SELECTIVE DNA DETECTION 90

Introduction 90
Experimental Section 94
Results and Discussion 97
Conclusions 106

6 MAGNETIC NANOPARTICLES FOR CAPTURING TRACE AMOUNTS OF OLIGONUCLEOTIDES FROM A COMPLEX MATRIX 108

Introduction 108
Experimental Section 111
Results and Discussion 115
Conclusions 121

7 SUMMARY AND FUTURE DIRECTIONS 122

APPENDIX

A ELECTRON MICROSCOPY 127
B FLUORESCENCE MICROSCOPY 131
C ULTRAPYCNOMETER 136

LIST OF REFERENCES 137

BIOGRAPHICAL SKETCH 144

LIST OF TABLES

Table page

2-1 Amounts of surfactants used for systems with different w_0 values..... 21

2-2 Average diameters and standard deviations in nm of nanoparticles prepared in different surfactants, reaction times, and water-to-surfactant molar ratios (w_0). 23

2-3 Average densities and standard deviations in g/cc of nanoparticles prepared in different surfactants, reaction times, and water-to-surfactant molar ratios (w_0). 35

2-4 Percent Si and percent Ru by ICP-MS of nanoparticles prepared in different surfactants reaction times, and water-to-surfactant molar ratios (w_0). 39

2-5 Number of Ru atoms per nanoparticle by ICP-MS and fluorescence measurements (FM) of nanoparticles prepared in different surfactants, reaction times, and water-to-surfactant molar ratios (w_0)..... 40

4-1 Reagents for the preparation of magnetic nanoparticles..... 74

4-2 Size of magnetic nanoparticles based on TEM..... 85

5-1 Efficiency of separation using MB-magnetic nanoparticles 111

LIST OF FIGURES

Table		page
1-1	Formation of reverse micelles	8
1-2	Schematic representation of avidin-biotin coupling	11
1-3	Chemical structure of d-biotin	12
1-4	Schematic representation of disulfide coupling	13
1-5	Schematic representation of amino-carboxyl coupling	13
1-6	Schematic representation of amino-carboxyl coupling	14
1-7	Schematic representation of amino-cyanate coupling.	14
2-1	TEM images of nanoparticles prepared in different surfactants	24
2-2	TEM images of particles reacted with different durations	25
2-3	TEM images of nanoparticles in Brij-97 with different w_0's	26
2-4	TEM images of nanoparticles in Igepal CO-520 with different w_0's	28
2-5	Chemical structure of RuBpy	29
2-6	Luminescence excitation and emission spectra	30
2-7	Photobleaching experiment.	31
2-8	Photobleaching experiment.	33
2-9	Schematic diagram for the calculation of number of Ru/particle	34
2-10	Density comparison of nanoparticles prepared in 3 hours (H3) and 24 hours (H24)	36

2-11 Percent Si (by ICP-MS) comparison of nanoparticles prepared in 3 hours (H3) and 24 hour(H24)..... 37

2-12 Percent Ru (by ICP-MS) comparison of nanoparticles prepared in 3 hours (H3) and 24 hours (H24) 38

2-13 Fluorescence intensity vs. dye concentration. 42

3-1 Structures of rhodamine 6G(a) and fluorescein (b)..... 55

3-2 Fluorescence intensity comparison of fluorescein-doped silica nanoparticles..... 56

3-3 Fluorescence intensity comparison of fluorescein-dextran-doped silica nanoparticles 57

3-4 Electron microscope images 58

3-5 Fluorescence intensity comparison of samples with different PTES:TEOS ratios 59

3-6 Comparison of fluorescence intensities of nanoparticles immersed in water for 3 days before (3o) and after (3r) centrifugation and re-suspension 60

3-7 Photostability comparison of dye-doped nanoparticle and pure dye Rh6G .....
61

3-8 Bioassay for biotinylated BSA. Biotin interaction of avidin-modified nanoparticles 62

3-9 Quantitative representation of Figure 3-8. 63

3-10 Nanoparticle biosensor for glutamate 64

4-1 TEM images of non-coated and coated magnetic nanoparticles prepared in Brij-97 using NaOH 75

4-2 TEM images of non-coated and coated magnetic nanoparticles prepared in Igepal CO-520 Using NaOH..... 75

4-3 TEM images of non-coated and coated magnetic nanoparticles prepared in Triton X-100 Using NaOH..... 76

4-4 TEM image of bulk magnetic particles 78

4-5 XRD diffractograms 79

4-6 Magnetization curve for non-coated particles prepared in microemulsion using Brij-97, Igepal CO-520, and Triton X-100 81

4-7 Magnetization curve for silica-coated particles prepared in microemulsion using Brij-97, Igepal CO-520, and Triton X-100 82

4-8 Magnetization curve for bulk material 82

5-1 Schematic representation of a sandwich-based DNA assay using dye-doped silica nanoparticles 93

5-2 Comparison of signal intensities between dye-label and dye-doped silica nanoparticle label 98

5-3 Fluorescence microscopy images of samples containing different concentrations of target DNA 100

5-4 SEM images at 50x magnification showing concentration dependence of deposited nanoparticle density as target (DNA2) concentration is increased 101

5-5 Luminescence intensity vs. log [DNA target] 102

5-6 Selectivity of assay 105

5-7 Selectivity of assay (A-T vs. G-C Mismatch) 105

6-1 Schematic digram for the separation of oligonucleotides 114

6-2 TEM image of silica-coated magnetic nanoparticle 116

6-3 Molecular Beacon 116

6-4 Efficiency of molecular beacon immobilization 117

6-5 Temperature profile of immobilized MB-DNA duplexes 118

6-6 Temperature profile of free MB-DNA duplexes 118

6-7 Temperature profile comparison 120

A-1 Specimen interaction 128

A-2 Schematic representation of a transmission electron microscope..... 129

A-3 Schematic representation of a scanning electron microscope..... 130

B-1 Jablonski Diagram 131

B-2 Cut-away diagram of an inverted fluorescence microscope..... 132

B-3 Schematic diagram of an inverted fluorescence microscope 134

B-4 Wide-field fluorescence Lens 135

Abstract of Dissertation Presented to the Graduate School
of the University of Florida in Partial Fulfillment of the
Requirements for the Degree of Doctor of Philosophy

SYNTHESIS AND CHARACTERIZATION OF SILICA-BASED NANOPARTICLES FOR BIOANALYTICAL APPLICATIONS

By

Rovelyn Tapec Dytioco

August 2002

Chair: Dr. Weihong Tan
Major Department: Chemistry

Novel silica-based nanoparticles that may improve and create an impact in bioanalyses have been developed. Highly luminescent dye-doped silica nanoparticles with excellent photostability were synthesized and used as probes or biomarkers for various biochemical processes. Ultra-small magnetic silica nanoparticles were also made and used as carriers in separation processes involving biomolecules. Due to the silica matrix, both types of nanoparticles can be easily conjugated to biomolecules for further use in bioanalyses.

RuBpy dye-doped silica and silica-coated magnetic nanoparticles were synthesized in reverse microemulsion. This size-selective microemulsion system allowed the formation of monodisperse nanoparticles with diameters from 2-3 nm to 70 nm. Rhodamine 6G dye-doped nanoparticles were prepared using a modified Stöber method. The procedure yielded 100-nm and bigger particles.

The dye-doped nanoparticles were characterized not only for their size but also for their optical properties. These particles have excellent photostability due to the shielding effect provided by the silica matrix. Composition analysis done on the nanoparticles showed that each particle contains thousands of dye molecules, which can be a basis for signal amplification. The nanoparticles were used in a DNA assay and detection down to 100 fM was achieved. In addition, signal amplification was observed when the intensities from assays using dye-doped nanoparticle label and organic fluorophore label were compared.

Silica-coated magnetic nanoparticles were characterized according to their size and magnetic susceptibility. The particles obtained were in the nanometer range and were superparamagnetic. These nanoparticles were used in the collection of trace amounts of oligonucleotides from a complex matrix. With the silica coating, the magnetic nanoparticles were bound to molecular beacons, which acted as probes and capturing elements for the target oligonucleotide. Collection efficiency using these magnetic nanoparticles conjugated with molecular beacons was as high as 98%.

Both the synthesis routes developed and the assay results may be used in future studies to either further improve the nanoparticles or optimize the nanoparticle-based assays. This work is one indication that nanotechnology can benefit, if not revolutionize, biotechnology.

CHAPTER 1
INTRODUCTION

Medical and biotechnological advances in the area of disease diagnosis and treatment are dependent on an in-depth understanding of biochemical processes. Diseases can be identified based on anomalies in the molecular level and treatments are designed based on activities in such low dimensions. A multitude of methods for disease identification as well as treatment already exist; some use molecules such as fluorophores or atoms in the form of isotopes, all with dimensions close to the molecular level, to better understand the mechanisms involved in the processes.

The use of fluorophores as biomarkers in bioanalyses may already be an established procedure but the use of such molecules still have some limitations. First, individual synthesis of fluorophores would be required for specific conjugation to different types of molecules. For example, fluorophores to be linked to an amine-containing molecule have to be synthesized separately from those that will be attached to biotinylated biomolecules. Second, the sensitivity of an assay using fluorophores may not be very high because a sufficiently high concentration would be needed to obtain discernable signal. Third, fluorophores suffer from photobleaching and this does not make them the ideal biomarkers for assays that require long-time light exposure. However, using alternative biomarkers may solve the problems of conjugation, sensitivity, and photostability.

Possible alternative biomarkers are dye-doped silica nanoparticles. The features of dye-doped silica nanoparticles can eliminate the problems of fluorophores. With the silica as a matrix, dye-doped nanoparticles are very versatile with regards to bioconjugation. Higher sensitivity of assays using dye-doped nanoparticles can be achieved because of signal amplification. To solve the photobleaching problem, the silica coating can act as a shield against quenchers and would leave the biomarkers photostable. With the limitations of the fluorophores addressed by dye-doped silica nanoparticles, the latter can be used as a better alternative if they are made in the same dimension range as biomolecules. Since advances in nanotechnology has allowed the fabrication of ultra-small dimension of materials bordering to the molecular level, nanoparticles can be made and used as a better alternative to traditional fluorophores for bioanalyses. Such a protocol is just one of many possible ways that nanotechnology can benefit biotechnology.

Biomedical sciences and biotechnology have benefited significantly from technological advancement in many fields [1-10]. Much as microfabrication technologies have revolutionized the electronics industry, nanotechnologies are now poised to revolutionize the biomedical fields ranging from basic studies to disease diagnosis and treatment. Nanotechnology, the process to generate, manipulate and employ nanomaterials, represents an area holding significant promise for health care and biotechnology in many years to come. Understanding the principles of nanotechnology may provide insights into critical biological systems related to disease control, correction of genetic disorders and longevity. Numerous works have been published on the use of nanomaterials for biotechnological research and more are certainly in progress. The

biotechnological applications of nanomaterials include the use of nanotechnology for DNA transfection [1-5], drug delivery [6, 7], and immunoassays [8-10].

Nanoparticles and Biotechnology

Technically defined, nanoparticles are materials with structural features in between those of atoms and bulk materials [11]. In addition, at least one of the dimensions should be 100 nm (1 nm = 10^{-9} m) or less. Nanoparticles have been developed and show great promise in biotechnology and bioanalysis due to their unique optical properties, high surface-to-volume ratio, and other size-dependent qualities. When combined with surface modifications and composition manipulation, these properties provide probes for highly selective and ultra-sensitive bioassays.

The size of nanoparticles distinguishes them from bulk materials and offers more diverse capabilities in bioanalysis. A class of nanoparticles that would demonstrate such capabilities includes particles made of semiconductors called quantum dots. Quantum dots, whose radii are smaller than the bulk exciton Böhr radius, are intermediate particles between molecular and bulk forms of matter [12, 13]. Due to quantum confinement, both the absorption and emission energies of quantum dots shift to higher energies as the size of the nanoparticles decreases [12-15]. The utilization of quantum dots for multiple-color multi-analyte analysis [15] and biological imaging [16] demonstrate the feasibility of using these semiconductor-based particles in biotechnological research.

Another class of nanoparticles includes metal nanoparticles in which different wavelengths of scattered light can be observed due to changes in size and compositions [17]. The class involving silica nanoparticles can also be adapted to specific applications by size control [18, 19]. The effects of fine-tuning the size of materials to obtain

desirable properties for biological applications observed in nanoscale materials can be advantageous in biotechnology.

Nanoparticle composition is also important to their applicability in biotechnology. The composition determines the compatibility and the suitability of the probes with the analytes and what assays are possible. The most common materials used are gold, silica, and semiconductors such as CdSe and ZnS [20]. These materials allow easy and efficient surface modifications that also make them applicable to biomedical and biotechnology applications.

Gold (Au) is an attractive material for merging nanotechnology with biotechnology due to its affinity toward thiol-modified molecules. Scientists have done extensive work using gold nanoparticles for oligonucleotide (oligo) detection [17, 21-28]. Gold nanoparticles immobilized with thiol-modified oligos were used as probes for detecting target oligo hybridization by changes in the solution's color due to the formation of polymeric Au nanoparticle/polynucleotide aggregates [21, 22]. Also, latex and gold particles have been immobilized with different DNA fragments complementary to DNA targets. Upon DNA duplex formation a color change was observed. Gold nanoparticles have also been extended to DNA detection on an array-based format. In a sandwich-based array method, a gold nanoparticle-labeled DNA hybridizes with a target sequence that has also formed a duplex with a capture sequence immobilized to a solid support. Signal is obtained from the bound nanoparticle probe and is further amplified by silver reduction over the gold probe [24]. By utilizing different light scattering properties of oligonucleotide-capped particles, a method has also been developed for multicolor

labeling and imaging of DNA arrays and has the capability to distinguish between two different DNA targets [17].

Other groups have also demonstrated gold nanoparticle based-DNA detection [29-32]. Based on reflected and transmitted light of surface-bound nanoparticles, the hybridization of gold nanoparticle-labeled DNA probes with their target DNA was monitored [33]. Gold has also been shown to act as a quencher for the fluorophore of a molecular beacon (MB) [34]. A molecular beacon is consists of a single-stranded DNA molecule in a stem-loop conformation with a fluorophore linked to the 5'- end and a quencher at the 3'- end. Upon hybridization of target oligonucleotide to the MB, the fluorophore and quencher are spatially separated causing the restoration of the fluorescence. By using the gold nanoparticle as the quencher of the fluorophore, the resulting structure demonstrated up to 2 orders of magnitude sensitivity enhancement over 4-(4'-dimethylaminophenylazo) benzoic acid or DABCYL-quenched beacons [34]. Increasing the sensitivity of DNA probes by using nanoparticles allows the development of more efficient bioanalytical tools for oligonucleotide detection.

The use of gold nanoparticles is, however, not limited to DNA detection [35, 36]. Gold, as well as silver, nanoparticles can also be used for immunophenotyping when coated with antibodies [35]. The magnitude and direction of the wavelength shifts will depend on the size, shape, and refractive index of the nanoparticles, and their relative effect on light scattering from the targeted cells.

Semiconductors that make up quantum dots are also making a significant impact in biotechnological research. Much work has been done involving ultrasensitive non-isotopic bioanalysis with quantum dot bioconjugates [37, 38]. The dots are claimed to be

20 times brighter, 100 times more stable against photobleaching, and one-third wider in spectral width compared to organic fluorophores [37]. These particles have also shown recognition capabilities to specific antibodies or antigens when labeled with the proper immunomolecules [37]. Quantum dots labeled with a protein transferrin have also been shown to undergo receptor-mediated endocytosis in cultured cells. The small size of quantum dots has also been utilized to embed them into microbeads [39]. When embedded at different ratios, the resulting microbeads also have different colors. Water-soluble silica coated quantum dots have also been developed which show promise in bioconjugation studies due to the versatility of silica chemistries [40]. Quantum dots offer new capabilities for multicolor optical coding in bioanalysis and show promise in gene expression studies, high-throughput screening, and medical diagnostics.

Other materials that have been used as nanoparticle probes are europium, latex, and metals other than gold [41-52]. Europium (Eu) nanoparticles were utilized as probes for time-resolved fluorescence detection of prostate-specific antigen [41-43]. Fluorescent latex nanobeads have been used to probe specific sequences on single DNA molecules [52]. Based on the current reported work done involving nanoparticles, a wide variety of available materials exist that can be employed to investigate several important and relevant biological problems. Also, since the composition of a material does not limit the type of analyte that can be analyzed, with the proper detection method a wide range of analytes can be used.

Nanoparticle Synthesis Routes

A variety of techniques are available for the preparation of nanoparticles; many of which involve colloidal chemistry while others involve ablation by high peak-power laser

pulses, electrodeposition, etching, and direct synthesis on surfaces or Langmuir-Blodgett films [53]. The two general synthesis routes for the developed silica-based nanoparticles in the projects that will be discussed are both colloid-based. One is by reverse microemulsion [18, 54-56], primarily for the inorganic dye-doped nanoparticles and the magnetic particles and the other is by Stöber method [19, 57-59] for the preparation of pure silica nanoparticles and organic dye-doped nanoparticles.

Reverse or water-in-oil microemulsion (W/O) is the primary route used in the synthesis of the silica-based nanoparticles in this work. This type of technique is a robust and efficient method of nanoparticle preparation. The microemulsion yields monodisperse particles in the nanometer range. Reverse microemulsion is an isotropic and thermodynamically stable single-phase system consisting of three prime components: water, oil, and a surfactant (Figure 1-1). A surfactant is a surface-active amphiphile that aggregates or self-assembles in water or other solvents to form various microstructures such as micelles or bilayers. In reverse microemulsion, water nanodroplets are contained in the reverse micelles formed by the surfactant molecules. These water nanodroplets formed in the bulk oil phase act as confined media, or nanoreactors, for the formation of discrete particles. The size of the nanoreactors, and consequently the nanoparticles, can be tuned by controlling the water-to-surfactant molar ratio (w_0). Systems with w_0= 10 using Triton X-100 can produce silica nanoparticles ranging from 60-70 nm diameters.

Using reverse microemulsion, silica nanoparticles have been synthesized and doped with either tris(2,2'-bipyridyl)dichlororuthenium (II) or (RuBpy), tetramethylrhodamine (TMR), TMR-dextran, or fluorescein-dextran [18, 55, 56]. The procedure allowed the doping of dye molecules in each nanoparticle. Ultra-small

magnetic nanoparticles of Fe_3O_4 and Fe_2O_3 were also obtained using the reverse microemulsion method [54]. These were then silica-coated for biomolecule immobilization.

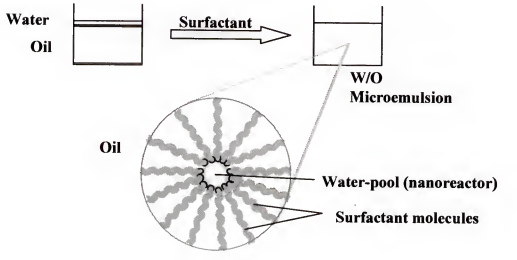

Figure 1-1. Formation of reverse micelles.

The Stöber method is an alternative procedure mainly used for the preparation of pure silica nanoparticles and hydrophobic organic dye-doped particles. Suspension of sub-micron silica-based spheres can be obtained by this method. The particle diameter can be controlled through the parameters involved in the process i.e., temperature and concentration. The mechanism of growth of silica particles by the Stöber method has been explained to start with the formation of small primary particle nucleates in ammonia-water, followed by aggregation to form a larger particle [59]. Particles obtained can be less than 100 nm to about 1μm in diameter. Although this method is relatively simple and can be carried out in only a few hours, it is limited by the non-uniformity of the products obtained. Filtration and further separation is needed to obtain highly uniform and ultra-small particles.

Nanoparticle Characterization

The synthesized silica nanoparticles (pure, dye-doped, and magnetic) were characterized by at least one of the following criteria: size, optical, and magnetic properties. Transmission electron microscopy (TEM) and scanning electron microscopy (SEM) were used to determine the size of the silica-based nanoparticles. Since the particles are mostly spherical, sizes were compared according to measured diameters. To evaluate spectroscopic properties, the nanoparticles were subjected to either fluorescence microscopy or spectrofluorometry or both. Optical properties such as emission, excitation, and photostabilities were analyzed. The size and the optical properties are the significant factors that would determine the usefulness of the dye-doped silica nanoparticles for bioassays [18, 55].

In addition to size and optical characterization, the magnetic properties of Fe_3O_4/ Fe_2O_3/SiO_2 particles were also evaluated. A powdered form of the nanoparticles was analyzed using superconducting quantum interference device (SQUID). The results obtained were used to determine the optimal synthesis conditions that would yield magnetic particles useful for bioanalysis. The crystalline properties of the magnetic particles were also analyzed by X-ray diffraction. The information obtained was expected to shed light as to what form of iron oxide (Fe_3O_4 or Fe_2O_3) was present in the nanoparticles and what the effect would be on the over-all magnetic properties of the particles.

Quantitation is an important aspect in bioanalysis. To be able to calculate how many nanoparticles are present in a certain weight of sample, the density of the material should be known. Density information as well as volume calculated from the size

information would allow the desired calculation. Although the densities of pure silica and pure dopants such as RuBpy are known, the densities of the composites or the dye-doped nanoparticles were not. For this purpose, an instrument called ultra-pycnometer was used. The information obtained helped not only determine the number of particles but also compare emission intensities of different nanoparticle samples.

Silica as a Matrix

The use of silica as a substrate in bioanalysis has special advantages as shown by its widespread use. Silica can be synthesized by various preparation techniques to prepare nanoparticles, transparent films, or solid flat materials. Silica synthesis is governed by the chemical properties of the surface, which in return are based on the silanols and siloxanes present on the surface [60].

Silanol groups can be functionalized through different procedures. The hydroxy group can react with various compounds to give amino, carboxy, or thiol groups. Silica surface modification is not limited to chemically mediated procedures. Passive adsorption of molecules such as avidin is also commonly used. The versatility of silica in synthesis and in surface modification offers a great advantage to the use of the material in bioanalysis.

Surface Modification and Bioconjugation

The silica-based nanoparticles can be useful in bioanalytical applications when conjugated to analyte recognition elements and/or signal generating components. The dye-doped nanoparticles already contain dye molecules ready to luminesce when interrogated, but such an event can only be useful when coupled to a biomolecular interaction of interest. To take advantage of the usefulness of silica nanoparticles, a

variety of surface modification and immobilization procedures were utilized and were developed to couple the nanoparticles to various biomolecule targets. For example oligonucleotides, enzymes, antibodies, and other proteins have been used for bioanalytical detection.

A clear advantage that the silica matrix/surface provides is versatility towards different surface modification protocols. The silica surface can be modified to contain avidin, disulfide, amine, or carboxylate groups. Avidin can be passively adsorbed on the silica surface followed by glutaraldehyde crosslinking. The resulting avidin-coated particle can then be conjugated with biotinylated molecules based on the strong avidin-biotin affinity (Figure 1-2). The capacity of silica to bind with avidin will allow the use of the nanoparticles to assays requiring commonly used and widely available biotinylated compounds.

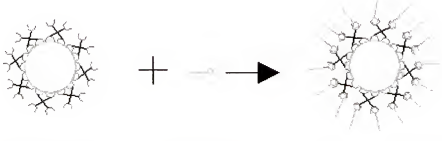

Figure 1-2. Schematic representation of avidin-biotin coupling.

Avidin is a tetrameric glycoprotein (MW 68 kDa) composed of four identical subunits. Each subunit is glycosylated at 17-Asparagineand has one binding site for d-biotin, Vitamin H (Figure 1-3). The great affinity of avidin to d-biotin ($k_d = 10^{-15}$ M)

results in a great number of applications in biochemistry (immunoassays, receptor and histochemical studies, bacteriophage inhibitions, etc.)

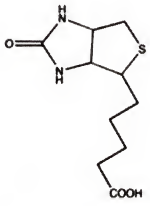

Figure 1-3. Chemical structure of d-biotin.

Disulfide-coupling chemistry has also been used for the immobilization of oligonucleotides onto silica nanoparticles [61]. Silica nanoparticles (procedure previously described) were silanized with 1% 3-mercaptopropyl-trimethoxysilane (MPTS). A thiol/disulfide exchange reaction would allow the conjugation of the thiol-modified nanoparticles to disulfide-modified oligonucleotides. The disulfide-modified oligonucleotides are directly coupled to the silane-activated silica surface without any pretreatment (Figure 1-4). In this reaction, the R group from the biomolecule should be a good leaving group for the exchange to occur. The procedure is a simple approach to bioconjugation.

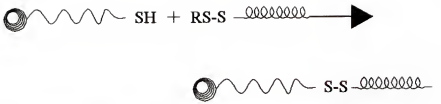

Figure 1-4. Schematic representation of disulfide coupling.

A commonly used protocol for the immobilization of enzymes and antibodies is the amino-group derivatization for isourea or peptide linkage. The particles are silanized with N^1-[3-(Trimethoxysilyl)propyl]diethylenetriamine (DETA) in acetic acid. After silanization, glutaraldehyde is added as a crosslinker before subsequent binding with amino-containing groups such as enzymes and antibodies (Figure 1-5). A slightly modified procedure can yield carboxyl-modified nanoparticles. Instead of using glutaraldehyde, the particles are then treated with succinic anhydride in dimethylformamide. The carboxyl-modified particles can be further reacted with carbodiimide hydrochloride before subsequent enzyme immobilization (Figure 1-6) [19].

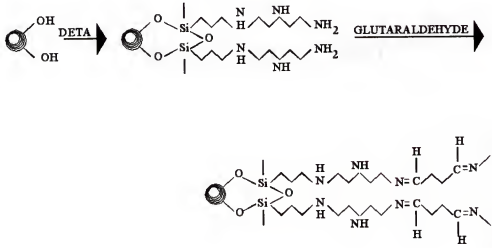

Figure 1-5. Schematic representation of amino-carboxyl coupling.

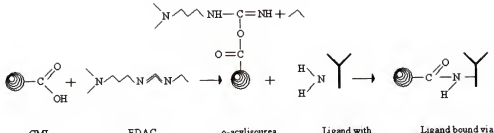

Figure 1-6. Schematic representation of amino-carboxyl coupling (adapted from Bangs Labs TechNotes). CML is carboxyl-modified ligand while EDAC is 1-Ethyl-3-(3-dimethylaminopropyl) carbodiimide.

Silica nanoparticles can also be surface-modified by activating them with sodium carbonate. A solution of cyanogen bromide in acetonitrile would then be added to the suspension to yield the reactive cyanate intermediate on the particle surface. The cyanate-modified particles would then be available for bioconjugation to biomolecules containing free amino groups (Figure 1-7).

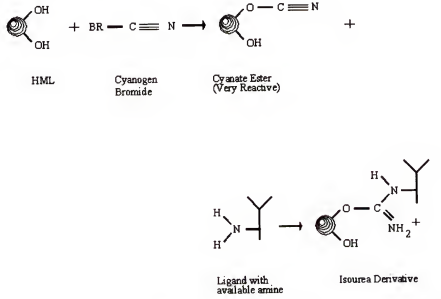

Figure 1-7. Schematic representation of amino-cyanate coupling (adapted from Bangs Labs TechNotes). HML stands for hydroxide-modified ligand.

After the appropriate surface modification, the nanoparticles can then be directly used in bioanalytical applications. Examples of such include biomarker, biosensor, and oligonucleotide detection applications.

Dissertation Overview

The need to understand mechanisms and interaction in the sub-cellular or even close to molecular level has made it necessary to have analyses done on platforms of sub-micro or nano dimensions. Although numerous strategies are already available, the size of nanoparticles gives them the potential to be used for such analyses. The over-all objective of this research was to develop general methods for the synthesis of silica-based nanoparticles that may be used for bioanalyses. The resulting particles were characterized according to their size, optical properties, and other parameters that were considered useful for the role of the nanoparticles role in bioanalyses. Actual bioanalytical applications using the nanoparticles were also demonstrated.

In Chapter 2, the synthesis and characterization of inorganic dye-doped silica nanoparticles, RuBpy-doped in particular, is explained. Chapter 3 focuses on the synthesis and characterization procedures of organic dye-doped silica nanoparticles that were investigated. The synthesis and characterization of another class of silica nanoparticles, magnetic nanoparticles, is the subject of Chapter 4. Bioanalytical applications of silica-based nanoparticles are demonstrated in Chapters 5 and 6. In Chapter 5, dye-doped nanoparticles are used as probes for highly sensitive and selective DNA detection. Magnetic nanoparticles coupled with molecular beacons are shown in Chapter 6 to be effective carriers in the extraction of trace amounts of oligonucleotides

from a complex matrix. Chapter 7 includes a summary of the research that has been done on silica-based nanoparticles as well as some future insights.

CHAPTER 2
SYNTHESIS AND CHARACTERIZATION OF INORGANIC DYE-DOPED SILICA NANOPARTICLES

Introduction

The development of reliable methods for detection and quantification is of great importance in bioanalyses. Radiolabeling is often employed on probe molecules in biochemical processes due to the sensitivity that can be obtained. This method is however hampered by a major drawback: it uses potentially hazardous radioisotopes and ^{32}P, a commonly used label, has a relatively short half-life. Non-radiosotopic methods that include the use of fluorophores, luminophores, and electroactive agents are thus gaining widespread use [33, 50, 51]. Fluorescence, chemiluminescence, and bioluminescence are widely used in many bioanalyses. Detection is based on the signal generated by fluorophores, quantum dots, or fluorescent nanoparticles. Although each group of labels has its own advantages, each has its share of limitation. Fluorophores suffer from rapidly decaying fluorescence decreasing sensitivity at very low target concentration [41, 62]. Quantum dots are showing great promise in bioanalyses. They have size-tunable spectra and can be very useful in multiplex analyses. Unless modified, however, these luminescent dots have poor solubility in water and may undergo agglutination. In addition, since these dots are made up of semiconductors, they are inherently bound to have low quantum yields.

Fluorescent latex particles have also been used as labeling moieties. Large size, tendency to agglomerate, and dye leakage have however prevented the effective

application of such particles as luminescent biomarkers for ultrasensitive analyses. In spite of several limitations, however, the development of nanoparticle-based luminescent markers has become a challenging field of research in recent years because such types of nanoparticles can be engineered to obtain desired luminescent properties.

In an effort to synthesize highly stable, sensitive and uniform biomarkers, novel dye-doped silica nanoparticles were developed for application as efficient biomarkers. The use of silica network as a matrix for the incorporation of the inorganic dye RuBpy prevents dye-photobleaching, communication to the outside environment and dye leakage. The silica matrix not only protects the dye but also provides some unique features, which are very important while working with biological systems. For example, silica is a biocompatible substrate and very stable in adverse environment. Moreover, silica nanoparticles form a clear dispersion in water and their surface can be modified very easily to attach biomolecules. Dye-doped nanoparticles can be very uniform when they are made in water-in-oil microemulsion, a medium that can control the size of the particle. Because of the much smaller dimension of the dye-doped nanoparticles, compared to the cellular dimension, they are suitable for biolabeling.

Various parameters were controlled in the synthesis of RuBpy-doped silica nanoparticles. These include the type of surfactant used, time of polymerization, water-to-surfactant molar ratio (w_0), and amount of dopant (RuBpy) used. The obtained nanoparticles were characterized according to size and optical properties. In addition, density measurements, mass spectrometry analyses, and fluorescence analyses were performed to determine the number of particles for a given weight of sample. The

measurements were also done to fairly compare the intensities of the particles prepared via the different methods.

Experimental Section

Materials. Tetraethylorthosilicate (TEOS), Triton X-100 or TX-100 {polyoxyethylene(10)isooctylphenylether, 4-(C_8H_{17})C_6H_4(OCH_2CH_2)$_n$OH, n~10}, Brij-97 {polyoxyethylene(10)oleylether, $C_{18}H_{35}$(OCH_2CH_2)$_n$OH, n~10}, Igepal CO-520 {polyoxyethylene(5)nonylphenylether, 4-(C_9H_{19})C_6H_4(OCH_2CH_2)$_n$OH, n~5}, Tris(2,2'-bipyridyl) dichlororuthenium(II) hexahydrate (RuBpy), and n-hexanol were purchased from Aldrich Chemical Co. Inc. (Milwaukee, WI). Cyclohexane, n-heptane, n-hexanol, acetone, and ammonium hydroxide (28-30 wt%) were obtained from Fischer Scientific Co. (Pittsburgh, PA). Distilled deionized water (EasyPure LF, Barnstead Co.) was used for the preparation of aqueous solutions.

Nanoparticle synthesis. The general procedure for the preparation of RuBpy-doped silica nanoparticles is as follows: a water-in-oil microemulsion was prepared by adding 1.77 mL of TX-100, 7.5 mL of cyclohexane, 1.8 mL of n-hexanol, and 400 μL of water. After thorough stirring, 80 μL of 0.1 M aqueous RuBpy solution was added. TEOS (100 μL) was then added as a precursor for silica formation followed by addition of 60 μL NH_4OH to initiate the polymerization process. This system has a water-to-surfactant molar ratio or w_0 of 10. The reaction was allowed to proceed for 24 hours with constant magnetic stirring. After completion of the reaction, adding acetone broke the reverse micelles, thereby releasing the dye-doped silica nanoparticles. The washing steps that ensued involved the use of ethanol, centrifugation, and ultrasonication. Washing with

ethanol and water several times was done to ensure the removal of surfactant molecules. Each step was done at ambient temperature.

Varied surfactant systems. Following the general procedure for the synthesis of dye-doped nanoparticles described above, two other surfactants were tried. The surfactants used were also non-ionic like the Triton-X-100 but the length of the hydrophobic tails varied. The other surfactants used were Brij-97 and Igepal CO-520. Based on the molecular weights of the surfactants, the needed amounts were measured to give a microemulsion system that would have the same w_0 (10). Brij-97 (1.424 g) was added to 18.6 ml of cyclohexane. For the Igepal CO-520 system, 0.892 g of the surfactant was used and 2.4 ml of n-heptane. The amount of water (400 μL), 0.1 M RuBpy (80μL), TEOS (100μL), and NH_4OH (60 μL) were all kept constant. The procedure allowed synthesis of particles made in reverse microemulsion systems of Triton X-100, Brij-97, and Igepal CO-520.

Varied water-to-surfactant molar ratio. In this experiment, the amount of surfactant were varied to yield microemulsions with w_0= 5 or 2. For the w_0=5 systems, the amounts of surfactant used were double that of the w_0=10 systems. The w_0=2 systems were prepared by using 5 times the amounts of surfactant used in the w_0=10 systems. All the other reagents were kept the same. Amounts of surfactants used are in Table 2-1.

Table 2-1. Amounts of surfactants used for systems with different w_0 values.

Surfactant	w_0 =10	w_0 =5	w_0 =2
Triton X-100	1.77 ml	3.54 ml	8.85 ml
Brij-97	2.14 g	4.27 g	10.68 g
Igepal CO-520	1.14 g	2.28 g	5.7 g

Varied reaction time. For this experiment, reverse microemulsions of the different surfactants and different w_0's were allowed to proceed not for 24 hours, but for 15 minutes, 1 hour, 3 hours, 6 hours, and 12 hours.

Varied amount of dopant, RuBpy. Using the Triton X-100 system with w_0=10, different amounts of 0.1 M RuBpy were used (40 μL, 80 μL, 160 μL). The amount of water was adjusted to keep the w_0 the same.

Nanoparticle characterization. The obtained nanoparticles were characterized with respect to their size and optical properties. The samples were subjected to either transmission electron microscopy (TEM, Hitachi H-7000) or scanning electron microscopy (SEM, Hitachi S-4000) to determine the size of the nanoparticles. Fluorescence microscopy (Olympus IX70 microscope) and spectrofluorometry (SPEX Fluorolog-2) were both employed to determine the optical properties of the nanoparticle samples. Excitation and emission wavelengths as well as signal intensities were compared. The photostabilities of the nanoparticles were also evaluated by subjecting them to long-time light exposure with the fluorescence signal being simultaneously

monitored. Other physical characterizations that were done on the nanoparticle samples include density measurements using ultra-pycnometer, mass spectrometry analyses, and fluorescence analyses. This set of measurements provided information needed for the calculation of number of particles for a given weight of sample, nominal values of ruthenium atoms per particle, and effective number of fluorescent ruthenium atoms per particle.

Results

Size. TEM sample preparation was done by putting a drop of the microemulsion on carbon-coated 200-mesh metal grids. After 2-day air-drying, TEM analysis was done. The diameter measurements of the produced nanoparticles are shown in Table 2-2. Based from the data it can be inferred that surfactant system, time of reaction, and the water-to-surfactant molar ratio affect the final size of the produced nanoparticles. For the experiment, the surfactants used were all non-ionic but they differed in their type of hydrophobic tails. Triton X-100 and Igepal CO-520 both have phenyl groups but the former has a longer polyoxyethylene group (10 versus 5). Brij-97 has a polyoxyethylene group as long as that of the Triton X-100 but did not have any phenyl group; it had an aliphatic group instead. The surfactants with the phenyl group yield bigger particles. In addition, among the aromatic ring-containing surfactants, the one with a longer polyoxyethylene chain produced bigger nanoparticles. The results are shown in Figure 2-1. The sample nomenclature was based on the following scheme: the letter for the surfactant system and the number for the w_0 value. The letter I stands for Igepal CO-520, T for Triton X-100, and B for Brij-97. I10 would then mean that the sample was prepared in Igepal CO-520 with w_0=10. H3 stands for 3-hour reaction time and H24 for 24 hours.

Table 2-2. Average diameters and standard deviations in nm of nanoparticles prepared in different surfactants, reaction times, and water-to-surfactant molar ratios (w_0).

Sample	H3 (nm)	H24 (nm)
I10	21 ± 4	26 ± 3
I5	27 ± 5	41 ± 7
I2	43 ± 5	53 ± 7
T10	43 ± 4	73 ± 5
B10	17 ± 2	28 ± 4

Reaction time has definitely an effect on the size of the nanoparticles made. From the measured diameter values, the polymerization is not yet complete at 3 hours. Between 3 hours and 24 hours, there is a significant difference in the diameter values, albeit not proportional with the time change. This data suggests that control of polymerization time can yield particles of the desired size. Figure 2-2 shows this result.

(a)

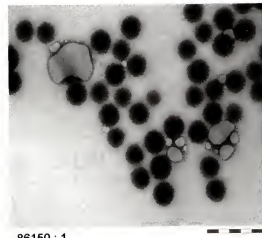

(b)

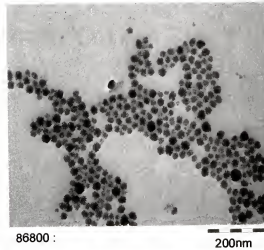

(c)

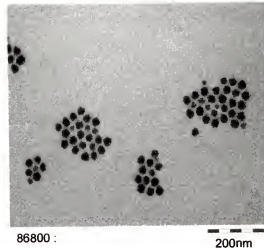

Figure 2-1. TEM images of nanoparticles prepared in different surfactants. (a) Triton X-100; (b) Igepal CO-520; (c) Brij-97. All were reacted for 24 hours and have w_0=10. Scale bars are 200 nm.

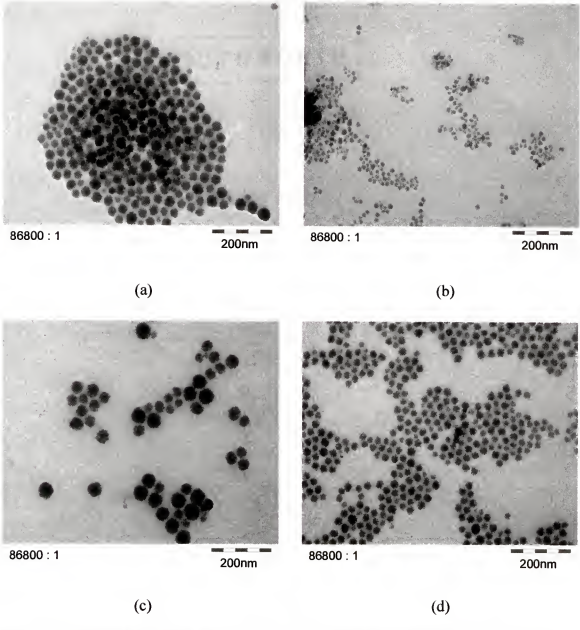

Figure 2-2. TEM Images of particles reacted with different durations. (a) and (c) are nanoparticles prepared in Igepal CO-520 with w_0= 5 but were reacted for 3 hours and 24 hours, respectively. (b) and (d) are nanoparticles prepared in Brij-97 with w_0= 5 but were reacted for 3 hours and 24 hours, respectively. Scale bars are 200 nm.

Another factor that can greatly influence the size of the nanoparticles is the water-to-surfactant molar ratio, w_0. It has been reported that an increasing w_0 value would lead to an increase in the size of the resulting nanoparticles due to the swelling of the reverse micelles. This phenomenon was observed in the case of the Brij-97 system where

samples of w_0= 10, 5, and 2 were compared (Figure 2-3). A decrease in size was observed from the samples with decreasing w_0.

(a)

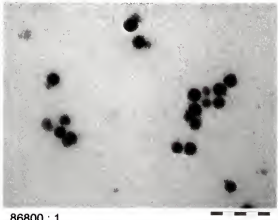

(b)

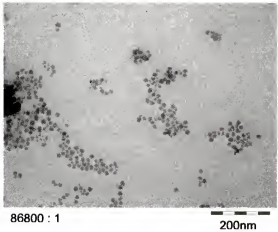

(c)

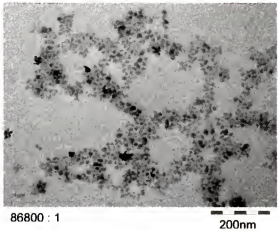

Figure 2-3. TEM Images of nanoparticles in Brij-97 with different w_0's. (a) w_0=10, (b) w_0=5, (c) w_0=2. The reaction time for all is 3 hours. Scale bars are 200 nm.

In the case of Igepal CO-520, a reverse trend was observed (Figure 2-4). Increase in size was seen from the samples with decreasing w_0. It can thus be inferred that both the structure of the surfactant and the w_0 play important roles in the formation of the micelles. It is possible that the phenyl-containing hydrophobic tail of the Igepal CO-520 has an effect on the size of the reverse micelles formed. A decrease in w_0 value can mean an increase in the amount of the surfactant. Since the hydrophobic tail has a bulky group present, an increase in the number of surfactant molecules would result to repulsion. To minimize repulsion, the surfactant molecules would tend to have a less compact distribution. A bigger reverse micelle with a bigger waterpool would then result. Thus, lower w_0 yields bigger particles in Igepal CO-520. A similar experiment was done with the Triton X-100 system. The reverse microemulsions obtained for the lower w_0 were however unstable. They were turbid and the particles did not stay suspended but coagulated instead. The cloudiness is an indication that particles or reverse micelles big enough to cause light scattering were present. The particles were relatively big and most of them were formed outside the reverse micelles. Evidence of such formation is the settling of particles at the bottom of the reaction vessel for the systems with lower w_0 values (5 and 2). Since the structure of Triton X-100 is more similar to that of the Igepal CO-520 than that of Brij-97, the w_0 effect should be similar to that of the Igepal CO- 520. Since Triton x-100 is more hydrophobic than Igepal CO-520, bigger particles would thus be obtained for lower w_0's. This explains the size of the reverse micelles and nanoparticles formed and also the cloudiness observed in the microemulsions.

(a)

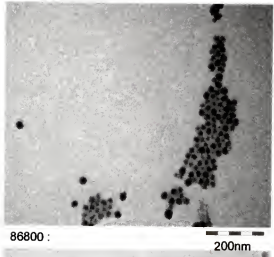

(b)

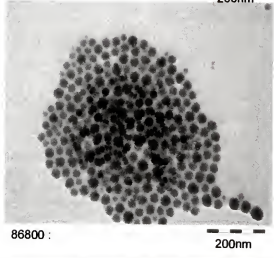

(c)

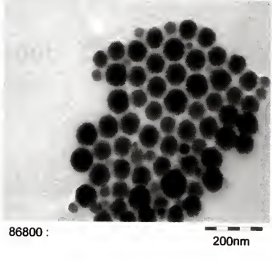

Figure 2-4. TEM Images of nanoparticles in Igepal CO-520 with different w_0's. (a) w_0=10, (b) w_0=5, (c) w_0=2. The reaction time for all is 3 hours. Scale bars are 200 nm.

Optical properties. RuBpy (Figure 2-5) is an inorganic luminophore whose optical properties are based on metal-to-ligand charge transfer. The metal donor in this case is the ruthenium and the ligands are the bipyridine moieties. The spectroscopic properties of the pure dye, RuBpy, were evaluated by obtaining the excitation spectra as well as emission spectra. The obtained spectra were compared to those of the dye-doped nanoparticles. In addition, the fluorescence signal of the dye-doped nanoparticles and the pure dye were separately monitored over a certain period of time. The results gave a comparison of the photostabilities of the samples.

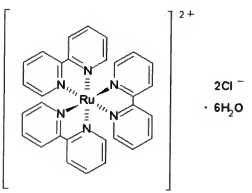

Figure 2-5. Chemical structure of RuBpy.

The excitation and the emission spectra of the pure RuBpy and dye-doped nanoparticles were measured in aqueous solution. Pure RuBpy shows emission at 594 nm when excited at the 458 nm excitation band maxima in aqueous solution. The excitation spectra remained the same for the pure RuBpy and dye-doped nanoparticles in the aqueous solution, but the emission band maximum of the nanoparticles shifted by 7 nm towards the longer wavelength when compared with the pure RuBpy luminophore

(Figure 2-6). This can be explained as an effect of the localization of the dye. Since the change was only very slight (~7 nm), this could indicate that there was not much conformational or structural change in the dye, if any. Since the RuBpy complex was trapped due to the electrostatic interaction between ruthenium ion and the partially negative oxygen of the silica, this could be the possible phenomenon that affected the shift in the emission [18].

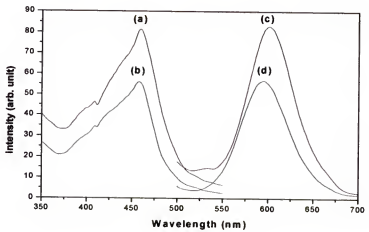

Figure 2-6. Luminescence excitation (left panel) and emission spectra (right panel). [(a) and (c)]for the dye-doped nanoparticles and the [(b) and (d)] for pure RuBpy. [18].

RuBpy has a lifetime longer than most organic fluorophores but it is also known to be a photosensitive compound. It can easily get quenched by oxygen. In a set of experiments, the emission intensities of RuBpy, RuBpy-doped nanoparticles, and Rhodamine 6G in aqueous solutions were monitored. The intensities were measured over a certain period of time. The photostability of the samples were observed in both the solution phase and the solid phase. The samples were either suspended in aqueous solution or dispersed in a thin film of polymethylmethacrylate (PMMA). These experiments were done to test the photostability of the dye-doped nanoparticles when

they are exposed to an aqueous environment for biological applications. The results from solution studies showed that there was basically no photobleaching for the nanoparticles over a long period of continuous intensive excitation with a 150-watt xenon lamp. The results were compared to that of rhodamine 6G (Rh6G) aqueous solution. An aliquot of the sample solution (200 µl) was taken in a cuvette and the spectrofluorometer was used for this experiment. For this experiment, emission spectra were recorded on a Perkin Elmer Spectrofluorometer, model LS50B. With this set-up, no noticeable photobleaching was observed (Figure 2-7) for dye-doped nanoparticles in solution for a period of one hour. However, a slight decrease in fluorescence intensity was observed for RuBpy, while a significant decrease was observed for Rh6G molecules. It is worth noting that in the solution phase photobleaching experiment, the luminophore-doped nanoparticles kept moving due to Brownian motion. Therefore, the particles were not continuously exposed to the excitation source.

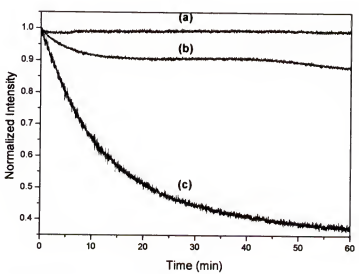

Figure 2-7. Photobleaching experiment: (a) dye-doped nanoparticles, (b) pure RuBpy and (c) rhodamine 6G (Rh6G), all in solution phase with a 150 W xenon lamp excitation source. Experiments were done on a spectrofluorometer. [18].

To test the photobleaching property in a more rigid situation, the nanoparticles were immobilized on PMMA films. The luminophores on the PMMA solid matrix were continuously exposed to optical excitation. A thin film sample doped with the nanoparticles was prepared on a microscope cover slip. A 0.1 % PMMA solution in toluene was used to prepare the thin film matrix by spin coating. The cover slip with the thin film sample was then mounted over the microscope stage with the laser excitation (a focused 500 mW argon laser, 488 nm, in the visible range was used with the appropriate filters, 575 nm long pass filter and 610 nm band pass filter for emission). Fluorescence emissions were monitored using an Olympus IX70 Microscope. Photobleaching for all the samples tested were observed as shown in Figure 2-8. As expected, photobleaching was much more severe for Rh6G (Figure 2-8a) when compared to both pure RuBpy (Figure 2-8b) and dye-doped nanoparticles (Figure 2-8c). Compared to the results obtained in Figure 2-7, photobleaching is more severe for all samples. This is explained by the continuous excitation of the same molecules for the whole duration of the experiment. This is quite different from the solution experiment where the molecules were free to move and the probability of the same molecules being excited all throughout is less than one.

It is believed that the RuBpy luminophores were not immune from photobleaching under intense excitation by a focused laser beam even when doped inside the nanoparticles. There are two possibilities for this photobleaching in the solid state. One is minute amount of oxygen penetration into the silica network and the other is the presence of some luminophores close to the silica particle surface. Since the surface

area/volume ratio is quite high for the nanoparticles, there might be a significant number of dye molecules on the surface. In both cases, additional silica coating on the nanoparticle surface would be a reasonable solution to minimize photobleaching of the luminophores. A second coating of pure silica was applied to the dye-doped nanoparticles expecting that further silica coating would completely prevent oxygen molecule penetration to the top surface and hence the photobleaching. These particles were synthesized and then used in photobleaching experiment. As shown in Figure 2-8d, it was demonstrated that post silica coated dye-doped nanoparticles nanoparticles were more photostable. There was no photobleaching observed over a long period of intensive laser excitation. This observation, therefore, suggests that further silica coating completely isolates the dye molecules from the outside environment thus preventing oxygen molecule penetration. The thickness of the post coating could be as thin as a few nanometers.

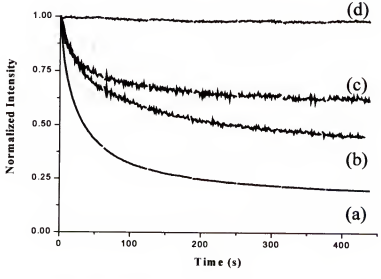

Figure 2-8. Photobleaching experiment: (a) pure Rh6G, (b) pure RuBpy, (c) dye-doped nanoparticles, (d) post silica coated dye-doped nanoparticles, all dispersed on a thin film of PMMA with excitation from a focused laser beam of a 0.503 W argon laser.

Luminescence signal was collected by an intensified charge coupled device (ICCD) camera coupled with a fluorescence microscope. [18].

Ru/Nanoparticle Ratio Calculation. The number of dye molecules per nanoparticle can give an indication of how much signal amplification a dye-doped nanoparticle-based bioanalysis could provide. To determine the number of ruthenium atoms present in each nanoparticle, the density of the dye-doped nanoparticles were determined. From the density measurements and the size information available from TEM and SEM images, the total number of particles in a sample of known weight was calculated. Using samples of known concentration, the absolute number of ruthenium atoms per nanoparticle was calculated. In addition, the total number of luminescing molecules per particle was also determined. Schematic is shown in Figure 2-9.

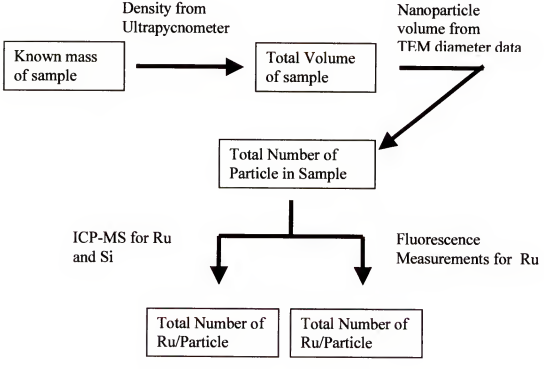

Figure 2-9. Schematic diagram for the calculation of number of Ru/particle.

For this experiment, known weights of vacuum-dried nanoparticle samples were subjected to density measurement using a nitrogen gas-based ultrapycnometer (Quantachrome 1000 Gas Ultrapycnometer). A sample of known mass was placed in the instrument in a cell with a known volume. Based on the gas law $P_1V_1=P_2V_2$, the volume of the sample was determined. This data was then subsequently used for density calculation. The density of each nanoparticle sample was measured 15 times and the first 5 were discarded. The remaining measurements were averaged and the results for all the samples are reported in Table 2-3. Using the known densities of the components of the dye-doped nanoparticles, the obtained densities were reasonable. The density for pure silica is 2.12 g/cc while that of ruthenium is 12 g/cc. Thus, it can be inferred that the nanoparticles may be porous but not at very high extent.

Table 2-3. Average densities and standard deviations in g/cc of nanoparticles prepared in different surfactants, reaction times, and water-to-surfactant molar ratios (w_0).

Sample	H3	H24
I10	3.73 $\pm$ 0.08	2.14 $\pm$ 0.02
I5	2.52 $\pm$ 0.02	2.44 $\pm$ 0.03
I2	3.92 $\pm$ 0.16	2.58 $\pm$ 0.07
T10	3.27 $\pm$ 0.06	2.48 $\pm$ 0.03
B10	2.94 $\pm$ 0.36	2.66 $\pm$ 0.03

Comparing the density values between the 3-hour (H3) nanoparticles and the 24-hour (H24) ones, it can be observed that there was a decrease in density in all samples. Figure 2-10 shows this information better. This suggests that the bulk of the dye molecules were trapped in the early stage of polymerization. As the polymerization progresses, the amount of dye molecules available for trapping was depleted thus less dye was doped on the newly polymerized surface. The decrease in the amount of dye trapped in the outer regions would lead to a lower density as shown in Figure 2-10.

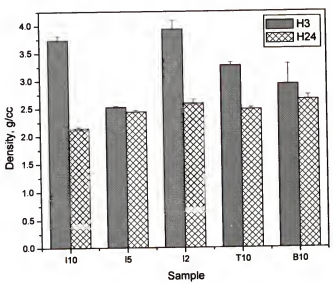

Figure 2-10. Density comparison of nanoparticles prepared in 3 hours (H3) and 24 hours (H24). Samples I10, I5, and I2 were prepared in Igepal CO-520 with w_0 of 10, 5, and 2, respectively. T10 was prepared in Triton X-100 and B10 in Brij-97, both with w_0 of 10.

The next set of information obtained for the determination of dye molecule/nanoparticle ratio was the amount of ruthenium atoms present per particle. Known amount of the samples were dissolved in hydrofluoric acid and later on in nitric acid. The resulting solutions were diluted to 50-ml volumes. Using ruthenium and silicon standards, calibration sets of solution were prepared in the same way as the nanoparticle

samples. Both the nanoparticle samples and the standard solutions were analyzed using Inductively Coupled Plasma Mass Spectrometry (ICP-MS). The results from the standard set were used to plot a calibration curve from which the actual concentrations of Si and Ru in the nanoparticle solutions were subsequently calculated. The results for the amount of Si (% Si) in the samples are shown in Figure 2-11. Similarly, the amounts of Ru (% Ru) in the nanoparticle solutions are shown in Figure 2-12.

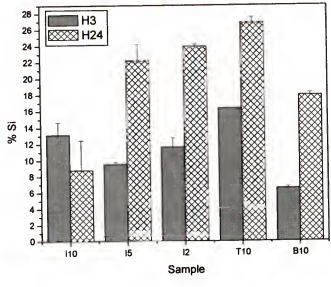

Figure 2-11. Percent Si (by ICP-MS) comparison of nanoparticles prepared in 3 hours (H3) and 24 hours (H24). Samples I10, I5, and I2 were prepared in Igepal CO-520 with w_0 of 10, 5, and 2, respectively. T10 was prepared in Triton X-100 and B10 in Brij-97, both with w_0 of 10.

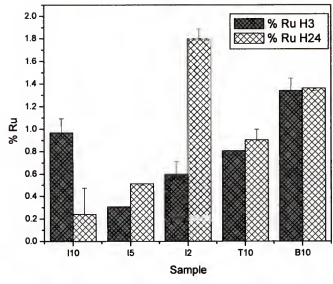

Figure 2-12. Percent Ru by (ICP-MS) comparison of nanoparticles prepared in 3 hours (H3) and 24 hours (H24). Samples I10, I5, and I2 were prepared in Igepal CO-520 with w_0 of 10, 5, and 2, respectively. T10 was prepared in Triton X-100 and B10 in Brij-97, both with w_0 of 10.

Both sets of information confirm the density information described previously. With the exception of sample I10, the percentage of silica in all the 3-hour nanoparticle samples were higher than those in the 24-hour ones. The data on ruthenium do not exactly reinforce such a claim when seen as differences in the concentration of Ru in the sample. Instead of a decrease, an increase is observed in the concentration of ruthenium atoms between the 3-hour nanoparticles and those of the 24-hour ones. However, the extent of increase in Ru was lower than in Si. This is shown by the data in Table 2-4. The amount of silica almost always doubled, an occurrence that was rare in the amount of Ru. Thus, it can be inferred that the current data validates the density data.

Table 2-4. Percent Si and percent Ru by ICP-MS of nanoparticles prepared in different surfactants, reaction times, and water-to-surfactant molar ratios (w_0).

Sample	% Si H3	% Si H24	% Ru H3	% Ru H24
I10	13.16	8.78	0.97	0.24
I5	9.49	22.20	0.31	0.51
I2	11.56	23.91	0.60	1.80
T10	16.29	26.83	0.81	0.90
B10	6.52	17.91	1.34	1.36

Samples I10, I5, and I2 were prepared in Igepal CO-520 with w_0 of 10, 5, and 2, respectively. T10 was prepared in Triton X-100 and B10 in Brij-97, both with w_0 of 10.

The ICP-MS data provided information on the absolute number of ruthenium atoms that might be present in each nanoparticle. An alternate method using fluorescence was also used to determine the number of Ru atoms. This method, instead of giving the absolute number of Ru atoms, supplied information on how many Ru atoms were effectively luminescing. Using spectrofluometry and fluorescence microscopy, the nanoparticle samples were analyzed. For spectrofluorometer measurements, sample solutions of known weights as well as standard solutions were prepared. The emission intensity at 605 nm was taken for all the solutions. Excitation was done at 454 nm. Based on a calibration curve using the data from the standard solutions, the number of Ru atoms

per particle was calculated. The data were compared to those obtained using ICP-MS (Table 2-5).

Table 2-5. Number of Ru atoms per nanoparticle by ICP-MS and fluorescence measurements (FM) of nanoparticles prepared in different surfactants, reaction times, and water-to-surfactant molar ratios (w_0).

Sample	ICP	FM
I10H3	1.07 E6	1.29 E4
I5H3	5.00 E5	9.14 E3
I2H3	5.72 E6	4.06 E5
T10H3	6.40 E6	5.24 E3
B10H3	6.23 E5	2.72 E4
I10H24	2.81 E5	1.22 E4
I5H24	2.61 E6	9.65 E4
I2H24	2.18 E7	5.62 E4
T10H24	2.78 E7	3.52 E5
B10H24	2.46 E6	1.56 E3

Samples I10, I5, and I2 were prepared in Igepal CO-520 with w_0 of 10, 5, and 2, respectively. T10 was prepared in Triton X-100 and B10 in Brij-97, both with w_0 of 10. H3 Samples were synthesized in 3 hours, H24 in 24 hours.

A closer look at the number of Ru atoms/ particle data reveals that there was a significant discrepancy between the ICP-MS data and the fluorescence data. This can be explained by the possibility that not all of the dye molecules trapped inside the nanoparticles were effectively excited. There are two possible reasons for this. One would be that the silica matrix and the overlying dye molecules prevent the rest of the luminophores from being exposed to the light of excitation. A second reason would be the possibility of self-quenching. At a very high concentration and highly localized condition, the tendency for the dye molecules to be in close proximity to each other is

very high. In cases like this that is similar to a very concentrated solution, the emission energy from one molecule is absorbed by the next molecule thus quenching the signal. These two reasons would thus explain the observed discrepancy. The number of effectively emitting dye molecules might be less than what is actually trapped in the nanoparticles, but the obtained values still show that signal amplification is possible. If these nanoparticles were used as probes in bioanalysis, each nanoparticle that would signal a single event would give off emission equivalent to at least a thousand individual probe dye molecules.

As described above, self-quenching can be an issue in dye-doped nanoparticles. In another experiment, self-quenching was also observed when different amounts of the dopant were used for the synthesis of dye-doped silica nanoparticles. Between the amounts 40 μL, 80 μL, 160 μL of the 0.1 M RuBpy used, the sample that had the highest fluorescence was the one with 80 μL [18]. There is therefore an optimum concentration of dopants that can be contained in a nanoparticle to give off the maximum emission signal. An increase in dye concentration does not necessarily mean that there is going to be an increase in fluorescence. As shown in Figure 2-13, fluorescence intensity decreases beyond the optimum concentration. Beyond such optimum, self-quenching becomes prominent and the fluorescence signal is reduced.

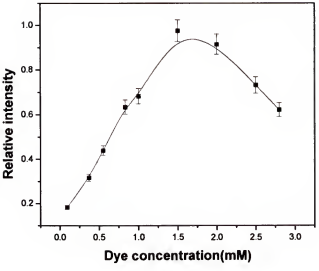

Figure 2-13. Fluorescence intensity vs. dye concentration.

Discussion

The synthesis procedure for dye-doped silica nanoparticles is affected by various factors. As have been shown by experimental results, reaction time, surfactant system, water-to-surfactant molar ratio, and amount of dopant have great influence on the final size and over-all characteristics of the resulting nanoparticles. These are the few variables that were studied but there are still other factors that may play influential roles on the formation of dye-doped nanoparticles. Some of these factors are the amount of silica precursor used, type of precursor used, and temperature at which the reaction is done. A systematic study addressing these factors might yield a more thorough understanding of the characteristics of resulting nanoparticles. In addition, generalized routes can be designed using the results from such a systematic study for the synthesis of specific types of nanoparticles. Nonetheless, the results that have been shown in this work can be used

as starting guide and complementary information for the evaluation of the factors necessary in the synthesis of dye-doped silica nanoparticles.

The factors that affect the formation of dye-doped silica nanoparticles were first studied in an attempt to create smaller and smaller but brighter particles. The first dye-doped silica nanoparticles that were made were about 60-70 nm. These particles were synthesized in Triton X-100 with w_0=10. It has been published that the size of the water pool is controlled by the water-to-surfactant molar ratio or w_0 [18]. Ideally, the synthesis of smaller particles is possible by reducing the w_0 value of the microemulsion system. This strategy was tried with the Triton X-100 but it was not successful. The microemulsion was cloudy, indicating that it was not stable when the w_0 used was less than 10. Since the goal was to have smaller particles, microemulsions with higher w_0 were not really studied. Instead the use of different surfactants was pursued. As discussed in the Results Section, such instability and cloudiness of the microemulsion can be attributed to the high hydrophobicity of the surfactant.

The surfactants that were used were all non-ionic like the Triton X-100. Brij-97 and Igepal CO-520 were both polyoxyethylene-containing substances. The difference between the three surfactants would be on the length of the hydrophobic tail or the presence or absence of an aromatic group. Since the resulting nanoparticles had different sizes when these three surfactants were used, it can be inferred that their structures affect the water pool size and the resulting nanoparticles. One possible reason is the varying degree of hydrophobicity of the surfactants. With Triton X-100 being the most hydrophobic, followed by the Igepal CO-520, and then by Brij-97, it can be deduced that the more hydrophobic surfactant produces the biggest particles. With higher

hydrophobicity, the surfactant molecules tend to have greater repulsion resulting to formation of bigger reverse micelles. Another behavior observed in the microemulsion systems containing Brij-97 and Igepal CO-520 was the possibility of having w_0 of less than 10. Such behavior can again be explained by the hydrophobicity. Igepal CO-520 and Brij-97 are not so hydrophobic that repulsion among surfactant molecules at lower w_0's is not so severe and formation of the small reverse micelles is possible. The microemulsions were quite stable and thus were used to make nanoparticles.

Microemulsions with w_0's equal to 5 and to 2 were prepared and nanoparticles were synthesized in them. The size of the nanoparticles changed with decreasing w_0. The expected trend, decreasing size with decreasing w_0, was observed in the Brij-97 system but not in the Igepal CO-520 system. The structure for the Igepal CO-520 was therefore playing a more important role than the change in w_0. As discussed earlier in the Results Section, increase in w_0 value resulted to increase in nanoparticle size from those prepared in Brij-97 system. It is believed that this is due to swelling caused by the increased amount of water available for each micelle [18, 55]. Nanoparticles obtained in Igepal CO-520 however decreased in size with increasing w_0. Since lower w_0 means there is a higher concentration of surfactant molecules, added to the fact that Igepal CO-520 is quite hydrophobic, bigger micelles would thus be formed. Consequently, bigger nanoparticles are obtained.

The reaction time allowed for the formation of the nanoparticle controls the final size as well as the brightness of the dye-doped silica nanoparticles. Shorter reaction time makes smaller particles and at the same time allows a high percentage of dopants to be incorporated into the matrix. A proper control of the reaction time can therefore yield to

a particular nanoparticle size with an optimum brightness. Note however that the amount of doped dye is not directly time-based. Based from the results obtained from ICP-MS and fluorescence studies, the amount of dye doped is dependent on the amount of silica present which in return was controlled by polymerization time.

A variable that has a direct impact on the over-all brightness of dye-doped nanoparticle is the amount of dye dopant used. It has been shown that increasing the amount of added dye does not necessarily increase the brightness of the resulting nanoparticle. Self-quenching can limit the brightness of nanoparticles depending on the final amount or concentration of doped dye [18].

Having evaluated some of the factors that affect the final size and the brightness of the nanoparticles, the general optical characteristics were also studied. The emission and excitation properties of the doped dye were compared to that of the free dye. A slight red shift in the emission spectrum of the doped dye was observed. The excitation spectrum was the same for the free dye and the doped dye.

Changes in the emission and excitation spectra might have been slight, but the photostabilities of the free dye and the doped dye were significantly different. The silica matrix was very effective in shielding the doped dye from photobleaching thus making the dye-doped nanoparticles almost impervious to photodegradation. A second coating of pure silica also made the surface-lying dye molecules immune to photobleaching.

A series of quantitation experiments was done to determine the dye to particle ratio in the synthesized nanoparticles. Density measurements were obtained to determine the volumes of samples with known weight. Using the diameters of the particles determined from TEM measurement, the volume of the individual nanoparticles were

calculated. This set of data and the volume of the weighed samples could yield information on the number of nanoparticles present in each sample. Such information became useful in determining the ruthenium atom/particle information after ICP-MS or fluorescence analyses.

Density measurements showed that the nanoparticles were more dense than pure silica but less dense than pure ruthenium. This result was expected since the materials obtained were composites of ruthenium, silica, and organic molecules. The lower density of the nanoparticles prepared in 24 hours compared to those obtained in 3 hours was however unforeseen. Two possible reasons might account for this phenomenon. One is that during the early stage of polymerization there is a high amount of ruthenium complexes available. As the reaction proceeds, depletion of the inorganic molecules led to fewer amounts being doped. A second possible reason for the lower density after a longer reaction time is the displacement of the bipyridine ligands by the coordination of oxygen atoms of the silica with the ruthenium ions. After a longer polymerization time, bigger particles were obtained with higher amount of silica. The probability of ligand displacement thus increases and even if ruthenium was still being doped, it was in the form of metal ion instead of a metal complex. The second reason also accounts for the increase in % Ru, however slight, after 24 hours of reaction. Since the density decreased and the particles got bigger with longer reaction time, it was expected that the % Ru would also decrease. Instead, an increase was observed. An increase in % Ru thus means that there was an increase in the amount of doped ruthenium and this is possible if more ruthenium ions instead of ruthenium complex molecules were being doped. This information might also explain why the fluorescence data was much lower than the ICP-

MS data in the determination of ruthenium/particle ratio. Aside from self-quenching that occurs among the highly localized ruthenium complex molecules, fluorescence was also greatly reduced by the displacement of the coordinated bipyridine ligands with the oxygen of the silica.

For the dye-doped silica nanoparticles to have an advantage over existing fluorescence probes in bioassays, it is not enough that they have excellent photostability. It would also be necessary that they are much brighter and that they can provide signal to even a low number of biochemical event. In a series of experiments, the brightness of nanoparticles was evaluated. The amount doped as well as the number of effectively fluorescing dye molecules in each nanoparticle was evaluated. Since the fluorescence results showed that at least a thousand molecules are contained in each nanoparticle, a minimum signal amplification of this magnitude can thus be expected when these dye-doped nanoparticles are used over fluorescent probes. Although the particular dye in this study, RuBpy, has a lower extinction coefficient than some organic fluorophores, there is a chance that each nanoparticle would still be brighter than a single organic fluorophore. In one hand, it is possible to apply the synthesis procedure employed here for the doping of dyes with higher extinction coefficient to maximize the signal amplification that can be obtained.

Conclusions

In an effort to make ultra-luminescent and highly photostable dye-doped silica nanoparticles, different synthesis parameters using reverse microemulsion system were evaluated. The parameters that have strong influence on the final size and brightness of the resulting nanoparticles were type of surfactant system, reaction time allowed for the

formation of particles, water-to-surfactant molar ratio, and amount of dopant used. Based on the results obtained, it can be inferred that these factors have significant effect on either the size and/or brightness of the resulting nanoparticles. The biggest particles obtained were from the Triton X-100 system, and the smallest were from the Brij-97 system. Water-to-surfactant molar ratio also had an influence on the final size of the nanoparticles obtained. Increasing the ratio had a corresponding effect on the Brij-97 system but had the opposite effect on the Igepal CO-520 system. The third factor evaluated was the reaction time for the formation of the nanoparticles. This factor had an effect on both the size and the brightness of the nanoparticles. Shorter time yields smaller particles with high percentage of dye molecules doped. The last factor evaluated was the amount of dye doped into the nanoparticles. Increasing the amount of dye did not necessarily increase the brightness of the nanoparticles. An optimum amount was needed to have the maximum luminescence on the nanoparticles. Beyond the optimum concentration, self-quenching becomes significant and it results to a decrease in the luminescence signal of the doped dye molecules. These data are supported by the quantitation experiments done on the nanoparticles. The absolute number of dye molecules contained was found to be much higher than the number that effectively luminesces. Taking all the information obtained, it is possible to synthesize dye-doped nanoparticles with different sizes and varying luminescence intensity. In addition, dye-doped nanoparticles have excellent photostability due to the silica matrix that acts as a shield. Thus, the synthesis of highly photostable dye-doped nanoparticles with varying sizes and luminescence for various bioanalytical applications is possible by manipulating the various synthesis parameters.

CHAPTER 3
SYNTHESIS AND CHARACTERIZATION OF ORGANIC DYE-DOPED SILICA NANOPARTICLES

INTRODUCTION

Luminescence techniques are highly and widely useful to detect events in many biochemical assays. For biochemical samples, signal measurement is often accomplished on a very small amount of sample containing limited number of optical signaling probes. The analysis of small volumes or small spatial areas can be a challenge, particularly for samples with low concentrations of analytes. Thus, highly fluorescent labels such as fluorescent organic molecules, quantum dots, and dye-doped nanoparticles are frequently used [41, 18, 55]. Of these, the dye-doped nanoparticles [18, 55] have great potential for biocompatible materials for signal amplification in bioanalysis due to the incorporation of a multitude dye molecules in each nanoparticle. In considerations of the number of dye molecules in each nanoparticle, each recognition event will bring in up to 10^3 dye molecules for signal transduction [18, 55]. In addition, the dye-doped nanoparticles have much-improved photostability due to the shielding by the silica matrix. Quantum dots are another recent development for luminescent biolabeling. They have very narrow emission bands and have been used successfully in a number of bioanalysis [15, 37, 52]. However, they are restricted by their low quantum yield and their compatibility with biomolecules in aqueous solutions. On the other side, organic fluorophores have been used extensively in bioimaging and bioanalysis [64, 65]. They have high quantum yield and excellent molar absorptivity. The major limitations for organic dye molecules are their rapid and

irreversible photobleaching. This gives rise to decreased analytical sensitivity and irreproducible measurements. These limitations of the organic fluorophores can be addressed by the dye-doped nanoparticles using the silica matrix as a protection layer for the incorporated dye molecules. In addition, current dye-doped nanoparticles mainly use inorganic luminescent materials such as ruthenium complexes whose intrinsic photostability is excellent.

Out of the many dye-doped nanoparticles, inorganic dye molecules such as tris(2,2'-bpyridyl) dichlororuthenium (II), or RuBpy [18, 55], and Eu(III) [43] have been used as dopants for the synthesis of luminescent nanoparticles. Ru(II)-doped [18, 55] and Eu(III) –doped [41] silica and polystyrene nanoparticles have been demonstrated to be effective optical reporters in biochemical analyses. Fluorescent latex nanobeads have also been used for DNA probing. Thousands of dye molecules are embedded in individual nanoparticles that give rise to reasonable signal amplification. In addition, the dye molecules are protected inside the matrix; hence, photobleaching as well as nonspecific luminescence are greatly reduced. However, inorganic dye molecules such as RuBpy [18, 55], and Eu(III) [43] have low intrinsic quantum yield and relatively low absorptivity. These limitations prevent inorganic molecule-doped nanoparticles from displaying the desired signal amplification for ultrasensitive analysis. On the other side, fluorescent organic molecules, having higher quantum yield and larger molar absorptivity, seem to be a better option for dye-doped nanoparticles for biolabeling and bioanalysis. Organic dyes such as rhodamine and fluorescein have been incorporated into polymer matrices such as polystyrene. The doping of these dyes in a silica matrix is, however, a challenge. The lack of a silica matrix in a polystyrene nanoparticle prevents easy and efficient

bioconjugation processes to link biomolecules with nanomaterials for biotechnology and biomedical applications.

In comparison to fluorescent organic molecules, metal complexes such as RuBpy are easily doped into silica matrix because of the charge interaction between the positively charged metal and the partially negatively charged silica. The synthesis can be done in a reverse microemulsion that yields monodisperse nanoparticles and at the same time allows control on the size nanoparticles [18, 55]. Using this method, various organic fluorophores were tried as dopants in a silica matrix. Fluorescein, tetramethylrhodamine, their dextran-conjugated forms, and rhodamine 6G were used. However, the doping of fluorescein, tetramethylrhodamine, and rhodamine 6G were unsuccessful. This could be attributed to the higher affinity of these organic dyes to the organic solvent than to the water pool inside the micelles. Hoping that larger molecules would be trapped better in the porous silica matrix, dextran-conjugated forms of fluorescein and tetramethylrhodamine were used. This set of experiment was more successful than the use of the unmodified fluorophores. Long-term immersion of the nanoparticles in solution however resulted to dye leakage. This indicates that the size of the dextran-conjugated dyes was not enough to keep them inside the silica matrix. Since this route of synthesis of organic dye-doped nanoparticles was not working, an alternative was sought.

An alternative to the reverse microemulsion system is the Stöber method. Hydrophilic dyes such as Nile Blue have been incorporated in silica matrices via this method to produce dye-doped microspheres [66]. The incorporation of hydrophobic dyes such as rhodamine 6G (Rh6G) and fluorescein in hydrophilic silica spheres could be

difficult. The dye molecules are most likely to dissolve in the organic solvent rather than get trapped inside the silica matrix due to the affinity bias. Both reverse microemulsion and Stöber method have been tried for the incorporation of Rh6G and fluorescein. The dye molecules are too hydrophobic to stay inside the matrix. For both methods, tetraethylorthosilicate (TEOS) was used as silica precursor. As an alternative precursor, relatively hydrophobic phenyltriethoxysilane (PTES) was used to trap the organic fluorophores. This method has been used for the synthesis of hydrophobic-dye-doped microspheres [60]. Although it was demonstrated that the resulting particles were in the micrometer range, the method could be adapted for the synthesis of organic dye-doped nanoparticles. The method could also be modified to contain TEOS to yield water-soluble particles.

Silica is a desirable matrix not only for its role in the dispersion of particles in water. More importantly, it can be modified to contain functional groups that will be useful for subsequent surface modification and/or biomolecule immobilization. Silica can be chemically modified to have an amine group, a carboxylic group, or even a thiol group. It can also be passively adsorbed with avidin for specific interaction with biotinylated biomolecules. With the aim of providing highly luminescent labels for bioanalytical applications, a new method was developed for the doping of organic dye molecules into a silica matrix for the preparation of Rh6G- doped silica nanoparticles. The feasibility of the conjugation between the nanoparticles and biomolecules was also demonstrated for applications in biosensors and bioanalysis.

Experimental Section

Materials. Tetraethylorthosilicate (TEOS), phenyltriethoxysilane and rhodamine 6G were purchased from Aldrich Chemical Co. Inc. (Milwaukee, WI). Fluorescein was obtained from Kodak Chemicals. Fluorescein-dextran and tetramethylrhodamine-dextran were purchased from Molecular Probes (Eugene, OR). Triton X-100 {polyoxyethylene(10)isooctylphenylether, 4-(C_8H_{17})C_6H_4(OCH_2CH_2)$_n$OH, n~10}, and n-hexanol were purchased from Aldrich Chemical Co. Inc. (Milwaukee, WI). Cyclohexane was obtained from Fischer Scientific Co. (Pittsburgh, PA). Distilled deionized water (EasyPure LF, Barnstead Co.) was used for the preparation of aqueous solutions.

Nanoparticle synthesis. Preliminary experiments on the doping of organic dyes in silica matrix were done in reverse microemulsion. Synthesis method is as described in the experimental section in Chapter 2. Instead of using RuBpy, however, the organic fluorophores fluorescein, rhodamine 6G, fluorescein-dextran, and tetramethylrhodamine-dextran were used.

To prepare the organic dye doped nanoparticles, the Stober process was adapted. The silica nanoparticle formation is a three-step process: (a) hydrolysis of the silica precursor such as TEOS or PTES to silanols, (b) polymerization, and (c) nanoparticle formation. For the preparation of the RH6G-doped nanoparticles, 3 ml of 1 mM solution of the dye in ethanol was mixed with 1.0 ml PTES. Hydrochloric acid or ammonium hydroxide was added to the resulting solution to start the hydrolysis of the PTES. The completion of the reaction is indicated by the formation of a one-phase system after a few hours. The 0.5 ml of the hydrolyzed solution was then added with 100 μL TEOS, dissolved to 5.0 ml with ethanol and further reacted with ammonium hydroxide via the

Stöber process. The reaction was done for an hour at 0°C with continuous sonication and frequent vortexing. Adding an excess amount of acetone to the mixture stopped nanoparticle formation.

Characterization. Size and morphology characterization were done using transmission electron microscopy (TEM, Hitachi H-7000) and scanning electron microscopy (SEM, Hitachi S-4000). Fluorescence measurements for the enzymatic reaction were taken using SPEX Fluorolog-2. Avidin-biotin binding experiments were done using an Olympus IX70 inverted fluorescence microscope for fluorescent imaging.

Surface modification. Nanoparticle modification with avidin was carried out by allowing the physical adsorption of avidin molecules (1 mg/ml in 10 mM phosphate buffer, pH 7.0) on cleaned glass silica surface. The avidin was then cross-linked with 1% glutaraldehyde in 100 mM phosphate buffer for an hour and then stored in Tris-HCl buffer (pH 7.5). Both nanoparticles and glass plate were coated with avidin with the same method. The coated glass plate was treated with two different concentrations of biotinylated bovine serum albumin (BSA). Each BSA molecule has 9 biotin molecules on average. Biotin-avidin interaction was checked by allowing the avidin-coated nanoparticles to bind with the available biotin molecules on the glass plate. The experiment was done under an Olympus fluorescence microscope where the 520 nm excitation and 550 nm emission of rhodamine 6G were utilized.

For bioconjugation with an enzyme, the nanoparticles were modified with 2% solution of an aminosilane, N^1-[3-(Trimethoxysilyl)propyl]diethylene triamine, in 1 mM acetic acid. The resulting nanoparticles were further treated with a bifunctional crosslinker, glutaric dialdehyde, before subsequent conjugation to an enzyme, glutamate

dehydrogenase (GDH) [19, 67]. Adequate washing was followed each step. The activity of the nanoparticle-conjugated enzyme was tested in the presence of the glutamate substrate and nicotinamide adenine dinucleotide (NAD^+). The reaction was monitored by observing the fluorescence of the newly produced NADH.

Results

Reverse microemulsion method. The doping of organic fluorophores was tried in reverse microemulsion system. The dyes that were tested were rhodamine 6G and fluorescein (structures shown in Figure 3-1). Negligible amounts of the dyes were found to have been trapped in the formed nanoparticles. Subsequent washing of the nanoparticles left them like pure silica nanoparticles. The difficulty of trapping the organic fluorophores could probably be attributed to the higher tendency of the dyes to dissolve in the organic phase rather than inside the reverse micelles where the polymerization would take place. In addition, the dye molecules have very small size. The small amount of dye dissolved in the water phase inside the reverse micelles were trapped in the silica matrix. Washing however removed the small amount of dye trapped.

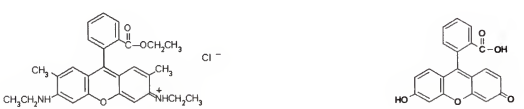

(a) (b)

Figure 3-1. Structures of rhodamine 6G (a) and fluorescein (b).

Fluorescein-doped nanoparticles were analyzed by measuring their fluorescence intensities using spectrofluorometer. By exciting the samples at 488 nm, emission signals

were obtained at 520 nm. The fluorescein suspensions were allowed to stand for 1 day after which they were centrifuged. The supernate was separated from the precipitate. The obtained precipitates were resuspended in the same volume of the original suspension. Emission signals of the samples were then taken. After 3 days the process was repeated and the emission data were compared (Figure 3-2).

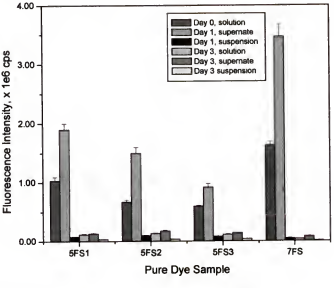

Figure 3-2. Fluorescence intensity comparison of fluorescein-doped silica nanoparticles. Samples were allowed to stand for 1 day and 3 days.

In an attempt to trap the organic fluorophores better, their dextran-conjugated forms now with much larger size were used. Dextran, a polymer with glucose subunits, is a much bigger molecule and it did help a little in trapping the organic dyes. This was shown by the fluorescence intensity of the dextran-conjugated organic fluorophore-doped nanoparticles. The nanoparticles were dispersed in water and their fluorescence intensities were recorded. The solutions were allowed to stand for 3 days, centrifuged, and decanted. The precipitates were resuspended in water again and their fluorescence measured. Results are shown in Figure 3-3. Significant amounts of dyes were trapped but

there were also significant losses over time. A better method was thus needed for the doping organic of fluorophores in silica matrix.

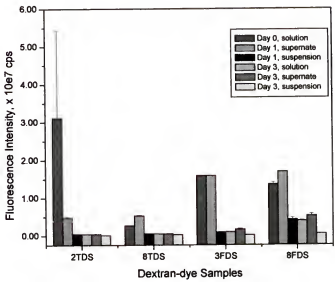

Figure 3-3. Fluorescence intensity comparison of fluorescein-dextran-doped silica nanoparticles. Samples were allowed to stand for 1 day and 3 days.

Stöber Method. The new method enabled the preparation of organic dye doped nanoparticles in the vicinity of 100-nm diameter. The newly synthesized nanoparticles were characterized by using Transmission Electron Microscopy (TEM) and Scanning Electron Microscopy (SEM), as shown in Figure 3-4. In the present state, the nanoparticles are not as monodisperse and uniform compared to those obtained from microemulsion method. It was observed that if the polymer formation was allowed to go on for more than 12 hours, larger particles were obtained in the micrometer range.

The amount of PTES was an important factor for the entrapment of Rh6G in the nanoparticles. An increase in the amount of PTES resulted in a corresponding increase in the amount of doped dye molecules. This can be seen in Figure 3-5 as an increase in the fluorescence intensity with increase in the amount of PTES. The data supports the

assumption that the driving force for the entrapment of the dye molecules is the affinity between the hydrophobic molecules of the dye and the PTES. Different PTES:TEOS volume ratios were tried, and there was a limiting ratio at which precipitate began to be formed. Fluorescence intensity comparison was done for samples with different PTES:TEOS ratios : (1SR1) 0.25:1, (1SR2) 0.5:1, and (1SR3) 1:1. Too high a concentration of PTES would yield nanoparticles with high hydrophobicity. A 2:1 or lower ratio was found to yield water-soluble nanoparticle products.

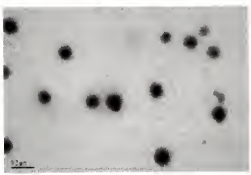

(a)

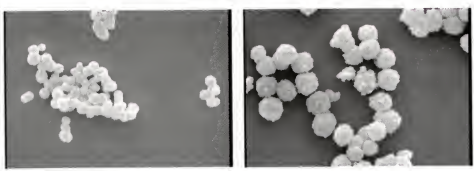

(b) (c)

Figure 3-4. Electron microscope images. (a) TEM and (b) SEM images of Rh6G doped nanoparticles allowed to hydrolyze and to polymerize for 12 hours. (c) SEM image of particles allowed to polymerize for 24 hours.

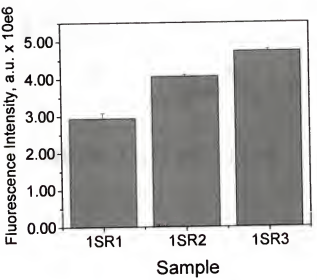

Figure 3-5. . Fluorescence intensity comparison of samples with different PTES:TEOS ratios : (1SR1) 0.25:1, (1SR2) 0.5:1, and (1SR3) 1:1). Increase in PTES allowed better trapping of Rh6G.

The effect of the concentration of Rh6G in the solution was tested by keeping the amount of PTES and TEOS constant. Increased fluorescence intensity was observed with increased nominal concentration of Rh6G. The fluorescence intensities of 1 mg samples dispersed in 1 ml solution were compared to various concentrations of pure Rh6G. The amounts of Rh6G trapped in the nanoparticles were calculated to be less than 1% based on a calibration curve established using pure Rh6G molecules. Even with only a 1% Rh6G concentration inside the nanoparticle, the nanoparticles showed higher luminescence intensity than RuBpy-doped nanoparticles, which optimally contains 20% of the dye [18, 55].

Once the dye molecules are trapped inside the silica matrix, the nanoparticles were washed with acetone and water. The doped dye molecules showed minimal leakage in aqueous solutions. Samples were immersed in solution for 3 days and the fluorescence of the solutions before (3o) and after centrifugation (3r) were compared (Figure 3-6). The

3-day aqueous solution was centrifuged to separate the dye-doped nanoparticles from the supernate that might contain dye molecules that leached out from the particles. After decanting the supernate, the precipitate was again resuspended in water to the original volume of the solution. Fluorescence intensities of the original solution (3o) and the resuspended precipitate (3r) were compared. No significant differences in the intensities were observed indicating that most of the dye molecules were kept trapped in the nanoparticles. The hydrophobic nature of the PTES made Rh6G kept in the matrix. The samples had decreasing TEOS: PTES ratio from samples 5SR1 to 5SR3. It can be observed that the higher the TEOS amount is in the particle, the greater is the tendency for the dye to be leached out. This is consistent with the results shown in Figure 3-5, where the higher concentrations of PTES made more Rh6G dye molecules trapped inside a nanoparticle.

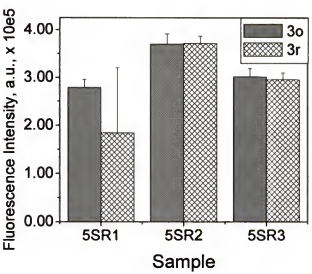

Figure 3-6. Comparison of fluorescence intensities of nanoparticles immersed in water for 3 days before (3o) and after (3r) centrifugation and re-suspension.

One of the major problems in using organic dye for bioanalysis is photobleaching, especially for surface studies such as biosensor development and cell membrane imaging. The newly synthesized nanoparticles provide the organic dye molecules a protection layer to minimize photobleaching. The photostability of the pure dye and the dye-doped nanoparticles were compared. The samples were continuously illuminated for 1000 seconds and the fluorescence intensities were monitored using solid-state spectrofluorometry. To minimize experimental instability, the samples were sandwiched between two coverslips for the monitoring. As shown in Figure 3-7, the intensity of the pure Rh6G was decreased rapidly, while the fluorescence intensity of the same Rh6G inside the nanoparticle was not changed significantly under the same conditions. The much-improved photostability of the organic dye in the nanoparticles would enable us to minimize photobleaching of bioassays and to improve the accuracy of bioanalysis.

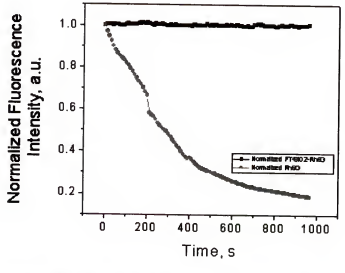

Figure 3-7. Photostability comparison of dye-doped nanoparticle and pure dye Rh6G.

To show the potentials for these nanoparticles in bioanalysis and biosensors, the nanoparticle was coated with avidin and allowed to bind with BSA linked biotin on a glass surface. This is like an enzyme-linked immunosorbent assay (ELISA); in this case the enzyme was replaced by the organic dye nanoparticle as the signaling element. Since thousands of dye molecules are contained in each nanoparticle, this assay was expected to have high sensitivity. As shown in Figure 3-8, the nanoparticles bound to the surface due to biotin-avidin binding were imaged. A greater amount of nanoparticles stayed on the glass surface containing the highest concentration of biotinylated BSA (2mg/ml) (Figure 3-9). There was almost nothing on the control glass that contained unmodified BSA. The result clearly showed that surface modified nanoparticles could be used as biosensors for bioanalysis. The nanoparticles could be used as a fluorescent signaling source as was shown here in the detection of biotinylated BSA. They could also be used for enzyme immobilization in enzymatic reaction for neurotransmitter analysis as shown below.

(a) (b) (c)

Figure 3-8. Bioassay for biotinylated BSA. Biotin interaction of avidin-modified nanoparticles : Fluorescence images of nanoparticles on the samples (a) treated with BSA, control; (b) 1mg/ml biotinylated BSA; and (c) 2mg/ml biotinylated BSA. All 3 images are in the same display range.

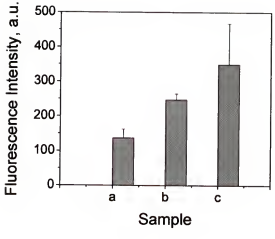

Figure 3-9. Quantitative representation of Figure 3-8.

To show the feasibility of using the Rh6G doped nanoparticles as biosensors for glutamate detection, the nanoparticles were tested by immobilizing an enzyme, glutamate dehydrogenase (GDH), onto the nanoparticle surfaces. GDH has been used in our lab for the monitoring of neurotransmitter glutamate release from living systems. We have used immobilized GDH for glutamate biosensor development [67]. Using an approach similar to glutamate biosensors [19,67], GDH molecules were immobilized onto the Rh6G doped nanoparticles. Once the GDH was immobilized, an enzymatic reaction, NAD^+ + glutamate→NADH + α-ketoglutarate, was used to test the activity of the GDH molecules on the nanoparticles. The fluorescence of NADH was monitored for the analysis of glutamate. As shown in Figure 3-10, the GDH molecule immobilized nanoparticles have adequate enzymatic activity. Their activity can be comparable with GDH biosensors based on pure silica nanoparticles [19]. This suggests that the Rh6G doped nanoparticles

could be further treated with biomolecules as the nanoparticle surface is silica. Therefore, a variety of nanoparticle-based biosensors could be prepared for different applications. With the Rh6G dye doped nanoparticles; the measurement of at least two different signals would be possible, one from the biosensing processes and the other from the Rh6G dye molecules inside the nanoparticles. This would serve well for ratiometric measurement for quantitation of the analytes.

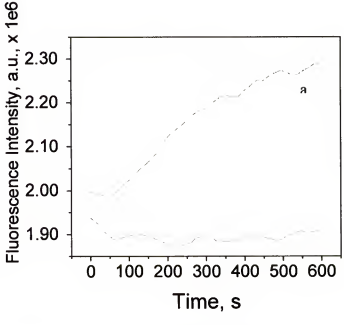

Figure 3-10. Nanoparticle biosensor for glutamate. NADH production, catalyzed by the GDH immobilized nanoparticles, was monitored over time with the following concentrations: (a) GDH-nanoparticle with 4 mM NAD^+ and 1 mM glutamate, (b) GDH-nanoparticle with NAD^+ only.

Discussion

Dye-doped silica nanoparticles have the potential to be very useful in bioanalyses due to their excellent photostability and high signal amplification. These characteristics

are attributed to the shielding provided by the silica matrix and the numerous dye molecules contained in each nanoparticle [18, 55]. The synthesis of these nanoparticles has been successful when inorganic dye molecules such as RuBpy were used [18, 55]. Such molecules are very hydrophilic and they have a very high tendency to stay inside the waterpool of the reverse micelles where silica polymerization would take place. During the polymerization process, these molecules get trapped in the silica matrix and remain there due to the electrostatic interaction between the positively charged metal cation and the partially negative oxygen of the silica matrix. The use of inorganic dye-doped silica nanoparticles for bioanalyses has one drawback. Inorganic dye molecules have inherently long lifetimes but they also have low molar absorptivity [55]. They are therefore not as bright as organic fluorophores. To have dye-doped silica nanoparticles that have excellent photostability with the highest signal amplification possible, it would be ideal then to use organic fluorophores instead of the inorganic dyes.

The doping of the organic fluorophores rhodamine 6G and fluorescein in silica matrix using reverse microemulsion were tried. These fluorophores have higher affinity to the organic solvent than to the waterpool, thus the possibility for them to get trapped during the silica polymerization was greatly reduced. The small amount of dye trapped in the nanoparticle was still hydrophobic and was easily removed during the washing step. Based on the results presented in Figure 3-2, it can be observed that the fluorescence intensities of the supernates removed after 1 day were consistently higher than those of the original suspensions. This is a proof that the dye molecules leached out from the nanoparticles. The fluorescence signal increased because the dye molecules are now in less localized environment, thus self-quenching has been greatly reduced. This

assumption is supported by the now much lower intensity of the precipitate resuspended to the original volume.

The synthesis procedure was modified by using dextran-conjugated fluorophores. The much bigger size of the dextran polymer significantly improved the amount of dye doped in the silica matrix but it was not enough to prevent dye leakage during washing. This indicates that big size is not enough to trap dye molecules in a silica matrix. Strong intermolecular interaction is a better option to rely on when trapping dye molecules in silica. Comparing the results obtained for the fluorescein-dextran-doped nanoparticles from the fluorescein-doped ones (Figures 3-2 and 3-3), it can be observed that dye leakage was apparent in both samples. However, there is no increase in the intensity of the 1st day supernate of the fluorescein-dextran-doped silica nanoparticle samples. This phenomenon can be explained by the distribution of the fluorescein molecules in the dextran polymer. Since the dye molecules are distributed along the dextran polymer chain, the tendency for self-quenching is minimized. Thus when the fluorescein-dextran or fluorescein molecules leak out of the nanoparticles, no increase in fluorescence signal due to decreased self-quenching is observed.

An alternative synthesis method to dope organic fluorophores in silica was designed based on the hydrophobicity of the molecules. In this method, the Stöber process was adapted. Since the medium for this reaction consists mostly of ethanol, ammonia, and water, organic fluorophores would localize in the presence of nonpolar molecules. To take advantage of this possibility, a mixture of two silica precursors were used. Tetraethylorthosilicate (TEOS) was used to obtain water-soluble nanoparticles and phenyltriethoxysilane (PTES) was added to have a hydrophobic portion in the

nanoparticles for the organic fluorophores to cling to. This method proved to be successful in trapping rhodamine 6G molecules in a silica matrix polymerized from TEOS and PTES [58].

The potential of the organic dye-doped nanoparticles in bioanalyses was demonstrated when used in a sandwich assay for the detection of protein [56]. The assay described for biotinylated BSA assay might not be the most precise method available for this type of protein but it does clearly demonstrate that dye-doped nanoparticles have the capability to be conjugated to biomolecules for subsequent bioanalysis. The assay can be refined further to give highly precise results.

Another application demonstration that may show the versatility of the dye-doped nanoparticle is their use in enzyme-based detection [58]. The assay demonstrated that enzymes can be immobilized on the nanoparticles and that enzymatic activity is maintained in the process. Since the goal for this demonstration was to show that the nanoparticles can be immobilized with enzymes and that they can be used for enzyme-based detection, the assay was not optimized to detect very low analyte concentrations.

In this work, the synthesis and bioanalytical applications of the obtained nanoparticles were shown. Again, it was proved that the nanoparticles could become useful in bionalyses.

Conclusions

In summary, organic dye molecules such as Rh6G can be trapped inside silica nanoparticles by using hydrophobic silica precursor such as PTES. This precursor can be blended with TEOS to yield nanoparticles that can be dispersed in water. Organic dye doped nanoparticles in the nanometer range can be obtained by controlling the

polymerization time. Nanoparticles obtained through this method exhibit minimal dye leakage and excellent photostability. The dye nanoparticles are highly fluorescent. The bioconjugation capability of the newly prepared organic dye nanoparticle was also demonstrated, indicating that the silica surface is available for bio-functionalization of the nanoparticles for bioanalysis and biosensor applications. It was also demonstrated that the Rh6G doped nanoparticles could be used for a sandwich or ELISA-like assay in BSA determination and for biosensors in glutamate analysis. A simple method was thus developed for the entrapment of highly fluorescent organic molecules inside silica nanoparticles for efficient bioassays without photobleaching.

CHAPTER 4
SYNTHESIS AND CHARACTERIZATION OF MAGNETIC NANOPARTICLES

Introduction

The synthesis of ultra-small magnetic nanoparticles with uniform size distribution is very important because of their wide applications in biology and medicine [68-76] e.g. magnetic resonance imaging (MRI) contrast agent [70, 73, 76], magnetic separation of oligonucleotides [74], cells and other biocomponents [74], magnetically-guided site specific drug delivery systems [70,71] etc. The industrial application of magnetic materials covers a broad range [77-82]. The strongly magnetizable fluids find numerous applications [77, 80-82] e.g. magnetic seals in motors and devices such as gas lasers, blowers, etc., lubricants and bearing in magnetic disk drive spindles, optical memory devices, magnetic inks for bank checks, magnetic refrigeration units and an efficient material for magnetic recording media. Therefore, the synthesis of stable magnetic fluid with much higher saturation magnetization is very important and that can be achieved if particles are made uniform and very small in size. Pure magnetic particles themselves may not be very useful in practical applications because of the following limitations: (i) they tend to form large aggregates, (ii) their original structure may change if they are not stable enough resulting in the alteration of magnetic properties, (iii) they can undergo rapid biodegradation when directly exposed to the biological system. Therefore, a suitable coating is very necessary to prevent such limitations. To make a stable suspension of particles for practical applications, their dimension should be sufficiently

small so that precipitation due to gravitational forces could be avoided. To achieve this, particles should be made very uniform and ultra-small (<5 nm in diameter). The basic need is, therefore, to synthesize ultra-small, coated and uniform particles with strong magnetic properties for their practical applications.

Water-in-oil (W/O) microemulsion has been widely used in the synthesis of uniform-size nanoparticles of various kinds [83-86], including magnetic materials [87-91] and has become a powerful tool. This is an isotropic and thermodynamically stable single-phase system that consists of three components: water, oil and an amphiphilic molecule, called surfactant. The surfactant molecule lowers the interfacial tension between water and oil resulting in the formation of a transparent solution. The water nanodroplets present in the bulk oil phase serve as a nanoreactor for the synthesis of nanoparticles of different kind of materials. The shape of the water pool is spherical. The size of the water pool greatly influences the size of the nanoparticles. Thus the size of the spherical nanoparticles can be controlled and tuned by changing the size of the water pool (w_0 value, the water-to-surfactant molar ratio).

In an effort to make ultra-small, coated and uniform size magnetic nanoparticles, W/O microemulsion-mediated sonochemical synthesis was used [78-79] to make superparamagnetic iron oxide nanoparticles in non-ionic surfactants using two different inorganic bases. These nanoparticles are also coated with a thin layer of silica [92-94] to protect the core. Particles so obtained have diameters as small as 1-2 nm and the thickness of the silica coating is as thin as 1-2 nm. Three different types of non-ionic surfactants (Brij-97, Triton X-100, Igepal CO-520) were used for the preparation of microemulsions and differences with respect to the particle size and their magnetic

properties were observed. The effect of surfactants on the particle size and uniformity is discussed in detail for both coated and non-coated particles. Following the microemulsion route, iron oxide nanoparticles are synthesized first by the co-precipitation of iron salts (ferrous and ferric) with the inorganic base (aqueous NaOH or NH_4OH solution). The effect of two different basic solutions on the particle formation is also discussed. The addition of TEOS directly to the microemulsion containing excess base undergoes hydrolysis and polymerization reaction [58, 95]. This reaction rate is much slower in microemulsion in comparison to the bulk aqueous solution. Therefore, with time, as the polymerization reaction goes on, a thin layer of uniform silica coating is formed surrounding each nanoparticle. This coating protects the core magnetite nanoparticles from possible degradation influenced by the outside environment. The outer silica surface is biocompatible and functionalizable. The surface chemistry of the silica surface is simple and can be modified in various ways. To protect agglomeration of particles the silica surface can be covalently modified into a neutral or charged surface.

Experimental Section

Materials. Chemicals were purchased from commercial sources. They were reagent grade of high purity and used as received. Iron (III) chloride, iron (II) sulphate, hexane, Triton X-100 {polyoxyethylene(10)isooctylphenylether, 4-$(C_8H_{17})C_6H_{10}(OCH_2CH_2)_nOH$, n~10}, Brij-97 {polyoxyethylene(10)oleylether, $C_{18}H_{35}(OCH_2CH_2)_nOH$, n~10}, Igepal CO-520 {polyoxyethylene(5)nonylphenylether, 4-$(C_9H_{19})C_6H_4(OCH_2CH_2)_nOH$, n~12} and tetraethylorthosilicate were purchased from Aldrich Chemical Co. Inc. (Milwaukee, WI). Cyclohexane, n-heptane, n-hexanol, sodium hydroxide, ammonium hydroxide (28-30 wt%) were obtained from Fischer Scientific Co.

(Pittsburgh, PA). Distilled deionized water (EasyPure) was used for the preparation of all aqueous solutions.

Ultrasonicator used for the synthesis of nanoparticles was purchased from Fischer Scientific Co. (Model number FS20).

Transmission electron microscopy (TEM) . Particle size has been characterized by a Hitachi H-7000 microscope (Japan). The maximum resolution of the instrument was 0.2 nm. TEM samples were prepared by placing a drop of microemulsion containing nanoparticles directly onto the carbon-coated copper grids. These grids were kept over the Kimwipes EX-L tissue papers to absorb excess microemulsion solution and then air-dried at room temperature for at least two days before taking images.

X-ray electron diffraction (XRD). The structure of the powder samples was measured by the Philips Electronic Instruments APD 3720 X-ray Diffractometer. The X-ray diffraction patterns were taken from 10 to 80 degree (2θ value) using Cu Kα radiation with an intensity ratio (α_2/α_1) = 0.5 and wavelengths of 1.54439 and 1.54056 Å, respectively.

Superconducting quantum interference device (SQUID) magnetometry. The magnetic properties of the nanoparticles were studied by a SQUID magnetometer (Quantum Design MPMS-5S). About 10 mg of sample in powder form was inserted in a gelatin capsule for the magnetic measurement at room temperature. Plots of magnetic moment versus applied magnetic field were obtained directly from the instrument. Field strength was varied in the range from –2.0 to 0.0 and 0.0 to +2.0 tesla (1 tesla = 10000 Oe) in each scan to get the hysteresis loop. Magnetic moment values were calibrated in terms of emu/g.

Synthesis of nanoparticles. Two separate microemulsions (ME1 and ME2) were prepared using each surfactant (see Table 4-1). The abbreviated terms B97, I520 and T100 refer to Brij-97, Igepal CO-520 and Triton X-100 surfactant containing microemulsions, respectively. ME1 contained the iron salts, $FeSO_4$ and $FeCl_3$, while ME2 had the base, either NaOH or NH_4OH. All aqueous solutions were prepared with deoxygenated water (nitrogen purged). Microemulsion is then placed in an ultrasonicator and magnetic stirrer was removed. ME2 was then added dropwise to ME1 using a glass syringe. Nitrogen gas was continuously purged during mixing and sonication when NaOH is used as a base. The resulting microemulsion was further sonicated for 2 hours. The formation of magnetic nanoparticles was visually realized by the appearance of deep brown color of the microemulsion mixture. The resultant fluid was then flocculated and washed several times with sufficient amount of ethanol (95%) and centrifuged. In each time of washing sonicator is used to completely disperse nanoparticles in ethanol. Surfactant molecules were almost completely removed during this process. Pure nanoparticles could then be collected either by magnetic separation directly from ethanolic dispersion or by centrifugation. The w_0 value was kept constant at 10 for all microemulsions. Silica coated particles were prepared following the similar way as the non-coated one with the exception that ME2 contained neat TEOS (Table 4-1). Also, ME2 was allowed to stir for an hour before it was added to ME1. Resultant silica coated magnetic nanoparticles were isolated after 24 hrs of aging.

With Brij-97, both microemulsion ME1 and ME2 were heated to 65^0 C in a water bath while stirring magnetically until a uniform single-phase solution resulted. Both ME1

and ME2 became cloudy upon addition of iron salts and base respectively. A complete transparent brown solution resulted when they were combined together at hot condition (65^0 C). Upon cooling, phase separation occurred with an appearance of a brown layer on top. This brown layer containing nanoparticles was collected by a separatory funnel. With Igepal CO-520 and Triton X-100, a transparent single-phase microemulsion always resulted at room temperature. For comparison, we have also made particles in deoxygenated pure water (bulk) using NaOH as a base.

Table 4-1. Reagents for the preparation of magnetic nanoparticles [54].

Micro-Emul-sion	Surfac-tant	Solvent (oil)	Co-Sur-factant	Water (nitro-gen purged)	$FeCl_3$ (0.15 M)	$FeCl_2$ (0.1 M)	NaOH (2.0 M)	NH_4OH (28-30 wt %)	TEOS (Neat)
B97	Brij-97	Cyclohexane							
ME1	3.5 g	45.6 ml	-	284.8 µl	300 µl	300 µl	-	-	10 µl
ME2	2.8 g	36.5 ml		354.0 µl	-	-	354 µl	354 µl	10 µl
I520	Igepal CO-520	n-Heptane							
ME1	7.6 g	20.0 ml	-	2.6 ml	500 µl	500 µl	-	-	10 µl
ME2	7.6 g	20.0 ml		2.6 ml	-	-	1.0 ml	1.0 ml	10 µl
T100	Triton X-100	Cyclohexanen-Hexanol							
ME1	5.3 ml	22.5 ml	5.4 ml	620 µl	500 µl	500 µl	-	-	10 µl
ME2	5.3 ml	22.5 ml	5.4 ml	810 µl	-	-	810 µl	810 µl	10 µl

Results

TEM measurements. TEM images of both non-coated and silica coated particles are shown in Figures 4-1, 4-2 and 4-3 for B97, I520 and T100, respectively. Most of the particles are aggregated and therefore, the determination of actual particle size becomes difficult.

B97

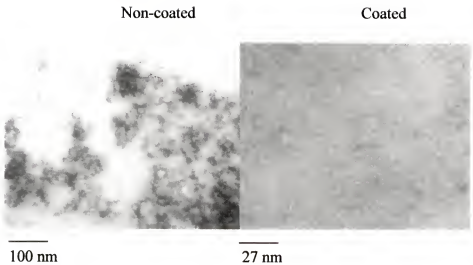

Figure 4-1. TEM images of non-coated (left panel) and coated (right panel) magnetic nanoparticles prepared in Brij-97 using NaOH [54].

I520

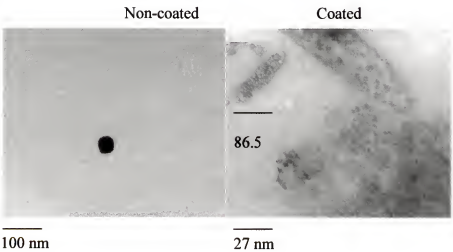

Figure 4-2. TEM images of non-coated (left panel) and coated (right panel) magnetic nanoparticles prepared in Igepal CO-520 using NaOH [54].

T100

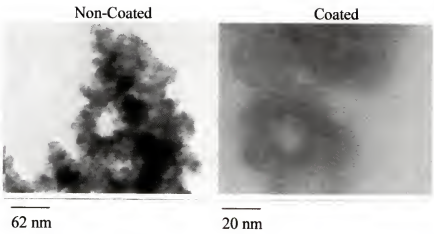

Figure 4-3. TEM images of non-coated (left panel) and coated (right panel) magnetic nanoparticles prepared in Triton X-100 using NaOH [54].

In Brij-97, non-coated particles are aggregated in two different fashions: hyper-branched and acicular- (ellipsoidal-) shaped structures irrespective of the nature of base used. The size of individual particles is about 1-2 nm (ultra-small). Because of their ultra-small size, the actual diameter of each particle and hence the particle size distribution were difficult to measure precisely. An approximate measurement of the size distribution is done and the percentage standard deviation is found to be less than 10% (uniform). The formation of hyper-branched structure is associated with the wire-like lining up of particles. In the acicular shaped structure, particles are not densely packed, rather, they are arranged in such a way that it creates uniform pores. They can be better identified as sieves (Figure 4-1). Some acicular shaped aggregations consist of uniformly spaced parallel layers of particles along the minor axis. These structural features get completely lost when they are coated with the silica. Monodisperse silica coated particles

of very uniform size (3-4 nm) are obtained when NaOH is used as a base. In NH_4OH, coated particles of uniform size (3-4 nm) tend to aggregate further to form spherical structure as if magnetic nanoparticles are doped inside the silica network.

In Igepal CO-520, particles are found less aggregated when NH_4OH is used. Their size ranges between 4 to 5 nm and interestingly, when they are coated with silica, particles aggregate to form tubule structure as long as 350 nm. The diameter of these nanotubes is very uniform (about 25 nm). Using NaOH, aggregated particles so obtained are mostly spherical composed of many small particles of 2-3 nm size. The typical size of spheres is 22±3 nm. When they are coated with silica, aggregated particles still retain their spherical shape with a very thin layer (1-2 nm) of coating and they remain well dispersed. Additionally, the formation of acicular shaped aggregation, as long as 400 nm, is also seen. The pattern of the interior of the acicular shaped structure is observed very similar to that obtained in Brij-97.

In Triton X-100, particles are again very uniform and small (1-2 nm) but they are aggregated. The aggregation pattern in NH_4OH is similar to that obtained in Brij-97. However, no acicular shaped structures are seen, rather, about 10% of particles are observed to be aggregated in a non-uniform and compact spherical fashion. Particles synthesized using NaOH have sponge-like porous structure that consists of small particles of about 2-3 nm sizes. The aggregation pattern in Triton X-100 does not change when particles are silica coated. Particles synthesized in pure deoxygenated water show extremely non-uniform, irregular shaped. They are mostly obtained in the form of large aggregates, as expected (Figure 4-4).

Figure 4-4. TEM image of bulk magnetic particles. Bulk magnetic nanoparticles were prepared in aqueous solution [54].

XRD measurements. X-ray diffraction spectra of non-coated and coated particles synthesized in microemulsions are shown in Figure 4-5 and they are compared with the same material prepared in the bulk water phase. From the Figure 4-5, it is clearly seen that particles synthesized from the microemulsions do not show any sharp diffraction peaks corresponding to the crystalline structure. Instead, a broad band appears in each spectrum. This observation is typical for amorphous materials and also for ultrasmall crystalline materials where diffraction peaks can not be well resolved. Although our bulk sample also does not show any sharp peak, still, diffraction peaks can be resolved. The diffraction pattern of our bulk magnetic sample is close to the standard pattern for crystalline magnetite (Fe_3O_4) or maghemite (γ-Fe_2O_3) or a mixture of both. Our experimental data can not clearly distinguish between these two types of iron oxides.

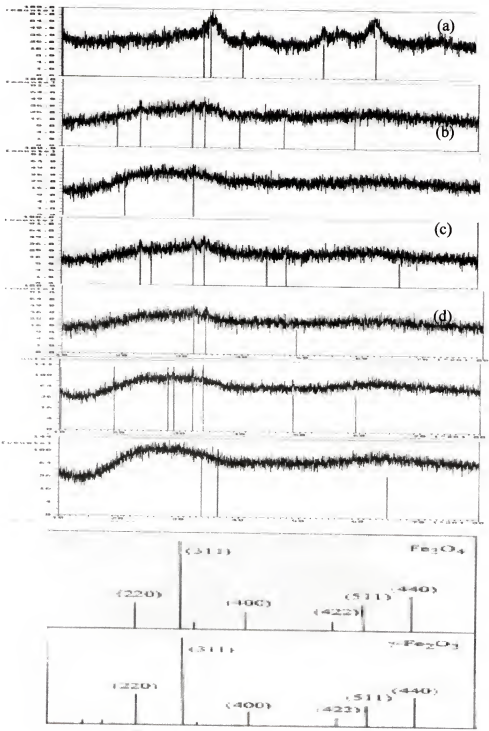

Figure 4-5. XRD diffractograms. Particles were prepared in (a) bulk, (b) Brij-97 usingNaOH, (c) Brij-97 using NH_4OH, (d), Triton X-100 using NaOH, (e) Triton X-100 using NH_4OH. Standard diffractograms for (e) Fe_3O_4 and (f) Fe_2O_3 [54].

However, we are not interested in identifying the specific form of iron oxide present because they have very similar magnetic properties. We have approximately calculated the relative broadness of the most intense diffraction peak (main diffraction line of the standard sample for magnetite, 311 peak) of the spectra for both coated and non-coated samples synthesized in microemulsions and compared with the bulk sample (See Table 4-2). The maximum broadness appears for the non-coated particles synthesized in Brij-97 using NH_4OH and minimum in the bulk sample.

SQUID measurements. The value of coercivity (coercive force, Oe), magnetization (magnetic moments, emu/g) with respect to the external magnetic field at 10 and 20 K Oe are compiled in Table 4-2 for particles synthesized in microemulsions as well as in the bulk water. Coercivity is described to be the amount of field necessary to "coerce" the material back to zero induction. Room temperature magnetization curves are shown in Figures 4-6 and 4-7 for non-coated and silica coated particles respectively. Figure 4-8 shows the magnetization curve for the bulk sample. The applied magnetic fields are not corrected for demagnetization effects. The inset of each plot represents the presence of hysteresis loop. Results thus obtained from SQUID magnetometric measurement show a very good correlation with that of TEM and XRD measurements (see discussion section). Hysteresis is observed for all samples except the non-coated one synthesized in Igepal CO-520 using NaOH as a base. At room temperature, no saturation of magnetization is observed when the applied field is increased up to the value of 20 K Oe for all samples. The magnetic moment value for the non-coated sample is always higher than that of the coated sample. As expected, much higher value of magnetic moment (about 25 times at 10 K Oe) is observed for the bulk sample when compared

with the samples synthesized via microemulsion route. The nature of the magnetization curve for the coated particles is very similar. The increase in the magnetic moment value with the applied field follows nonlinear fashion and therefore, a point of intersection is always obtained at about 1.2 K Oe. No such intersection point is observed for the non-coated particles synthesized in Igepal CO-520 and Triton X-100 but the same is observed in Brij-97. The magnetization curve for the bulk sample becomes flat at 20 K Oe although saturation magnetization value has not yet been reached. The behavior of the coated particle synthesized in Brij-97 is close to the bulk sample.

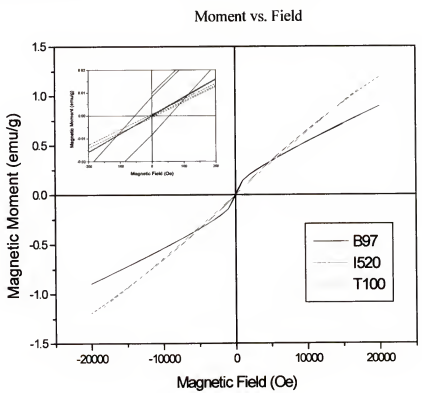

Figure 4-6. Magnetization curve for non-coated particles prepared in microemulsions using Brij-97, Igepal Co-520, and Triton X-100 [54].

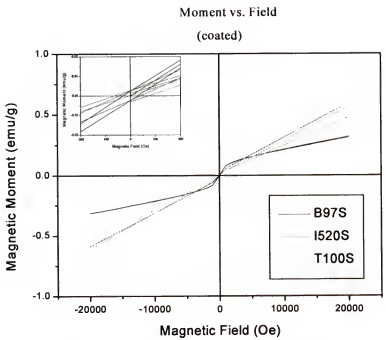

Figure 4-7. Magnetization curve for silica-coated particles prepared in microemulsions using Brij-97, Igepal Co-520, and Triton X-100 [54].

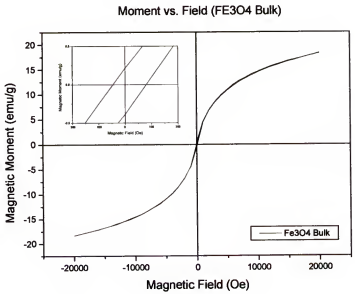

Figure 4-8. Magnetization curve for bulk material [54].

Discussion

The water-in-oil microemulsion has been prepared using nonionic surfactants. The water nanodroplets (nanoreactor) containing reagents undergo rapid coalescence that allow mixing, precipitation reaction and aggregation process for the synthesis of magnetic nanoparticles. The nanoreactor water pool is spherical in shape and surfactant molecules surround the nanodroplet wall. These walls act as cages for the growing particles and thereby reduce the average size of the particles during collision and aggregation process. In the present study we have observed very clearly that nonionic surfactants affect the particle size and the aggregation process. We believe that the formation of particles is first accompanied by very fast precipitation reaction and aggregation process. The nascent particles so formed are spherical in shape. They are very uniform (percentage standard deviation is less than 10%) and ultrasmall (<5 nm in diameter) as shown in TEM images in Figure 4-1, 4-2 and 4-3 and also from TEM data compiled in Table 4-2.

In the next step, interparticle collisions occur under the influence of ultrasonication which lead to the agglomeration, changing the morphology of the particles [96]. This agglomeration process facilitates the preferential adsorption of the surfactant molecules on to the particle's surface. Nonionic surfactants consist of polyoxyethylene moiety with a terminal hydroxyl group as a polar part and a long hydrocarbon chain as a tail part. It is thus very reasonable that the terminal hydroxyl group will interact by a weak hydrogen bonding force with the oxygen atoms present on the particle surface. The tail part, thus, will be away from the particle surface. The preferential surfactant adsorption restricts the sideways interconnection of the particles

and allows further aggregation process in an ordered fashion. During this process, hydrophobic tails of the surfactants remain parallel and interact with each other to stabilize the system and finally acicular particles are formed. Depending on the chemical structure of the surfactant molecules, the extent of surfactant molecule adsorption on to the surface of the nanoparticle varies. Looking at the structure of nonionic surfactants (see materials and methods section), it appears very clear that Brij 97 surfactant has longer hydrophobic chain (oleyl group) when compared to Igepal CO-520 (nonylphenyl group) and Triton X-100 (isooctylphenyl group). It is, therefore, expected that there will be strong hydrophobic-hydrophobic interaction between oleyl groups attached to adjacent nanoparticles. This could be the reason why we have observed more ordered fashion in particle aggregation in case of Brij 97 when compared to other surfactants. When coated with silica, the extent of surfactant molecule adsorption onto the silica surface is less compared to the bare particles resulting in the formation of more discrete particles. Also the ultrasound radiation generated from the ultrasonicator affects the adsorption process. This could be the reason why particles synthesized using different surfactants had different morphology. The formation of spherical particle occurs at the very first step of aggregation. Depending on the nature of surfactant molecules and their adsorption capabilities, individual spherical particle can further aggregate to form tube-like structure. We have observed this phenomenon in Igepal CO-520 during the silica coating process with NaOH. The hydrolysis and polymerization reaction by NH_4OH generally form stable spherical particles [95], that too was observed in Igepal CO-520. The magnetic dipole-dipole interaction sometimes plays also an important role in forming elongated

particles [97]. The use of strong base for the precipitation reaction of iron salts can also affect the particle morphology.

Table 4-2. Size of magnetic nanoparticles based on TEM [54].

Sample		TEM (particle size in nm)	XRD (peak broadness in mm)	SQUID		
				Magnetic Moment		Coercevity Field (in Oe)
				10 KOe	20 Koe	
Bulk (Non-coated)			9 ± 4	14.6	18.3	309.5
B97						
NaOH	Coated	2.5 ± 1	27 ± 4	0.212	0.311	27.4
	Non-coated	2 ± 1		0.540	0.896	52.9
NH_4OH	Coated	2 ± 1	40 ± 4			
	Non-coated	2 ± 1				
I520						
NaOH	Coated	2.5 ± 1		0.352	0.688	42.2
	Non-coated	22 ± 3		0.650	1.190	0
NH_4OH	Coated	9 ± 4		0.246	0.474	36.1
	Non-coated	4 ± 2		0.437	0.852	37.5
T100						
NaOH	Coated	2.5 ± 0.5	22 ± 4	0.286	0.555	63.7
	Non-coated	3 ± 1		0.636	1.22	5.9
NH_4OH	Coated	6.5 ± 1.5	21 ± 4			
	Non-coated	4 ± 1				

In the presence of strong base, the total ionic strength of the water pool increases. This causes instability of the microemulsion system resulting in the appearance of slight cloudiness. Therefore, particles formed in this medium should have different morphology when compared to that using mild base. In the experiment, very small amount of base was used that was sufficient for the precipitation reaction (non-coated) followed by the polymerization reaction of TEOS (silica-coated, Stober's synthesis) [58,95]. No major difference was observed in particle morphology using strong base and mild base. TEM results compiled in Table 4-2 clearly show that the present method has certainly produced very uniform and ultrasmall magnetic particles with and without silica coating.

The absence of sharp peak in the X-ray electron diffraction spectra (Figure 4-5) does not necessarily mean that magnetite particles so prepared by the microemulsion method are all amorphous. It is well known that the broadness of the peak increases with the decrease in the particle size [87]. Therefore, they might be crystalline, just for their ultrasmall size, diffraction peaks are not well defined. Table 4-2 shows that there exists a good correlation between the particle size (TEM data) and the peak broadening (XRD data). The maximum broadness appears for the non-coated particles synthesized in Brij-97 using NH_4OH that agrees with TEM results that particles are made very small (1-2 nm). The magnetic particles prepared in the bulk water phase did not show very sharp peak confirming that particles are poorly crystalline.

The magnetization of ferromagnetic materials is very sensitive to the size and structure of the sample. If a sample consists of small particles, its total magnetization (magnetization per unit volume) decreases with the particle size when compared to the large particles at a certain applied field. This is due to increasing dispersion on the

exchange integral that causes small particles to finally reach a superparamagnetic state with reduced exchange interaction between the particles [97,98]. It is also known that below some critical size (<10 nm) magnetic particles become single domain due to the interplay between the energy of dipole fields and domain wall creation [81, 99-101]. The lack of saturation in magnetization and the absence of hysteresis are the typical indication of superparamagnetic materials. Therefore, an assembly of single domain nanoparticles of ferromagnetic materials typically shows superparamagnetism. From the coercivity data (Table 4-2) and magnetization plot showing hysteresis (Figures 4-6, 4-7, 4-8) it is clearly revealed that non-coated nanoparticles synthesized in Igepal CO 520 using NaOH are purely superparamagnetic. Other nanoparticles, synthesized by the microemulsion route show low coercivity and very large value of saturation magnetization (Figures 4-6 and 4-7 and Table 4-2) compared to the bulk sample. Therefore, they remain in the transition-state from ferromagnetism to superparamagnetism. The bulk sample shows magnetic behavior very close to the ferromagnetic materials (Figure 4-8).

The presence of silica coating has been confirmed by the fluorescamine assay test [102] (results not shown). The decrease in the magnetic moment value (Table 4-2) when particles are coated with silica clearly distinguishes coated and non-coated particles. This silica coating protects the magnetic particles from possible decomposition induced by the surrounding environment, prevents further aggregation, and reduces inter-particle magnetic cross-talk retaining magnetic property of each particle intact. Moreover, the silica surface can be functionalized using a variety of known surface chemistry [67].

Conclusions

This work demonstrates a robust methodology for the synthesis of both non-coated and silica coated magnetic nanoparticles of ultra-small (<5 nm) and very uniform size distribution. Their magnetic properties are very close to the pure superparamagnetic materials. Therefore, they can be of potential use in power transformers, magnetic recording heads and microwave applications. The silica (a non-magnetic matrix) coated magnetic particles retain their magnetic properties intact. They might show giant magnetoresistance (GMR) effect, which would have potential applications for magnetic sensors and new storage devices with very high density. Also the silica coated magnetic nanoparticles (nanocomposites) can have good potential in magnetic refrigeration technology. The silica surface can also be coated with biomolecules (enzymes, antibody, DNA etc.), sugars (dextrans, starch, albumin, poly(ethylene glycol)) for a variety of applications. Studies on the different MRI contrast agent show that the biodistribution depends on the overall particle size, surface charge and the nature of the coating materials. The ultra-small silica coated particles can be easily immobilized with the antibody to deliver them into a specific target via the antibody-antigen recognition. Unlike polystyrene based magnetic particles, silica-coated nanoparticles can be easily dispersed in organic and aqueous solutions. These coated particles would also be very useful for efficient biomolecule separation technology e.g. DNA/RNA separation, cell separation etc. and also for magnetically guided biosensor applications. We have successfully attached DNA molecules on to our magnetic nanoparticles to make them useful as a magnetic probe for the specific separation of target oligonucleotides. In near

future, research can be focused on biomedical applications of these magnetic nanoparticles in the above-mentioned areas.

CHAPTER 5
ULTRA-LUMINESCENT NANOPARTICLES FOR SEQUENCE-SELECTIVE DNA DETECTION

Introduction

The demand for highly sensitive non-isotopic bioanalysis systems for biotechnology applications such as DNA sequencing, clinical diagnostics, and drug delivery has opened a niche for nanoparticles as a tool in biomedical fields and biotechnology. Nanoparticles offer great potential in bioanalyses due to their unique optical properties, high surface-to-volume ratio, and other size-dependent qualities. When combined with surface modification and composition control, these properties will provide probes or agents for highly selective and ultra-sensitive assays. Nanomaterials have demonstrated their unique advantages when they are combined with biomolecules for bioanalysis and biotechnology applications [6, 33, 37, 41, 103]. In this chapter, the use of the highly luminescent dye-doped silica nanoparticles for ultrasensitive DNA detection is discussed.

The use of nanoparticles in DNA detection has started to become a reality. Nanoparticles can be used as effective probes in hybridization-based assays. In a report, a new method for analyzing combinatorial DNA arrays using oligonucleotide-modified gold nanoparticle probes and a conventional flatbed scanner has been developed [24]. This nanoparticle-based assay used three different DNA sequences, of which a capture sequence was immobilized on a silica surface, while a probe sequence and a target

sequence were in a solution before hybridization. The probe sequence was labeled with a gold nanoparticle. The DNA hybridization took place between the target and both the probe and the capture to produce a surface bound hybridized complex. When coupled with a signal transduction method based on nanoparticle-promoted reduction of silver (I) [24], the complex was detected sensitively. The main reason for the better detection capability was due to signal amplification brought by the silver coating on the gold nanoparticles. Each hybridization event enabled one gold nanoparticle to be attached to the silica surface for complex-formation detection. However, the procedures involved in this assay can be complicated. The detection of the target was dependent on silver surface formation induced by a reduction-oxidation reaction. After the formation of a complex on the silica surface, the gold nanoparticles were "silver" coated for detection. How efficiently the silver coating can be carried out directly affects the efficiency of the assay for DNA analysis. This aggravates additional difficulties and uncertainty for this assay. In addition, the assay was not a direct reflection of the hybridization process and cannot be used for real-time DNA analysis. It is believed that this assay could be greatly improved if the gold nanoparticles are replaced with highly luminescent nanoparticles [18].

Overall, luminescence techniques are sensitive and reproducible in bioanalysis [18, 37, 41]. Recent progress in single molecule imaging and detection has attested their capability in ultrasensitive analysis [65, 104]. However, most of current luminescence techniques are limited by the photostability of the signal source that is usually an organic fluorophore. Practical biotechnological applications are often difficult. Problems arise from photobleaching, low signal intensities and intermittent light emission or blinking [18, 37, 42]. Although many new dye molecules have been synthesized, photobleaching

has been a problem that greatly hinders the application of luminescent techniques in bioanalysis and biotechnologies. Radioactive labeling is a highly established technique, however, it can be hampered by its inherent safety limitations. Therefore, the development of a highly photostable, nonisotopic, and extremely sensitive luminescent probe is needed for biotechnological applications.

The development of Tris(2,2'-bipyridyl)dichlororuthenium (II) hexahydrate- or RuBpy-doped silica nanoparticles might just be the tool needed for highly sensitive biotechnological applications (discussed in detail in Chapter 2) . These nanoparticles have been prepared using a water-in-oil (W/O) microemulsion method. The controlled hydrolysis of tetraethyl orthosilicate (TEOS) in W/O microemulsion led to the formation of monodisperse dye-doped silica nanoparticles. The dye molecules were doped inside the nanoparticles, and the particles' surfaces could be used for biochemical functionalization with biomolecules such as DNA strands. The amount of dye content in the nanoparticle could be varied. It is expected that each nanoparticle, depending on its size, should contain a large number of dye molecules, which forms the foundation for luminescence detection with high signal amplification. The dye molecules are well protected from the environmental oxygen when they are doped inside the silica network. The RuBpy-SiO_2 composite nanoparticles, which can be made from a few to tens of nanometers, are uniform, and the size distribution is within 2% [18, 55]. The dye molecules in the nanoparticles are stable, and the silica coating prevents photobleaching. In addition, the silica surface serves as a biocompatible and versatile substrate for biomolecule immobilization. The silica surface also aids in the dispersion of the

nanoparticles in aqueous solution. The nanoparticle's surfaces have been biochemically modified to suit the various applications using known immobilization mechanisms [105-109].

In this work, the use of highly luminescent RuBpy-doped silica nanoparticles as efficient signaling probes for ultrasensitive DNA analysis is demonstrated. This assay takes advantage of the strong luminescence provided by RuBpy-doped silica nanoparticles. The assay will not require further amplification in order to give highly discernable signals. The mechanism of the DNA assay is based on a sandwich method of three different sequences of oligonucleotides (scheme shown in Figure 5-1).

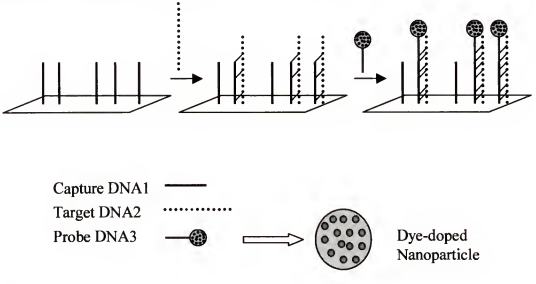

Figure 5-1. Schematic representation of a sandwich-based DNA assay using dye-doped silica nanoparticles. There are three DNA strands: capture DNA1 is immobilized on a silica surface; probe DNA 3 is linked to a highly luminescent nanoparticle, and DNA 2 is the target of this assay.

A capture DNA complementary to a fragment of the target DNA was immobilized on a modified glass substrate. The remaining portion of the target DNA is complementary to the sequence immobilized on the dye-doped silica nanoparticle-probe. The

hybridization events are followed by an imaging process to monitor the luminescence signal of the surface-bound nanoparticle-probes. An inverted fluorescence microscope and a wide-field lens were used for sensitive detection of luminescent signals and a scanning electron microscope (SEM) for visual confirmation of the binding between the probes and the target on the surface. The luminescent nanoparticle based DNA assay has been found to have high sensitivity, excellent selectivity and easy to carry out.

Experimental Section

Materials. Avidin was purchased from Molecular Probes (Eugene, OR). Biotinylated, amine-modified, and unmodified DNA sequences were obtained from IDT (Coralville IA). DNA1 had the sequence (5' TAA CAA TAA TCC T-biotin 3'), DNA2 (5' GGA TTA TTG TTA AAT ATT GAT AAG GAT 3'), and DNA 3 (5' biotin- TAT CCT TAT CAA TAT T 3'). Glutaraldehyde, succinic anhydride, 1-Ethyl-3-(3-dimethylaminopropyl)carbodiimide hydrochloride (EDC), and sulfo-N-hydroxysuccinimide (NHSS) from Sigma Chemical Co. (St. Louis, MO). N^1-[3-(Trimethoxysilyl)propyl]diethylenetriamine (DETA) was purchased from United Chemical Technologies (Bristol, PA). Acetic acid and N, N'- dimethylformamide (DMF), and glass coverslips (22x50x1mm) were from Fisher Scientific ((Pittsburgh, PA). Dye-doped nanoparticles were obtained from the synthesis procedure described in Chapter 3.

DNA Immobilization on glass substrates. For biotin-avidin based immobilization, coverslips cleaned by overnight immersion in 10 M NaOH were incubated for 12h in a 1-mg/ml avidin solution in 10 mM phosphate buffer (pH7.0). The avidin layer was stabilized by cross-linking reagent by first coating substrates with glutaraldehyde (1% in 100 mM potassium phosphate buffer for 1h at room temperature)

and subsequently incubated in 1 M Tris-HCl (pH 7.5). 250 nL of 20 μM biotinylated DNA1 (Figure 6-1). The incubation of DNA1 took 12 h in a humidified chamber.

For amine-carboxyl based immobilization, coverslips cleaned by overnight immersion in 10 M NaOH were incubated for 1 hour in 1% DETA (1 mM acetic acid), washed and dried. They were then immersed in 10% succinic anhydride in DMF for 10 hours under argon. The slides were put in an activation buffer (carbonate buffer pH 4.8). Amine-modified DNA1 was immobilized by adding 10 mg EDC and 1 mg NHSS to 500 μL solution of 10^{-8} M solution. Spots (2-μL) of the solution were deposited on the surface-modified glass slides.

DNA Immobilization on nanoparticle-probe. For biotin-avidin based immobilization, 10 mg of RuBpy-doped nanoparticles was incubated in 1 ml of the avidin solution. The avidin coating was cross-linked with 1% glutaraldehyde. The nanoparticles were then incubated in Tris-HCl solution prior to 12h biotinylated DNA3 (20 μM) immobilization (Figure 5-1). Stringent washing and centrifugation followed each step. The nanoparticles had a final concentration of 0.5 mg/ml when the DNA3 concentration for incubation was at 1 μM.

For amine-carboxyl based immobilization, 10 mg of RuBpy-doped nanoparticles was incubated for 1 hour in 1ml 1% DETA (1mM acetic acid). After centrifugation and washing, the particles were suspended with continuous stirring in 10% succinic anhydride in DMF under argon for 10 hours. The particles were then immersed in an activation buffer (carbonate buffer pH 4.8). After washing, they were put in amine-modified DNA3

solution with adding 10 mg EDC and 1 mg NHSS. The solution had a volume of 500 μL and a DNA concentration that would immobilize about 100 strands on one nanoparticle.

DNA hybridization. The target solution, DNA2 (IDT, Coralville IA) (Figure 6-1), was incubated onto the immobilized coverslip (with DNA1 immobilized) for 2 hours. After washing with buffer, the nanoparticle-DNA3 complex was allowed to hybridize for 2 hours. Stringent washing followed each step. Incubations were done in humidified chamber.

Optical testing and imaging. Luminescence images were obtained by an inverted fluorescence microscope (Olympus, model IX70) with an intensified charge coupled device (ICCD). For wide-field viewing and signal collection, the set-up is as described in the Appendix. Scanning electron microscopy images were taken by Hitachi S-4000 FE-SEM. The photobleaching of the dye-doped nanoparticles was compared to that of an organic dye, TAMRA. A fluorescence microscope was used to monitor luminescence signal change over time. Results are similar to those shown in Chapter 2.

Assay characterization experiments. Varied concentrations ranging from 10^{-16} to 10^{-6} M of target DNA2 were analyzed. The hybridization process was done as previously described. The concentration dependent luminescence intensity data were used to evaluate the detection limit. Selectivity experiments were done similarly. Luminescence signals from both complementary target and one base mismatched DNA were compared. Equal concentrations (1 μM) of the probe DNA and capture DNA were used in all these experiments.

Results and Discussion

Highly luminescent and ultra-photostable dye doped nanoparticles surface modified for biomolecular conjugation. The nanoparticles used for the DNA assay in this work were prepared using a water-in-oil microemulsion method (described in Chapter 2). RuBpy dye molecules were doped inside the nanoparticles whose silica surfaces can be used to covalently bind with biomolecules [18, 55, 56]. As reported before, an excellent molecular conjugation mechanism is used for direct linking the nanoparticles with interesting biomolecules for important biochemical functionalizations. Unique biochemical properties of the biomolecules, like DNA hybridization, can thus be associated with the photostable dye molecules. This opens a general approach to conjugate desired biomolecules with a sensitive signal transduction mechanism. The conjugation mechanism uses the uniform dye-doped silica nanoparticles as a signal transduction source. The nanoparticles have been characterized with microscopy and spectroscopic methods. The dye-doped silica nanoparticles were uniform in size, as characterized by TEM (data shown in Chapter 2). The dye-doped silica nanoparticles used in this work were 63±4 nm in diameter. The size of the nanoparticles can be controlled and tuned by changing the water-to-surfactant molar ratio (w_0 value) [18]. Using Triton X-100/cyclohexane/n-hexanol system and a W_0 value=10, silica nanoparticles with 63 nm and loaded with RuBpy dye molecules were obtained.

Spectrofluorometric analysis of the nanoparticles show that the dye molecules inside the nanoparticles demonstrate very similar properties as those in an aqueous solution (discussed in Chapter 2). The excitation and the emission spectra of the pure

RuBpy and dye-doped silica nanoparticles were similar, showing emission around 598 nm when excited at the 458 nm excitation band maxima in aqueous solution.

Signal amplification by using dye-doped silica nanoparticles. In a set of experiments, two complementary DNA sequences were separately immobilized on surface-modified glass substrate and on dye-doped silica nanoparticles. Various concentrations from 10^{-8} M to 10^{-16} M amine-modified DNA were immobilized on carboxyl-modified substrate. The DNA had the following sequence: 5' GGA TTA TTG TTA AAT-Amine 3'. Two sets of samples were prepared, one for hybridization with TMR-labeled complementary DNA and the other with dye-doped silica nanoparticle-labeled complementary DNA. The results are shown in Figure 5-2.

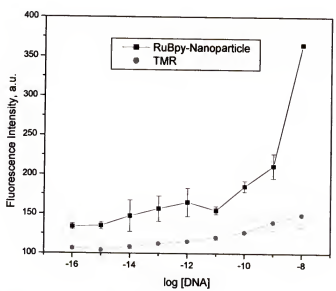

Figure 5-2. Comparison of signal intensities between dye-label and dye-doped silica nanoparticle label. Two complementary DNA's were used in this experiment.

The signal amplification from the dye-doped nanoparticles was expected to be thousand-fold compared to the pure RuBpy. Since it was not possible to directly compare the signal amplification from the RuBpy-doped nanoparticle and the pure RuBpy nanoparticle due to the bioconjugation limitation of the latter, comparisons were made between the nanoparticle and an organic label, TMR. The signal amplification observed was 2-3 times for the nanoparticle compared to the TMR dye. To better compare the signal from the dye-doped nanoparticle to that of the pure RuBpy dye, the relative quantum yields of TMR and RuBpy can be used. Since TMR, being an organic fluorophore, has a quantum yield which is 100 times better than the pure RuBpy molecule, the effective amplification for the assay using dye-doped nanoparticle is therefore 200-300 times more. The other discrepancy probably came from the difference in efficiency of hybridization between the two assays. The hybridization between oligonucleotides immobilized on bulky surfaces may not be as good as free flowing ones. Thus, between the TMR-immobilized and the nanoparticle-immobilized oligonucleotides, hybridization is probably more efficient in the former.

DNA detection assay using dye doped nanoparticles. To demonstrate that the dye-doped nanoparticles could be used in the detection of unmodified target oliogonucleotides, the hybridization scheme in Figure 5-1 was used for a highly sensitive DNA detection. A 12-mer biotinylated capture DNA (5' TAA CAA TAA TCC T-biotin 3') was immobilized on an avidin-coated glass substrate. The capture DNA was then allowed to hybridize to one end of a 27-mer target DNA (5' GGA TTA TTG TTA AAT ATT GAT AAG GAT 3'). The remaining 15 bases of the target were hybridized with the DNA (5' biotin- TAT CCT TAT CAA TAT T 3') attached to the dye-doped silica

nanoparticles. The completion of the hybridization of the three sequences of oligonucleotides via the sandwich assay was indicated by the presence of the nanoparticle probes on the coverslip surface. The coverslip surface was imaged after washing away any unhybridized DNA probes and physically adsorbed nanoparticles. Both fluorescence (Figure 5-3) and SEM (Figure 5-4) images were obtained to confirm the presence of the dye-doped silica nanoparticles attached to the surface, which is an indication of the hybridization of the three sequences. Both SEM and fluorescence microscopy results clearly show that the nanoparticles are attached to the surface after hybridization. By monitoring the luminescence intensity from these surface bound nanoparticles, varying concentrations of the DNA target were detected (Figure 5-5).

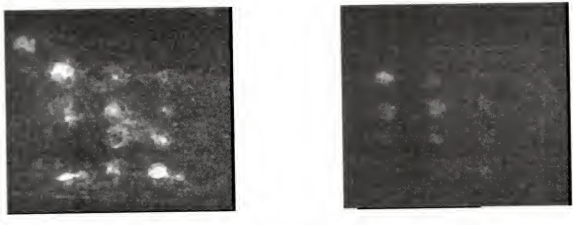

Figure 5-3. Fluorescence microscopy images of samples containing different concentrations of target DNA. The left panel shows results for samples containing 10^{-8} M to 10^{-11} M target DNA (top to bottom). The right panel shows results for samples containing 10^{-12} M to 10^{-15} M target DNA (top to bottom).

(a)

(b)

(c)

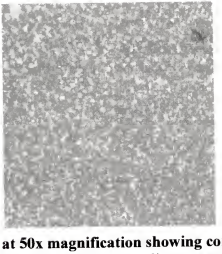

Figure 5-4. SEM images at 50x magnification showing concentration dependence of deposited nanoparticle density as target (DNA2) concentration is increased. (a) 0, (b) 1E-11 M, (c) 1E-7 M.

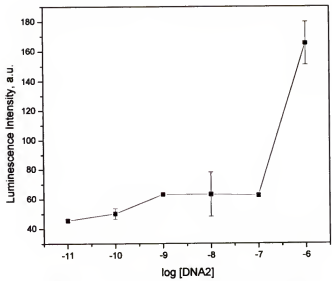

Figure 5-5. Luminescence intensity versus log [DNA target]. The experiment is based on a sandwich-assay using dye-doped silica nanoparticles.

A similar procedure was followed for covalent-coupling based immobilization. Instead of using biotin-modifed oligonucleotides, amine-modified DNA strands were used.

Since each nanoparticle has numerous dye molecules doped inside while only one probe DNA strand would ideally hybridize to the target DNA, this generates an excellent opportunity for signal amplification after hybridization. The basic idea is that one molecule of the probe DNA hybridizes one target DNA, and thus brings one dye-doped silica nanoparticle to the surface, leaving a large number of dye molecules for signaling. Large amplification of luminescent signal due to hybridization is thus possible with the following two favorable factors: the large number of dye molecules associated with a single hybridization event and the excellent photostability of the nanoparticles

It is worth noting that correlation between luminescence intensities and the concentration of target DNA molecules exists in a relatively wide concentration range. This clearly indicates that physical adsorption is not a major concern in the current assay.

Only when the target DNA concentration is higher than 1 μM can physical adsorption of the nanoparticles on the surface becomes a significant factor of concern in our DNA assay. It is a known phenomenon that nanoparticles have a high tendency to agglomerate. At low target DNA concentrations and low number of hybridization events, nonspecific binding due to nanoparticle agglomeration is not significant because there is a lower amount of previously deposited nanoparticles at which subsequent deposition can occur. Direct physical adsorption of the nanoparticle-probe on the surface-modified is negligible. Dependence of the target concentration on the signal can thus be observed. The detection limit determined for the described assay is down to the femtomolar level. An even lower detection limit is possible with the following four measures: improvement in the imaging system; more efficient excitation of the dye-doped silica nanoparticles on the surface; optimized number of dye molecules inside each nanoparticle; more efficient hybridization process. The concentration dynamic range for this assay can also be extended with higher throughput optical detectors.

Differentiating A-T and G-C mismatch. The large signal amplification of dye-doped silica nanoparticles-based assay enabled the differentiation of even the smallest variations in DNA binding affinity. This is due to the fact that even small differences could be greatly amplified, as shown by the dye-doped silica nanoparticles used in this work. It could then be used to amplify the minute differences in DNA binding affinity into detectable differences in luminescence intensities. Using this approach, we were not only able to identify single base mismatch in a linear DNA of 27 base pairs, but also able to differentiate an A-T mismatch from a G-C mismatch. As shown in Figure 5-7, there is a large difference in luminescence intensity obtained from the one-base mismatched

DNA (5' GGA TaA TTG TTA AAT TTA GAT AAG GAT 3') from that of the complementary DNA of equal concentration. The result shows that the assay can readily discriminate the perfect matched sequence from that of the one-base mismatched even at room temperature with a 5:1 selectivity in favor of the perfect complement sequence. Furthermore, the extraordinary signal amplification by the dye-doped silica nanoparticles enabled the differentiation between a mismatch by A-T from that by G-C. Usually, for a linear DNA with 27 bases, it is rather difficult to differentiate between a single base mismatch at room temperature (only a 3.5% difference in base composition) [110]. As shown in Figure 5-8, discrimination between the A-T mismatch from the G-C mismatch is possible. This assay will be highly useful in single point mutation as a capability in differentiating a G-C mismatch from an A-T mismatch is critically important. Single base mismatches have a pronounced impact on hybridization and this fact, coupled with identification, can be exploited for diagnostic studies [111].

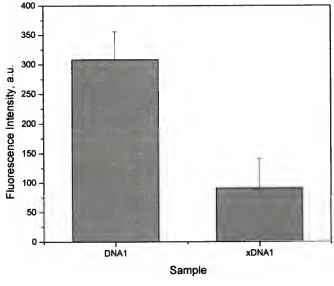

Figure 5-6. Selectivity of assay. DNA1 is perfect match while xDNA 1 is a single-base mismatched sequence.

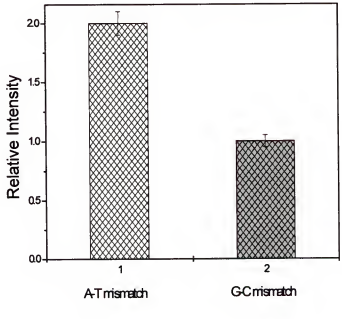

Figure 5-7. Selectivity of assay (A-T vs G-C mismatch).

It was shown that the DNA analysis assay based on dye-doped silica nanoparticles is an effective approach of monitoring DNA hybridization events with a few important advantages. The assay is highly sensitive, with a detection limit of 3 pM concentration and can easily detect 100 fM concentration [57]. The RuBpy-doped nanoparticles are highly photostable, and there is little photobleaching. This gives the assay excellent reproducibility. The assay is robust and convenient. With the dye-doped silica nanoparticles as the probes for DNA analysis, the assay can readily discriminate sequences even if they differ by only one base. The assay has a greater than five-fold selectivity to the target over a one-base mismatched sequence. Furthermore, the assay can differentiate an A-T mismatch from a G-C mismatch. This is due to a large amplification factor in signaling, brought by the dye-doped silica nanoparticles, during the hybridization. The assay can be used for a large range of target concentrations. Compared with other nanoparticle-based assays, the current one is simple and easy to carry out. The assay also enables a direct observation of the hybridization event. It is thus expected that this assay will be widely useful in a number of biotechnology applications in DNA analysis and imaging.

Conclusions

Oligonucleotide detection and separation is a bioanalytical process important in disease diagnosis. Research for the improvement of the process is continuously being pursued for it has a profound impact on the betterment of health care. A new route for oligonucletide detection using nanoparticles was demonstrated. This method was based on the use of dye-doped nanoparticles as

labels or probe for DNA detection. This assay is highly useful for the detection of very low concentrations of DNA target. Due to the presence of numerous dyes doped in one nanoparticle, high signal amplification can be obtained. Thus, a single event in a biochemical process such as hybridization can be indicated by the presence of one nanoparticle probe, which in turn gives off a signal equivalent to thousand dye molecule probes. The assay involving the use of dye-doped nanoparticle has been shown to detect concentration down to the 100 fM level.

CHAPTER 6
MAGNETIC NANOPARTICLES FOR CAPTURING TRACE AMOUNTS OF OLIGONUCLEOTIDES FROM A COMPLEX MATRIX

Introduction

The use of magnetic carriers in scientific and clinical applications, particularly for separation, is not new, but intense research in the field is still on going. This could be brought about by the development of new magnetic particles with improved properties for various procedures. The effectiveness of magnetic particles for biotechnological applications is governed by different factors: size, magnetic susceptibility, and biocompatibility. Magnetic particle size should be small enough to be easily dispersed in a suspension, but big enough to have a high susceptibility. In applications that involve circulation, they are desired to be big enough to stay localized in the target area. This is because circulation time depends reciprocally on particle size. Size and magnetic properties should therefore be optimized to obtain the particles with the right size and sufficient magnetic susceptibility for a particular application. For magnetic particles to be used in biotechnological applications, they should be compatible for conjugation with biomolecules needed for probing or capturing molecules, organelles, or cells of interest.

In this section, magnetic particles in the nanometer dimension are shown as carriers for the extraction of trace amounts of a target oligonucleotide from a complex matrix. These particles are small enough to stay suspended in solution and have enough magnetic properties to be attracted to a hand magnet. The nanoparticle have been silica-coated for easy conjugation with a probe/capture oligonucleotide. The probe/capture

oligonucleotide used in this work is a specially designed molecular beacon (MB). Using the molecular beacon as a probe and a capture sequence, oligonucleotides complementary to the loop sequence hybridize with the molecular beacon. Using a hand magnet, the ensemble of the magnetic nanoparticle with immobilized molecular beacon capturing a target oligonucleotide can be separated from a complex matrix. Oligonucleotides with sequences close to the complementary strand may also get captured. Purifications of the capture oligonucleotides are dealt with in a subsequent process. The procedure is expected to be useful in the collection of trace amounts of oligonucleotides from a complex matrix.

The separation and collection of trace amounts of gene products are of great interest for disease diagnostics, biomedical studies and biotechnology development. This is especially true for single base mismatched DNA/RNA strands in a complex mixture such as cell lysates and tissue samples. It has been reported that most cancers originate from genetic mutations starting with a single base change in a DNA sequence [110]. The detection and collection of DNA sequence with single base difference should thus play a major role in mutation detection and in gene expression studies. In particular, the collection and characterization of trace amounts of single base mismatched DNA can be potentially useful for early correction and elimination of mutant genes before cancer occurs. Currently, however, there is a lack of efficient technologies to collect trace amounts of target DNA from a complex matrix with single base accuracy. The collection of rare gene products from a complex mixture has always been a huge challenge.

DNA hybridization is one of the most selective molecular recognition mechanisms with the capability of detecting target DNA sequences from a mixture. However, discriminating between two DNA sequences that differ by only one single base is difficult to accomplish when linear DNA probes are used due to a small difference in thermodynamic stability between the two DNA duplexes. Usually, the melting temperatures between two DNA duplexes formed by linear DNA targets with one base difference are less than 10°C [112]. Better DNA molecules or DNA probes are thus needed for more effective discrimination between two DNA strands with single base difference. Recently, molecular beacons (MBs) have been developed for real-time DNA/RNA detection with high specificity and excellent sensitivity [112]. As a result of their special stem-loop structure, MBs have a much better capability to discriminate perfect complementary DNA from single base mismatched DNA [112]. MBs also have an excellent built-in signal transduction, which enables them to be used as gene probes for "detection without separation" [113]. Since MBs' development, they have been used in real-time monitoring of DNA/RNA in solution and inside living specimen, in protein-DNA interaction studies, and in biosensor development [114, 115]. However, using MB for DNA collection will have to rely on a suitable biomolecule carrier between liquid and solid phases.

Nanomaterials are excellent molecule carriers due to their high surface to volume ratio and ultrasmall size [54]. Nanomaterials have demonstrated many unique advantages when they are combined with biomolecules for bioanalysis and biotechnology applications [18, 55]. Actually, magnetic materials and microparticles

have been used for magnetic separation of biomolecules [116] and biological cells [117]. The separation of biotinylated DNA and non-biotinylated DNA has been carried out using avidin-coated magnetic nanoclusters [118]. However, the collection and separation of single base mismatched DNA strands has not been demonstrated.

In this work, the high selectivity and excellent sensitivity of MBs are combined with the superior magnetic properties of a recently developed magnetic nanoparticle [54] for the collection of trace amount of DNA strands with single base difference from a complex mixture. Genomagnetic nano-capturers have been developed using magnetic nanoparticles functionalized with MBs. Single base mismatched DNA could be easily separated, collected and monitored from perfectly complementary DNA by applying a magnetic field and by controlling the temperature for duplex melting. The separation and collection processes can be monitored easily with the changes of the intrinsic fluorescence signal of MBs.

Experimental Section

Materials. All biochemicals were purchased and used as received. Lysozyme(Lyz), hemoglobin(Hb) and bovine serum albumin(BSA) were purchased from Sigma. Ferric chloride, ferrous chloride, Triton X-100 (polyoxyethylene (10) isoooctylphenylether, 4-(C_8H_{17})C_6H_4(OCH_2CH_3)$_n$OH, n~10), and TEOS (tetraethylorthosilicate) were purchased from Aldrich Chemical Co. Inc. (Milwaukee, WI). Cyclohexane, n-hexanol, and sodium hydroxide were obtained from Fisher Scientific Co. (Pittsburgh, PA). Distilled deionized water (Easy Pure

LF) was used for the preparation of all aqueous solutions in the synthesis of magnetic nanoparticles.

FS20 ultrasonicator (Fisher Scientific Co.), Centrifuge 5810 R (Eppendorf), Hitachi H-7000 Transmission Electron Microscopy (Japan) and MPMS-5S Superconducting Quantum Interference Device (SQUID) Magnetometer were used for the synthesis and characterization of magnetic nanoparticles (Chapter 4). Fluorolog TAU-3 Spetrofluorometer (Jobin Yvon-Spex, Instruments S. A., Inc.) was used to detect fluorescence intensity at different temperatures.

Molecular beacon design. A molecular beacon with a 15-base loop and 5-base arms was synthesized by TriLink BioTechnologies Inc. The loop had the sequence 5' ATC AAT ATT TAA CAA 3'. For this molecular beacon, the fluorophore used was fluorescein and the quencher was DABCYL, 4-(4'-dimethylaminophenylazo) benzoic acid.

Synthesis of magnetic nanoparticles. The silica-coated magnetic nanoparticles were synthesized using a water-in oil microemulsion method described in Chapter 4. The microemulsion was prepared using Triton X-100 surfactant. $FeCl_2$ and $FeCl_3$ were used to form iron oxide nanoparticles. The silica layer was formed by adding 10 μL TEOS to the microemulsion.

Immobilization of biotinylated molecular beacons on the magnetic nanoparticles. MB was immobilized onto nanoparticles through avidin-biotin linkage as described in the first section of this chapter. Biotinylated molecular beacon (1.0×10^{-6} M) was incubated with magnetic nanoparticles for 12 h at 4°C. To make sure each exposed biotin group on the MB coupled to the avidin molecules

on the magnetic nanoparticles (each avidin molecule has four biotin binding sites), avidin was added in excess. The resultant nano-capturer was then washed three times with 20 mM Tris-HCl -5 mM $MgCl_2$ buffer (pH=8) and stored at 4°C for future use.

Separation and collection method. The complex matrix in this study was a 9.90 ml of mixture containing trace amounts of target DNA1 and DNA2, large amounts of random DNA 3 and DNA4 (100 times more concentrated) as well as BSA, Hb and Lyz proteins (1000 times more concentrated). DNA1 was a perfectly complementary target to the MB while DNA2 was a single base mismatched sequence. Three separation steps were used in the experiments. First, DNA1 and DNA2 were separated and collected from the components of the complex matrix. A solution (100 μL) of the MB-containing magnetic nanoparticles was added to the mixture for 30 min at 18 ° C. DNA1 and DNA2 were assumed to have hybridized with the MB on the nanoparticle surface while the random DNA sequences and proteins would not. By subjecting the mixture to a hand-held magnet, the magnetic nanoparticles carrying the DNA1 and DNA2 samples were separated from the various components of the mixture. The second step of the separation would then be between DNA1 and DNA2. The separation of DNA1 and DNA2 was based on the difference in melting temperatures of the duplexes they formed with the MB. A 20-μL solution of 20 mM Tris-HCl-5 mM $MgCl_2$ buffer was added to the collected magnetic nanoparticles in the first step. DNA1 and DNA2 were separated by bathing the magnetic nanoparticle suspension at 32°C for 15 min. At this temperature, DNA2 completely dissociated from the MB on the magnetic

nanoparticles, while DNA1 remained bound. The suspension was then exposed again to a magnetic field, and DNA1-carrying nanoparticles were retrieved. The supernate contained DNA2, accomplishing the individual collection of DNA1 and DNA2 from a mixture. The third step of the separation was the collection of DNA. A 20 μL of 20 mM Tris-HC, 5 mM $MgCl_2$ buffer was added to the magnetic nanoparticles containing DNA1. The temperature of the solution was raised and fixed at 52°C for 15 min, resulting in the complete dissociation of DNA1 from the MB of the nanoparticles. The nanoparticles were removed from the solution thereafter using an applied magnetic field. A schematic diagram of the separation is shown in Figure 6-1.

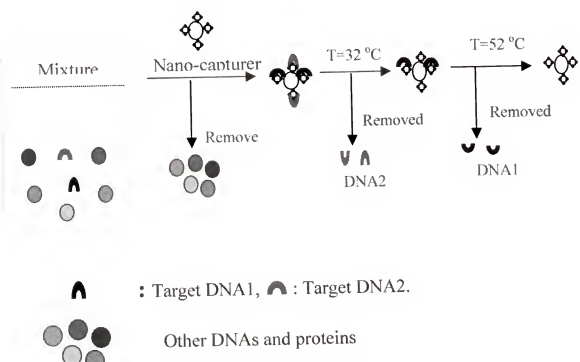

Figure 6-1. Schematic digram for the separation of oligonucleotides.

Results and Discussion

The search for highly accurate, specific, and sensitive oligonucleotide detection and collection still exist with the ever-present need for improved disease diagnosis. Using the carrying-capability of magnetic nanoparticles coupled with the surface-modification potential of silica, the collection of trace amount of target oligonucleotides from a complex matrix is demonstrated. The separation capability of the silica-coated magnetic nanoparticles is further combined with the highly sensitive oligonucleotide recognition of molecular beacon. The ensemble can thus be used for a highly efficient collection of trace amounts of oligonucleotide from samples such as lysates and other matrices. In addition, by manipulating the temperature both the target oligonucleotide and the one-base mismatched sequences can be collected. By subjecting the collected sequences, now bound to the MB on the nanoparticles, to different temperatures the target and mismatched sequences are separated. These temperatures are based on the individual melting point of the formed duplexes.

For the separation procedure, silica magnetic nanoparticles such as the one in Figure 6-2 are used. These particles are in the nanometer range thus they have high surface-volume-ratio. Such a property would allow the immobilization of high amount of molecular beacon for use in the recognition and capture process.

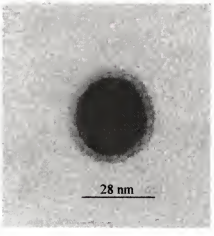

Figure 6-2. TEM image of silica-coated magnetic nanoparticle.

Molecular beacon molecules (Figure 6-3) were conjugated to the silica-coated magnetic nanoparticles by avidin-biotin coupling. The nanoparticles now containing the molecular beacons were washed and resuspended in solution. The supernate, the new suspension, and the wash solutions were stored. To determine the efficiency of the immobilization process, equal amounts of DNA1 were added to the stored solutions and their fluorescence intensities were compared. Results are shown in Figure 6-4.

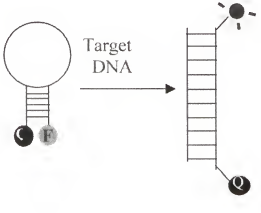

Figure 6-3. Molecular Beacon. In its stem-loop conformation, the quencher and fluorophore are in close proximity. Signal is obtained when a target DNA hybridizes with the loop part of the MB.

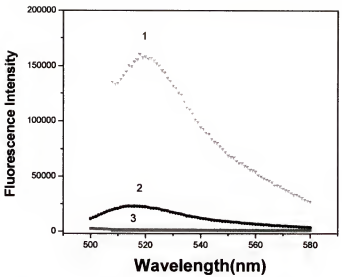

Figure 6-4. Efficiency of molecular beacon immobilization. (1) Suspension containing magnetic nanoparticles with immobilized molecular beacon, (2) supernate containing unbound molecular beacon, (3) wash solution.

The results show that the amount of immobilized molecular beacon was significantly higher than what was left in the supernate. The signal from the wash solution further indicates that the coupling was stable and that insignificant amount of molecular beacon dissociated from the magnetic nanoparticles.

The separation of the captured DNA's (DNA1 and DNA2) would involve the use temperature. Since melting points of the duplexes formed by captured DNA with molecular beacon vary, it would be possible to dissociate one of the DNA, the mismatched sequence in particular, while the other DNA was kept hybridized with the molecular beacon. To determine the melting points of the duplexes, temperature profiles of the duplexes were obtained. One set of experiment used immobilized molecular beacons (Figure 6-5) while the other used molecular beacons free in solution (Figure 6-6).

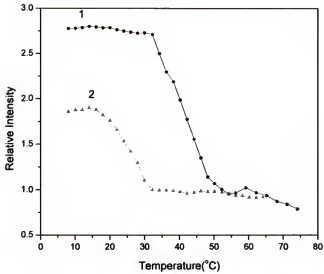

Figure 6-5. Temperature profile of immobilized MB-DNA duplexes. (1) MB-DNA1 duplex, (2) MB-DNA2 duplex.

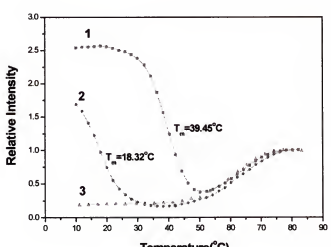

Figure 6-6. Temperature profile of free MB-DNA duplexes. (1) MB-DNA1 duplex, (2) MB-DNA2 duplex, (3) MB.

The fluorescence signal was highest when the hybridization between the DNA and the molecular beacon was at maximum. As the temperature was increased, dissociation of the DNA allowed the reconstitution of the molecular beacon into its stem-loop structure. As the temperature was further increased, the closed form of the molecular beacon started to denature thus the increase in fluorescence signal. This increase in signal was however less than when the molecular beacon was hybridized to a target DNA. Temperature profile results (Figures 6-5 and 6-6) showed that the duplex of the perfect target had a higher melting point compared to the duplex of the mismatched sequence. This difference in melting temperature allowed the separation of the two sequences. The temperature profiles of the duplexes have similar trends whether the molecular beacon was in solution or immobilized on magnetic nanoparticles (Figure 6-7). In the case of the immobilized molecular beacon however, the melting point of the duplex was at a higher temperature. Since the melting point of the duplexes of the captured DNA were significantly different, separation was possible. The melting temperature for the DNA1 duplex was 39.4^{0}C and 18.3 ^{0}C for the DNA 2 duplex. From Figure 6-5, it can be seen that when the temperature is 35 ^{0}C the amount of hybridized DNA1 was still at maximum while that of DNA2 was already at minimum. Separation of the two DNA's would be optimal at this temperature. The efficiency of separation using the molecular beacon-magnetic nanoparticle ensemble is shown in the results in Table 6-1.

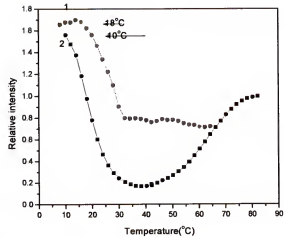

Figure 6-7. Temperature profile comparison. (1) Immobilized MB-DNA1, (2) Free MB-DNA1.

Table 6-1. Efficiency of separation using MB-magnetic nanoparticles.

Sample No.	Concentration before separation (pM)		Concentration after separation (pM)		Recovery(%)	
	DNA1	DNA2	DNA1 Mean±SD,n=5	DNA2 mean±SD,n=5	DNA1 (%)	DNA2 (%)
1	12.5	50.0	11.8±0.74	48.5±0.72	94.4	96.9
2	25.0	25.0	24.4±0.45	24.3±0.63	97.6	97.2
3	50.0	12.5	46.9±0.71	11.1±0.57	93.8	88.8
4	8.25	8.25	7.57±0.52	8.15±0.44	91.8	98.8

Using different combinations of oligonucleotide concentrations, it was shown that almost full recovery of the target DNA's is possible. The results show that magnetic nanoparticles coupled with molecular beacons could be very effective in capturing oligonucleotides of interest. A minor drawback but a factor that enhances the selectivity of this assay is the need to design a specific molecular beacon for a particular DNA needed to be captured. Nevertheless, the use of the magnetic nanocapturers in bioanalyses show great promise and this preliminary work can be basis for a more in-depth work.

Conclusions

A method for oligonucleotide detection coupled with separation was demonstrated using magnetic nanoparticles conjugated to molecular beacons. Due to the magnetic property of the nanoparticles and the recognition ability of the molecular beacons, oligonucleotides of interest were collected from complex matrices. Both perfect complementary sequences and one-base mismatch ones are captured from the matrix. Separation and purification of the two sequences was done by taking advantage of the difference in the melting points of their duplexes with the molecular beacon. Recovery of up to 98% was demonstrated.

CHAPTER 7
SUMMARY AND FUTURE DIRECTIONS

Summary

The development of novel silica-based nanoparticles with features such as high luminescence, excellent photostability, and versatile biomolecule conjugation capability can have a very high impact in bioanalyses. In this work, the syntheses of such silica-based nanoparticles for use in bionalytical applications were described. Since nanoparticles and many molecules, organelles, and cells involved in many biochemical reactions exist in the same dimension range, silica-based nanoparticles have the potential to be used as probes for such processes. Some of these applications were described in a few chapters (Chapters 3, 5, and 6).

The most extensively studied silica based nanoparticles in this work are the RuBpy-doped silica nanoparticles. RuBpy-doped silica nanoparticles were prepared in reverse microemulsions. The obtained particles are in the nanometer range with diameters ranging from 15 nm to 70 nm depending on the parameters used for the process. The physical properties of inorganic dye-doped nanoparticles are governed by the parameters used during the synthesis procedure. Size as well as optical properties are affected by the type of surfactant used, the water-to-surfactant molar ratio in the microemulsion, the time the polymerization reaction is allowed to proceed, and the amount of dye added as dopant. Evaluation of the optical properties of the nanoparticles showed that there was a slight difference between the emission spectrum of the doped dye compared to that of the

free dye. No significant change was observed in the excitation spectra of the dye-doped nanoparticleand the free dye. A comparison of the photostability of free dye and doped dye showed that it was greatly reduced in the latter. This improved photostability is due to the shielding effect provided by the silica matrix. Such property can be very useful for bioanalyses that require long-time light exposure. Another property that can be very desirable is the signal amplification that can be obtained when using the dye-doped nanoparticles in bioanalyses. Quantitation studies showed that each nanoparticle contain thousands of dye molecules, thus giving amplified signal for each single biological recognition event.

RuBpy, like other inorganic dyes, has a low quantum yield and low molar absorptivity. Although it has a long lifetime that allows it to have an inherent good photostability, it might not be the most ideal dye dopant for nanoparticles to be used in bioanalyses. Organic fluorophores are brighter than inorganic dyes, thus, a research thrust to dope the former in silica matrix was started. A problem with organic fluorophores is that they are too hydrophobic to be trapped in waterpools inside the reverse micelles. Trapping them in silica matrix using reverse microemulsion was a challenge. An alternative procedure was thus used. Using the Stöber process and a combination of tetraethylorthosilicate (hydrophilic) and phenyltriethoxysilane (hydrophobic) silica precursors, rhodamine 6G-doped silica nanoparticles were successfully made. The silica matrix provided the shielding effect expected and allowed the trapped organic dye to have excellent photostability.

Silica is good not only for shielding but also as a surface for bioconjugation through surface modification. In the preparation of magnetic nanoparticles, silica was

used as a coating to allow the conjugation of the nanoparticles to biomolecules for use in bioanalyses. Magnetic nanoparticles were prepared in reverse microemulsion using different surfactants and the obtained products were characterized according to their size, magnetic susceptibility, and crystallinity. Magnetic nanoparticles with diameters less than 10 nm and thin silica coating were obtained. These nanoparticles were later used in the separation of target oligonucleotides from a complex matrix.

The synthesized silica-based nanoparticles, both dye-doped and magnetic, were shown to be useful in bioanalytical applications. The dye-doped nanoparticles were used as probes in protein detection as well as in oligonucleotide assay. Using the dye-doped nanoparticles, the DNA assay was shown to easily detect 100 femtomolar concentration. The magnetic nanoparticles were also used in oligonucleotide collection and separation. With molecular beacon as a capturing element and as a signal source, the collection efficiency of the assay was seen to be as high as 98 %.

Future Directions

Inorganic dye-doped silica nanoparticles. It has been established that various parameters affect the size and optical properties of dye-doped silica nanoparticles. This set of parameters and the corresponding results may be used to build-up a synthesis guide for the preparation of nanoparticles with a particular size and optical properties. The set of parameters studied is not yet complete. Factors such as temperature, amount of silica precursor, different types of silica precursor, and a wider range of surfactants systems should be studied. A more complete and systematic study of the parameters mentioned will reduce the trial-and-error aspect of dye-doped silica nanoparticle synthesis. For

bioanalytical applications, the size effect on the process such as hybridization can be studied.

Organic dye-doped silica nanoparticles. The use of Stöber process is not the best process to obtain highly uniform nanoparticles. Although control of temperature can greatly improve the uniformity of the particles, the process is not as reproducible as the reverse microemulsion method. A possible extension of this work would be a modification of the reverse microemulsion system that would render the organic fluorophores to be more hydrophilic and allow them to get trapped inside the reverse micelles. Another line of work that might be pursued would be the use of dye-containing silica precursors. Such a procedure would eliminate the problem of forcing the organic fluorophores into the waterpool where the silica is localized.

Silica-coated magnetic nanoparticles. The silica coating on the prepared magnetic nanoparticles makes the composite biocompatible. Since many clinical applications require magnetic carriers to be biocompatible, the silica-coated magnetic nanoparticles might have the potential to be used in such applications. These applications include directed transport and controlled release of drugs or radionuclides, for use as sources of local temperature increase (hyperthermia), and for local contrast enhancement in magnetic resonance imaging.

Different types of nanoparticles can be made for many applications. The ideal nanoparticle is however different for every application. New possibilities in design, preparation methods, materials and modifications will in the future lead to more proposal of their use.

Nanoparticle-based assays. It has been shown that silica-based nanoparticles can be very useful in bioanalyses. Further evaluation and improvement of the procedures might however be still needed. One course of work that might be pursued is the size effect of the nanoparticles on the processes involved. The efficiency of immobilization, hybridization, and other processes might be affected by the size of the nanoparticles. Results obtained from such evaluation might improve the assays significantly.

In the case of separation assay, an evaluation of the interaction of the other components of the matrix with the target oligonucleotides should be made. Although it was shown that the oligonucleotides were collected, their purity was not ascertained. It is possible for the DNA's to have an interaction with the some proteins and this may affect the results of the assay.

Although future work might still be necessary before extensive use of silica-based nanoparticles in bioanalyses can be made, a foundation has been made and a follow-through and further development is the only way that this work can be put to real use.

APPENDIX A
ELECTRON MICROSCOPY

Electron microscopes have made it possible to examine samples down to near atomic levels in the innermost structures of most materials. They can thus be easily the choice of instrument for size characterization of samples that have dimensions in the nanometer level. Electron microscopes are scientific instruments that use a beam of highly energetic electrons to examine objects on a very fine scale. The use of such instruments can yield information on topography, morphology, composition, and crystallographic information. In a way, electron microscopes are similar to light microscopes. Both types of microscopes require an illuminating system, a specimen stage, an imaging system, and an image recording system. Although the main difference between these two types of microscopes lies in the type of illumination source, light versus electron, the types of lenses used are also not the same. Electron microscopes use magnetic lenses made of ferromagnetic materials while light microscopes have optical lenses made up of glass. More importantly, electron microscopes can magnify samples up to 500,000x while light microscopes can only do so to 1000x.

Electron microscopes are very powerful instruments and they come either as a transmission electron microscope (TEM) or scanning electron microscope (SEM). In electron microscopy (EM), images are formed through a series of steps. First, a stream of electrons is formed (by the Electron Source) and accelerated toward the specimen using a

positive electrical potential. This stream is confined and focused using metal apertures and magnetic lenses into a thin, focused, monochromatic beam. This beam is focused onto the sample using a magnetic lens. When the beam hits the sample, interactions occur inside the irradiated sample, affecting the electron beam. These interactions and effects are detected and transformed into an image. The above steps are carried out in all EMs regardless of type.

Specimen interaction is what makes Electron Microscopy possible. The energetic electrons in the microscope strike the sample and various reactions can occur as shown below. The reactions noted on the topside of the diagram are utilized when examining thick or bulk specimens (SEM) while the reactions on the bottom side are those examined in thin or foil specimens (TEM). A diagram showing the generation depths of the interactions is shown in Figure A-1.

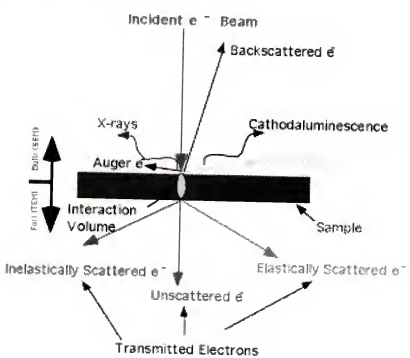

Figure A-1. Specimen interaction.

TEM forms a true image of the specimen, in the same way a light microscope does. The true image is formed when the specimen is illuminated with the radiation or electrons, with some of the radiation transmitted through the specimen, while some of the radiation is absorbed by the specimen. The schematic representation of TEM is shown in Figure A-2.

The important components of a TEM are the electron gun, the condenser lens system and its apertures, the specimen chamber, the objective aperture, the projector lens.

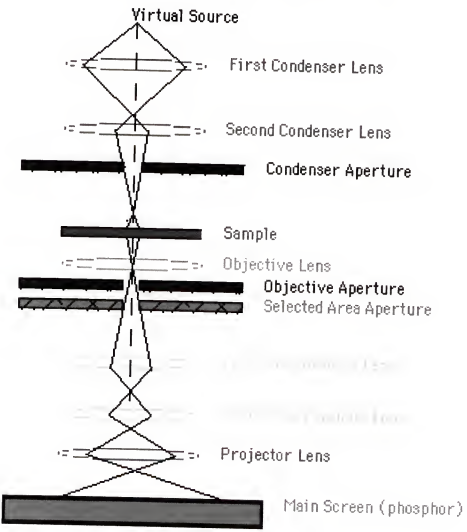

Figure A-2. Schematic representation of a transmission electron microscope.

SEMs are different in a way from TEMs because they are patterned after Reflecting Light Microscopes and yield similar information. A diagram showing a representation of the SEM is shown in Figure A-3.

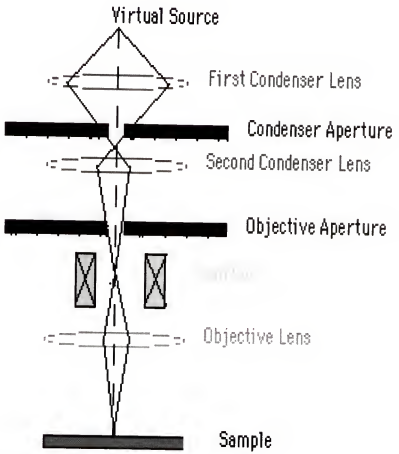

Figure A-3. Schematic representation of a scanning electron microscope.

The general features of the TEM and SEM are similar, that is, they can be used in the characterization of small particles. The choice of instrument is however governed by the type of sample available and the specific information need. For topography information, SEM may be the better choice but for greater detail TEM would be the better option.

APPENDIX B
FLUORESCENCE MICROSCOPY

Fluorescence activity is sometimes depicted diagrammatically as shown in Figure B-1 (a so-called Jablonski-type diagram). Prior to excitation, the electron configuration of the molecule is described as being in the ground state. Upon absorbing the excitation light, usually of short wavelengths, electrons may be raised to a higher energy and vibrational excited state; this may take a trillionth of a second (10 to the minus 12th seconds).

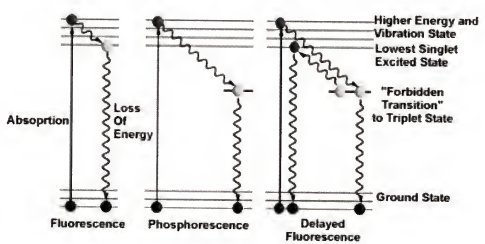

Figure B-1. Jablonski Diagram

In fluorescence, in an interval of approximately a billionth of a second (10 to the minus 9th seconds), the excited electrons may lose some vibrational energy and return to the so-called lowest excited singlet state. From the lowest excited singlet state, the electrons "drop back" to the ground state with simultaneous emission of fluorescent light

as illustrated in Figure B-1. The emitted light is always of longer wavelengths than the excitation light (Stokes' Law). If the exciting radiation is halted, the fluorescence ceases. If the excited electrons, instead of "dropping back" to the lowest singlet state, make a "forbidden transition" to the triplet state and then to the ground state, the emission of radiation may be considerably delayed--up to several seconds or more. This phenomenon is characteristic of phosphorescence as shown in Figure B-1(b). In some instances, the excited electrons may go from the triplet state to the lowest excited singlet state and then return to the ground state, emitting fluorescent light. This action takes a little longer (about a microsecond or two) than usual fluorescence and is called delayed fluorescence (Figure B-1(c)). Under some circumstances, e.g. photobleaching or the presence of salts of heavy metals, etc., emitted light may be significantly reduced or halted altogether.

Based on the above concept, fluorescence illumination and observation has become the most rapidly expanding microscopy technique employed today, both in the medical and biological sciences, a fact which has spurred the development of more sophisticated microscopes and numerous fluorescence accessories.

For the luminescence measurements of nanoparticles on the DNA assay, two types of set-up were used. One was similar to the inverted fluorescence microscope shown in Figure B-2 for low concentration detection.

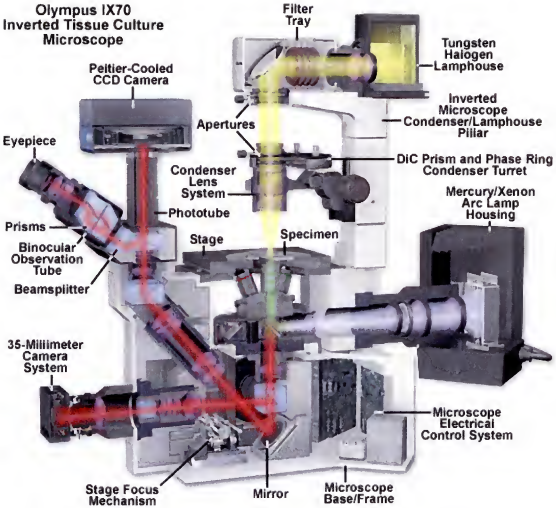

Figure B-2. Cut-away diagram of an inverted fluorescence microscope.

Inverted microscopes are capable of producing fluorescence illumination through an episcopic and optical pathway. Epi-illuminators usually consist of a mercury or xenon lamphouse (or laser system) stationed in a port at the rear of the microscope frame. Fluorescence illumination from the arc lamp passes through a collector lens and into a cube that contains a set of interference filters, including a dichroic mirror, barrier filter, and excitation filter. After excitation of the specimen, secondary fluorescence is collected by the objective and directed through the microscope optical train. The set-up used was

equipped with an ICCD (intensified charge-coupled device) instead of a CCD (charge-coupled device). A schematic diagram is shown in Figure B-3.

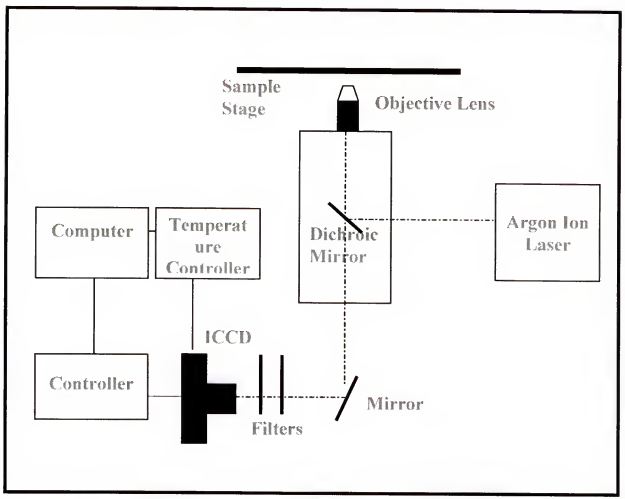

Figure B-3. Schematic diagram of an inverted fluorescence microscope (Courtesy of L. Hillard).

The other set-up had a wide-field imaging capability for bigger area of analysis (Figure B-4).

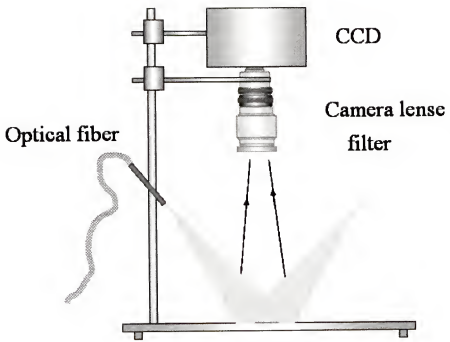

Figure B-4. Wide-field fluorescence lens.

Both set-ups of microscopes were used for the quantitative analyses based on the dye-doped nanoparticle assay. Images obtained were analyzed using a WinView program.

APPENDIX C
ULTRAPYCNOMETER

A gas pycnometer measures the structural or apparent density of solid or particulate materials using gas displacement. In this method, helium gas is used to access the open porosity in the sample. The apparent density of the material is calculated by determining the volume of the sample by introducing a known quantity of gas into the chamber at two different pressures. The relationship $P_1V_1=P_2V_2$ is used to calculate the volume, and the density is determined by dividing this into the mass of the sample. For materials with closed porosity, this results in the apparent density. For materials without closed porosity, this results in the true density

LIST OF REFERENCES

1. C. Kneuer, M. Sameti, U. Bakowsky, T. Schiestel, H. Schirra, H Schmidt, C. M. Lehr, *Bioconjugate Chem.* **11,** 926 (2000).

2. C. Kneuer, M. Sameti, E.G. Haltner, T. Schiestel, H. Schirra, H. Schmidt, C. M. Lehr, *Int. J. Pharm.* **196,** 257 (2000).

3. H. Q. Mao, K. Roy, V. L. Troung-Le, K. A. Janes, K. Y. Lin, Y. Wang, J. T. August, K. Leong, *J. Control Release* **70**, 399 (2001).

4. J. M. Benns, S. W. Kim, *J. Drug Target* **8,** 1 (2000).

5. V. L. Truong-Le, S. M. Walsh, E. Schweibert, H. Q. Mao, W. B. Guggino, J. T. August, K. M. Leong, *Arch. Biochem. Biophys.* **361,** 47 (1999).

6. K. S. Soppimath, T. M. Aminabhavi, A. R. Kulkarni, W. E. Rudzinski , *J. Control Release* **70,** 1 (2001).

7. S. R. Sershen, S. L. Westcott, N. J. Halas, J. L. West, *J. Biomed. Mater. Res.* **51,** 293 (2000).

8. S. Kubitschko, J. Spinke, T. Bruckner, S. Pohl, N. Oranth, *Anal. Biochem.* **253,** 112 (1997).

9. L. A. Lyon, M. D. Musick, P. C. Smith, B. D. Reiss, D. J. Pena, M. J. Natan, *Sensor Actuat. B-Chem.* **54,** 118 (1999).

10. S. Shaertl, F. J. Meyer-Almes, E. Lopez-Calle, A. Siemers, J. Kramer, *J. Biomol. Screen.* **5**, 227 (2000).

11. C. N. R. Rao, A. K. Cheetham, *J. Mater. Chem.*, **11,** 2887 (2001).

12. B. O. Dabbousi, J. Rodriguez-Viejo, F. V. Mikulec, J. R. Heine, H. Matoussi, R. Ober, K. F. Jensen, M. G. Bawendi, *J. Phys. Chem. B* **101,** 9463 (1997).

13. D. Y. Godovsky, *Adv. Polym. Sci.* **153,** 163 (2000).

14. A. P. Alivisatos, *J. Phys. Chem.* **100**, 13226 (1996).

15. M. J. Bruchez, M. Moronne, A. P. Alivisatos, S. Weiss, *Science* **281**, 2013 (1998).

16. M. Dahan, T. Laurence, F. Pinaud, D. S. Chemla, A. P. Alivisatos, M. Sauer, S. Weiss, *Optics Letters* **26,** 825 (2001).

17. T. A. Taton, G. Lu, C. A. Mirkin, *J. Am. Chem. Soc.* **123,** 5164 (2001).

18. S. Santra, K. Wang, R. Tapec, W. Tan, *J. Biomed. Opt.* **6,** 160 (2001).

19. M. Qhobosheane, S. Santra, P. Zhang, W. Tan, *Analyst* **126,** 1274 (2001).

20. C. M. Niemeyer, *Angew. Chem. Int. Ed.* **40,** 4158 (2001).

21. R. Elghanian, J. J. Storhoff, R. C. Mucic, R. L. Letsinger, C. M. Mirkin, *Science* **277,** 1078 (1997).

22. J. J. Storhoff, R. Elghanian, R. C. Mucic, C. A. Mirkin, R. L. Letsinger, *J. Am. Chem. Soc.* **120,** 1959 (1998).

23. R. A. Reynolds, C. A. Mirkin, R. L. Letsinger, *Pure Appl. Chem.* **72,** 229 (2000).

24. T. A. Taton, C. A. Mirkin, R. L. Letsinger, *Science* **289,** 1757 (2000).

25. R. C. Mucic, J. J. Storhoff, C. A. Mirkin, R. L. Letsinger, *J. Am. Chem. Soc.* **120,** 12674 (1998).

26. J. J. Storhoff, A. A. Lazarides, R. C. Mucic, C. A. Mirkin, R. L. Letsinger, G. C. Schatz, *J. Am. Chem. Soc.* **122,** 4640 (2000).

27. R. A. Reynolds, C. A. Mirkin, R. L. Letsinger, *J. Am. Chem. Soc.* **122,** 3795 (2000).

28. Y. W. Cao, R. Jin, C. A. Mirkin, *J. Am. Chem. Soc.***123,** 7961 (2001).

29. H.Cai, C. Xu, P. He, Y. Fang, *J. Electroanal. Chem.* **510,** 78 (2001).

30. D. Zanchet, C. M. Micheel, W. J. Parak, A. P. Alivisatos, *Nano. Lett.* **1,** 32 (2001).

31. Y. Weizmann, F. Patolsky, I. Willner, *Analyst* **126**, 1502 (2001).

32. G. R. Souza, T. J. Miller, *J. Am. Chem. Soc.* **123,** 6734 (2002).

33. J. Reichert, A. Csaki, M. Kohler, W. Fritzsche, *Anal. Chem.* **72,** 6025 (2000).

34. B. Dubertret, M. Calame, A. P. Alivisatos, J. Y. Libchaber , *Nat. Biotechnol.* **19,** 365 (2001).

35. O. Siiman, K. Gordon, A. Burshteyn, J. A. Maples, J. K. Whitesell, *Cytometry* **41,** 365 (2000).

36. A. Gole, C. Dash, C. Soman, S. R. Sainkar, M. Rao, M. Sastry, *Bioconjugate Chem.* **12,** 684 (2001).

37. W. C. W. Chan, S. M. Nie, *Science* **285,** 2016 (1998).

38. S. R. Emory, S. Nie, *J. Phys. Chem. B* **102**, 493 (1998).

39. M. Han, X. Gao, J. Z. Su, S. Nie, *Nat. Biotechnol.* **19,** 631 (2001).

40. D. Gerion, F. Pinaud, S. C. Williams, W. J. Parak, D. Zanchet, S. Weiss, A. P. Alivisatos, *J. Phys. Chem. B* **105,** 8861 (2001).

41. H. Harma, T. Soukka, T. Lovgren, *Clin. Chem.* **47**, 561 (2001).

42. T. Soukka, H. Harma, J. Paukkunen, T. Lovgren T. *Anal. Chem.* **73,** 2254 (2001).

43. T. Soukka, J. Paukkunen, H. Harma, S. Lonnberg, H. Lindroos, T. Lovgren, *Clin. Chem.* **47**, 1269 (2001).

44. D. J. Qian, H. G. Liu , H. X. Huang, Q. Fu, X. S. Feng, *Mater. Lett*. **51,** 525 (2001).

45. M. Brasuel, R. Kopelman, T. J. Miller, R. Tjalkens, M. A. Philbert, *Anal. Chem.* **73,** 2221 (2001).

46. H. Xu, J. W. Aylott, R. Kopelman, T. J. Miller, M. A. Philbert, *Anal. Chem.* **73,** 4124 (2001).

47. M. H. Charles, M. T. Charreyre, T. Delair, A. Elaissari, C. Pichot, *STP Pharma. Sciences* **11,** 251 (2001).

48. B. Q. Sun, G. S. Yi, S. Y. Zhao, D. P. Chen, Y. X. Zhou, J. Cheng, *Anal. Lett.* **34,** 1627 (2001).

49. S. Schultz, J. J. Mock, D. R. Smith, D. A. Schultz, *J. Clin. Ligand Assay* **22,** 214 (1999).

50. S. Schultz, D. R. Smith, J. J. Mock, D. A. Schultz , *P. Natl. Acad. Sci.* **97,** 996 (2002).

51. J. Wang, R. Polsky, D. Xu, *Langmuir* **17,** 5739 (2001).

52. J. R.Taylor, M. M. Fang, S. M. Nie, *Anal. Chem*. **72,** 1979 (2000).

53. A. N. Shipway, E. Katz, I. Willner, *Chemphyschem* **1,** 18 (2000).

54. S. Santra, R. Tapec, N. Theodoropoulou, J. Dobson, A. Hebard, W. Tan, *Langmuir* **17,** 2900 (2001).

55. S. Santra, P. Zhang, K. M. Wang, R. Tapec, W. H. Tan, *Anal. Chem.* **73,** 4988 (2001).

56. R. Tapec, X. Zhao, G. Yao, S. Santra, W. Tan, Submitted 2002.

57. W. Stober, A. Fink, E. Bohn, *J. Colloid. Interface Sci.* **26,** 62 (1968).

58. R. Tapec, X. Zhao, W. Tan, *J. Nanosci. Nanotech.* **2,** 1 (2002).

59. S. Shibata, T. Taniguchi, T. Yano, M. Yamane, *J. Sol-Gel Sci. and Tech.* **10**, 263 (1997).

60. S. Spange, *Progress in Polymer Science* **25,** 781 (2000).

61. L. R. Hilliard, X. Zhao, W. Tan, Submitted 2002.

62. B. P. Maliwal, Z. Gryczynski, J. Lakowicz, *Anal. Chem.* **73,** 4277 (2001).

63. J. Ji, N. Rosenzweig, I. Jones, Z. Rosenzweig, *Anal. Chem.* **73,** 3521 (2001).

64. J. Bui, T. Zelles, H. J. Lou, V. Gallion, M. I. Phillips, W. Tan, *J. Neurosci. Method* **89,** 9 (1999).

65. X. Fang, W. Tan, *Anal. Chem.* **71**, 3101 (1999).

66. S. Shibata, T. Yano, M. Yamane, *Jpn. J. Appl. Phys.* **37**, 41 (1998).

67. J. Cordek, W. Wang, W. H. Tan, *Anal. Chem.* **71**, 1529 (1999).

68. V. Tchikov, S. Schutze, M. K. Kronke, *J. Magn. Magn. Mater.* **194**, 242 (1999).

69. S. Winotomorbach, W. Mullerruchholtz, *Eur. J. Pharm. Biopharm.* **41**, 55 (1995).

70. A. Truchaud, B. Capolaghi, J. P. Yvert, Y. Gourmelin, G. Glikmanas, M. Bogard, *Pure Appl. Chem.* **63**, 1123 (1991).

71. T. Fukushima, K. Sekizawa, Y. Jin, M. Yamaya, H. Sasaki, T. Takishima, *Am. J. Physiol.* **265**, 167 (1993).

72. L. Babes, B. Denizot,G. Tanguy, J. J. Le Jeune, P. Jallet, *J. Colloid Interface Sci.* **212**, 474 (1999).

73. H. H. Bengele, S. Palmacci, J. Rogers, C. W. Jung, J. Crenshaw, L. Josephson, *Magn. Reson. Imaging* **12**, 433 (1994).

74. DYNALogue, *News and Views from Dynal Bioscience*, (2000), *Issue 1* (http://www.dynal.net) 03/2000.

75. J. T. Kemshead, J. G. Treleaven, F. M. Gibson, J. Ugelstad, A. Rembaum, T. Philip, *Prog. Exp. Tumor Res.* **29**, 249 (1985).

76. D. Pouliquen, H. Perroud, F. Calza, P. Jallet, J. J. Le Jeune, *Magn. Reson. Med.* **24**, 75 (1992).

77. F. E. Kruis, H. Fissan, A. Peled, *J. Aerosol Sci.* **29**, 511 (1998).

78. X. Cao, R. Prozorov, Y. Koltypin, G. Kataby, I. Felner, A. Gedanken, *J. Mater. Res.* **12**, 402 (1997).

79. K. Suslick, S. Choe, A. Cichowlas, M.W. Grinstaff, *Nature* **353**, 414 (1991).

80. B. M. Berkovsky, V. F. Medvedev, M. S. Krokov, *Magnetic Fluids: Engineering Applications*, Oxford University Press, Oxford (1993).

81. R. M. Cornell, U. Schwertmann, *The Iron Oxide. Structure, Properties, Reactions, Occurrence and Uses*, VCH, Weinheim (1996).

82. K. Raj, R. Moskowitz, *J. Magn. Magn. Mater.* **85**, 233 (1990).

83. T. Li, J. Moon, A. A. Morrone, J. J. Mecholsky,. D. R. Talham, J. H. Adair, *Langmuir* **15**, 4328 (1999).

84. S. Shiojiri, T. Hirai, I. Komasawa, *Chem. Commun.* **14**, 1439 (1998).

85. E. Stathatos, P. Lianos, F. Del Monte, D. Levy, D. Tsiourvas, *Langmuir* **13**, 4295 (1997).

86. S. -Y. Chang, L. Liu, S. A. Asher, *J. Am. Chem. Soc.* **116**, 6739 (1994).

87. J. A. Lopez Perez, M. A. Lopez Quintela, J. Mira, J. Rivas, S. W. Charles, *J. Phys. Chem. B.* **101**, 8045 (1997).

88. J. A. Lopez Perez, M. A. Lopez Quintela, J. Mira, J. Rivas, *IEEE Trans. Magn.* **33**, 4359 (1997).

89. P. A. Dresco, V. S. Zaitsev, R. J. Gambino, B. Chu, *Langmuir* **15**, 1945 (1999).

90. K. M. Lee, C. M. Sorensen, K. J. Klabunde, G. C. Hadjipanayis, *IEEE Trans. Magn.* **28**, 3180 (1992).

91. C. Liu, B. Zou, A. J. Rondinone, Z. J. Zhang, *J. Phys. Chem. B.* **104**, 1141 (2000).

92. T. Atarashi, Y. S. Kim, T. Fujita, K. Nakatsuka, *J. Magn. Magn. Mater.* **201**, 7 (1999).

93. G. Wang, A. Harrison, *J. Colloid Interface Sci.*. **217**, 203 (1999).

94. M. Ohmori, E. Matijevic, E. *J. Colloid Interface Sci.* **150**, 594 (1992).

95. F. J. Arriagada, K. Osseo-Asare,. *J. Colloid and Interf. Sci.* **211**, 210 (1999).

96. S. J. Doktycz, K. S. Suslick, *Science* **247**, 1067 (1990).

97. W. Luo, S. R. Nagel,T. F. Rosenbaum, R. E. Rosenseig, *Phys. Rev. Lett.* **67**, 2721 (1991).

98. S. R. Elliot, *Physics of Amorphous Materials*, Longman, London and New York, pp. 350-357 (1984).

99. D. L. Leslie-Pelecky, R. D. Rieke, *Chem. Mater.* **8**, 1770 (1996).

100. K. E. Gonsalves, S. P. Rangarajan, A. Garcia-Ruiz, C. C. Law, *J. Mater. Sci. Lett.* **15**, 1261 (1998).

101. Y. S. Kang, S. Risbud, J. F. Rabolt, P. Stroeve, P. *Chem. Mater.* **8**, 2209 (1996).

102. L. A. Chung, *Anal. Biochem.* **248**, 195 (1997).

103. L. He, M.D. Musick, S. R. Nicewarner, F. G. Salinas, S. J. Benkovic, M. J. Natan, C. D. Keating, *J. Am. Chem. Soc.* **122**, 9071 (2000).

104. S. Weiss, *Science* **283**, 1676 (1999).

105. F. Kleinjung, S. Klussman, V. A. Erdmann, F. W. Scheller, J. P. Furste, F. F. Bier, *Anal. Chem.* **70**, 328 (1998).

106. L A. Chrisey, G. U. Lee, C. E. O'Ferral, *Nucleic Acid Res.*, **24**, 3031 (1996).

107. Y. Rogers, P. Jiang-Baucom, Z. Huang, V. Bogdanov, S. Anderson, M. Boyce-Jacino, *Anal. Biochem.* **266**, 23 (1999).

108. M. A. Osborne, W. S. Furey, D. Klenerman, S. Balasubramanian, *Anal. Chem.* **72**, 3678 (2000).

109. X. Fang, X. Liu, S. Schuster, W. Tan, *J. Am. Chem. Soc.*, **121**, 2921 (1999).

110. R. G. H Cotton, *Mutation Detection* Oxford University Press, New York (1997).

111. P. Zhang, W. Tan, *Chemistry, A European Journal*, **6**, 1087 (2000).

112. S. Tyagi, D. P. Bratu, F. R. Kramer, *Nature Biotech.* **16**, 49 (1998).

113. X. Fang, J. Li, J. Perlette, K. Wang, W. Tan, *Anal. Chem.* **72**, 747A (2000).

114. L. G. Kostrikis, S. Tyagi, M. M. Mhlanga, D. D. Ho, F. R. Kramer, *Science* **279**, 1228 (1998).

115. X. Fang, J. Li, S. Schuster, W. Tan, *Angew. Chem. Inter. Ed.* **39**, 1049 (2000).

116. Y. R. Chela, H. L. Grossman, Y. Poon, R. McDermott, R. Stevens, M. D. Alper, J. Clarke, *Proc. Natl. Acad. Sci. USA* **26**, 14268 (2000).

117. I. Safarik, M. Safarikova, *J. Chromatog. B* **722**, 33 (1999).

118. V. S. Srinivas, B. Arijit, *Colloids Surfaces B: Biointerfaces* **8**, 199 (1997).

BIOGRAPHICAL SKETCH

Rovelyn Tapec Dytioco, born 1973 in Sanchez Mira, Cagayan, Philippines, studied chemistry at the University of the Philippines where she obtained her Bachelor of Science degree in chemistry in 1994. From 1994 to 1998, she stayed on and started her graduate studies and at the same time worked full-time as a chemistry laboratory instructor. She then moved to the University of Florida and worked in the bioanalytical chemistry group of Dr. Weihong Tan. She completed her research in August 2002, obtaining the degree of Doctor of Philosophy.

I certify that I have read this study and that in my opinion it conforms to acceptable standards of scholarly presentation and is fully adequate, in scope and quality, as a dissertation for the degree of Doctor of Philosophy.

Weihong Tan
Associate Professor of Chemistry

I certify that I have read this study and that in my opinion it conforms to acceptable standards of scholarly presentation and is fully adequate, in scope and quality, as a dissertation for the degree of Doctor of Philosophy.

Robert T. Kennedy
Professor of Chemistry

I certify that I have read this study and that in my opinion it conforms to acceptable standards of scholarly presentation and is fully adequate, in scope and quality, as a dissertation for the degree of Doctor of Philosophy.

James D. Winefordner
Professor of Chemistry

I certify that I have read this study and that in my opinion it conforms to acceptable standards of scholarly presentation and is fully adequate, in scope and quality, as a dissertation for the degree of Doctor of Philosophy.

Benjamin Horenstein
Associate Professor of Chemistry

I certify that I have read this study and that in my opinion it conforms to acceptable standards of scholarly presentation and is fully adequate, in scope and quality, as a dissertation for the degree of Doctor of Philosophy.

Michael I. Phillips
Professor of Physiology and Functional Genomics

This dissertation was submitted to the Graduate Faculty of the Department of Chemistry in the College of Liberal Arts and Sciences and to the Graduate School and was accepted as partial fulfillment of the requirements for the degree of Doctor of Philosophy.

August 2002

_____

Dean, Graduate School